Development of Bimetallic Pd-Zn Catalysts for Methanol Steam Reforming: Hydrogen Production for Fuel Cells

Submitted by

Philasande Xalabile

In partial fulfilment of the requirements for the degree of

Master of Science in Chemical Engineering

September 2015

HySA/Catalysis Centre of Competence

Department of Chemical Engineering

University of Cape Town

Synopsis

Proton exchange membrane fuel cell (PEMFC) has been reported as clean and efficient energy technology from conversion of H_2. However, one of the main challenges remains the storage and transport of hydrogen. The promising alternative is to produce H_2 on site by a reformer using a H_2-dense liquid as a fuel, a technology known as fuel processing. Methanol is an attractive source of H_2 compared to other fuels as it presents several advantages, i.e. it is obtained sulphur-free, has a high H to C ratio and therefore produces a H_2-rich reformate, can be reformed at low temperatures (200 - 300°C) and is a liquid at ambient conditions so that it can be easily handled. Typically, Cu-based catalysts are used for steam reforming of methanol due to their high activity (i.e. H_2 production) and high selectivity towards CO_2. As CO poisons anodic catalyst of PEMFC, high selectivity towards CO_2 is crucial so as to eliminate or at least minimize CO removal load downstream a fuel processor. However, Cu-based catalysts are thermally unstable and suffer deactivation due to sintering at high temperatures (> 250°C). Moreover, Cu-based catalysts are pyrophoric and therefore difficult to handle. Recent studies show that PdZn catalysts are very promising as they exhibit comparable activity and selectivity to Cu-based ones. Furthermore, PdZn catalysts are thermally stable in the typically methanol steam reforming temperature range (200 - 300°C). Most literature attributes high CO_2 selectivity of PdZn catalysts to formation of PdZn alloy. It is generally agreed that PdZn alloy is formed when PdZn catalysts are reduced in H_2 at high temperatures (> 250°C).

In this work, a Pd/ZnO catalyst aimed at 2.5 wt% Pd was successfully prepared via incipient wetness impregnation and the duplicate preparation of the catalyst was successful. Both impregnation catalysts were confirmed by ICP-OES to contain similar weight Pd loadings i.e. 2.8 and 2.7 wt%, respectively. The actual Pd loading (ICP-OES) was slightly higher than the target loading (2.5 wt%) due to Pd content of Pd salt underestimated during catalyst preparation. Furthermore, crystallite size distribution, i.e. PdO crystallites on ZnO support, was similar (i.e. 6.7 ± 2.4 nm and 6.3 ± 1.9 nm) for both impregnation catalysts.

The TPR analysis of the catalyst showed two peaks, i.e. a narrow peak at 87°C and a broader peak starting at approximately 260°C with a maximum at 348°C and ending around 385°C. The peak which occurred at the lower temperature was due to reduction of PdO to metallic

Pd. The H_2-TPR analysis of pure ZnO shows that ZnO (in the absence of Pd) did not reduce below 600°C. Therefore the peak which occurred at the higher temperature in the case of the impregnation catalyst was due to reduction of ZnO and this was facilitated by H_2 spill-over from the metallic Pd. To confirm the difference in selectivity towards CO_2 between the 'only PdO reduced' and the 'PdO and ZnO' reduced catalysts, the impregnation catalyst was reduced at different temperurates (i.e. 120, 180 and 450°C) prior to catalyst performance tests. However, selectivity towards CO_2 remained > 99% for all conditions. To not influence the reduction by *in-situ* reduction due to H_2 produced by the methanol steam reforming reaction, reforming was carried out at low temperatures. Consequently, CH_3OH conversion was low (< 30%). Since the feed molar steam to carbon ratio was 1.1, sligthly higher than the stoichiometric ratio, the low CH_3OH conversions (< 30%) resulted in excess steam (compared to CO and CO_2) in the reactor and this condition drove the water-gas shift reaction to high or equilibrium selectivity towards CO_2 (~ 99%).

The co-precipitation preparation method was not successful.i.e. the co-precipitation catalyst was aimed at 3 wt% but was confirmed by ICP-OES to be only 1 wt%. A significant fraction of Pd was lost as it did not precipitate during catalyst preparation. The uncontrollable precipitation of Pd makes the method irreproducible. Hence less focus was paid on the co-precipitation catalyst.

Acknowledgements

I owe my deepest gratitude to the following people and organisations who assisted me during the course of this thesis and who made it a success;

Prof. Jack Fletcher, for the opportunity he granted me to be part of the HySA/Catalysis Research group, for his guidance and support during the course of the project

Niels Luchters, for his encouragement and day-to-day assistance, ensuring that the project was progressing and that I develop a better understanding of the subject

Dr Peter Malatji, for his encouragement and day-to-day supervision especially during the initial phase of the project and his help in setting the scope and the objectives of the project

HySA/Catalysis Fuel Processing Team (UCT), for being a family, for their advices on challenges related to the project, and for their input in helping me to have a better understanding of fuel processing technology

Waldo Koorts, for his technical assistance, especially to challenges related to the testing rig I used for the project

Electron Microscope Unit (UCT), for taking microscope images of my samples

Analytical Laboratory (UCT), for analysing my solid samples

Dirk Reyskens, for his assistance in processing my equipment and chemicals orders, and for making sure that the laboratory was a safe working environment

HySA/Catalysis Centre of Competence (UCT), for financial support, and for providing equipment and materials required for the project

Lastly, but not least, I would like thank God for giving me health, strength and soundness of mind during the course of the project

Declaration

I know that plagiarism is wrong. Plagiarism is to use another's work and to pretend that it is one's own. This report is my own work. I have not allowed, and will not allow anyone to copy my work with the intention of passing it off as his or her own work.

…… Date……

Philasande Xalabile

Table of Contents

List of Figures

List of Tables

Nomenclature

ATR	Auto-thermal Reforming
barg	Gage pressure i.e. pressure in bar above atmospheric pressure
DMFC	Direct Methanol Fuel Cell
DRIFTS	Diffuse Reflectance Infrared Fourier Transform Spectroscopy
FID	Flame Ionization Detector
FTIR	Fourier Transform Infrared spectroscopy
GC	Gas Chromatography
GHSV	Gas Hourly Space Velocity
h	Hour
$\Delta_{rxn}H$	Heat of reaction
MD	Methanol Decomposition
PEMFC	Proton Exchange Membrane Fuel Cell
PGM	Platinum group Metal
POx	Partial Oxidation
ppm	Parts per million
PrOx	Preferential Oxidation
PSD	Particle Size Distribution
RMFC	Reformed Methanol Fuel Cell
S/C	Molar Steam to Carbon Ratio
sccm	Standard cubic centimetres per minute
S_{CO_2}	Selectivity towards carbon dioxide
SD	Standard Deviation
SelMeth	Selective Methanation
SRM	Steam Reforming of Methanol
$T_{reduction}$	Reduction temperature
T_{rxn}	Reaction temperature
UNFCCC	United Nations Framework Convention on Climate Change
WGS	Water-gas shift
X_{MeOH}	Methanol conversion
XRD	X-ray Diffraction

Chapter 1 Introduction

The growth of the world population and an ambition to achieve economic growth has led to high energy demands. In addition, environmental concerns resulting from emissions of greenhouse gases when using conventional fossil fuel combustion technologies necessitates research and development of cleaner and efficient energy generation sources or technologies (Chianese *et al*., 2015; Cipriani *et al*., 2014).

Literature reports a growing trend for the use of PEMFC technology, amongst others, as a clean and efficient energy conversion technology. PEMFCs convert chemical energy stored in hydrogen directly into electrical energy while producing water as the only by-product. Due to their relatively low operating temperature (60-120°C) and fast start-up, PEMFCs are suitable for transport and portable power generation applications (Mekhilef *et al*., 2012; Wang *et al*., 2011).

One of the main challenges, however, is that PEMFCs require hydrogen as a fuel. Hydrogen does not occur naturally and once it is produced it is energy intensive to store and dangerous to transport. The promising alternative in fuel cell systems is to produce hydrogen on site by a reformer using hydrogen carrier as a feedstock, a technology known as fuel processing. Typically, as a fuel, hydrocarbons such as methane, LPG or diesel and alcohols e.g. methanol, ethanol etc., are used as feedstock for reformer to produce hydrogen. Currently, methane is the primary fuel used globally for the production of hydrogen through steam reforming reaction using a catalyst. This is mainly due to its large abundance, high hydrogen to carbon ratio and the existing pipeline infrastructure for its distribution (Roh and Jeong, 2012; Mondal and Ramesh Chandran, 2014).

Methanol presents several advantages compared to other fuels, i.e. it is obtained sulphur-free, has a high H to C ratio and therefore produces a H_2-rich gas upon reforming, can be 'steam reformed' at lower temperatures (200-300°C) and is liquid at ambient conditions to be stored and transported easily (Sá *et al*., 2010). On the other hand, catalyst development plays a significant role in improving efficiency of the reformer and therefore of fuel cell-reformer integrated system. Typically, Cu-based catalysts are used for methanol steam reforming due to their high activity (i.e. hydrogen production) and high selectivity towards CO_2. High selectivity towards CO_2 is crucial so as to eliminate or at least reduce CO removal

load. Cu-based catalysts, however, are thermally unstable and suffer from deactivation due to sintering at high temperatures (> 250°C) and due to their pyrophoricity, Cu-based catalysts are difficult to handle (Zhang and Farrauto, 2011; Ilinich *et al*., 2008). On the other hand, ZnO supported Pd catalysts have been reported in literature to have comparable activity and selectivity to Cu-based ones. In addition, these catalysts are thermally stable in the typical methanol steam reforming temperature range (200 – 300°C). Many researches attributed high selectivity towards CO_2 of ZnO supported Pd catalysts to the formation of PdZn alloy upon reducing the catalysts at high temperatures (Sá *et al*., 2010). In this work methanol was used as a fuel for methanol steam reforming reaction investigating the selectivity towards CO_2 of ZnO supported Pd catalysts reduced at different temperatures.

Chapter 2 Literature Review

2.1. Hydrogen and Fuel Cells

The world economy is heavily dependent on fossil-fuel based energy since the beginning of the industrial revolution in the 18th century (Cabtree *et al*., 2004). Moreover, energy demands are continuing to rise due to population growth and industrialization. On the other hand, there are growing concerns over the use of fossil fuel-based energy as unsustainable due to dwindling of fossil fuels. In addition, conventional technologies (i.e. burning of fossil fuels) to produce energy or electricity are inefficient and results in emission of green-house gases (GHGs). It is generally agreed by scientists that an increase in concentrations of GHGs in the atmosphere enhances the green-house effect thus resulting in global warming and that this is detrimental to our planet (Pachauri *et al*., 2014). In an effort to stabilise or reduce GHG emissions, many countries, including South Africa, have committed themselves under the Kyoto Protocol of the United Nations Framework Convention on Climate Change (UNFCCC) adopted in 1997. Consequently, policies aimed at reducing GHG emissions are discussed and implemented worldwide.

Amongst other solutions, H_2 is considered as a potential fuel for the future due to its environmental advantages over fossil fuels (Ball and Weeda, 2015). Hydrogen can be burned in O_2 to produce large amount of energy as heat (e.g. internal combustion engines) while producing water as the only by-product. Fuel cell (FC) technology is even more considered and is undergoing serious research and development as a potential clean and high efficient technology (Wang, 2004). Platinum group metals (PGMs) are the key catalytic material for FCs. This makes the FC technology even more attractive in South Africa where ~ 80% of the world PGMs are found (Yang, 2009).

There are different types of FCs. Table 2-1 shows the common types of FCs, their power output range, typical application, fuel, advantages and efficiency. In principle, all FCs work in a similar way i.e. FCs convert chemical energy stored in a fuel.

Table 2-1: Different types of fuel cell technologies (after FuelCell Energy, 2013)

Technology	Size range	Typical Application	Fuel	Advantages	Electrical efficiency
MCFC[a]	300 kW- 2.8 MW	Utilities, large universities, industrial-based load	Natural gas, biogas, others	High efficiency, scalable, fuel flexible & CHP	43% - 47%
PAFC[b]	400 kW	Commercial buildings - baseload	Natural gas	CHP	40% -42%
SOFC[c]	up to 200 kW	Commercial buildings - baseload	Natural gas	High efficiency	50% - 60%
PEM/SOFC	< 10 kW	Residential and small commercial	Natural gas	Load following & CHP	25% - 35%
DMFC	up to 5 kW	Portable power	Methanol	High energy density	-
PEMFC[d]	up to 100 kW	Transportation & portable power	Hydrogen	Load following & CHP	25% - 35%

[a]Molten carbonate, [b]Phosphoric Acid, [c]Solid Oxide and [d]Polymer Electrolyte Membrane FCs. CHP = Combined Heat and Power.

This work focuses on PEMFC. Due to its low operating temperature, typically, 60-180°C (Sharaf and Orhan, 2014), PEMFC is attractive for transport and portable power applications. A PEMFC consists of two electrodes (i.e. anode and cathode) separated by an electrolyte or proton exchange membrane (refer to Figure 2-1).

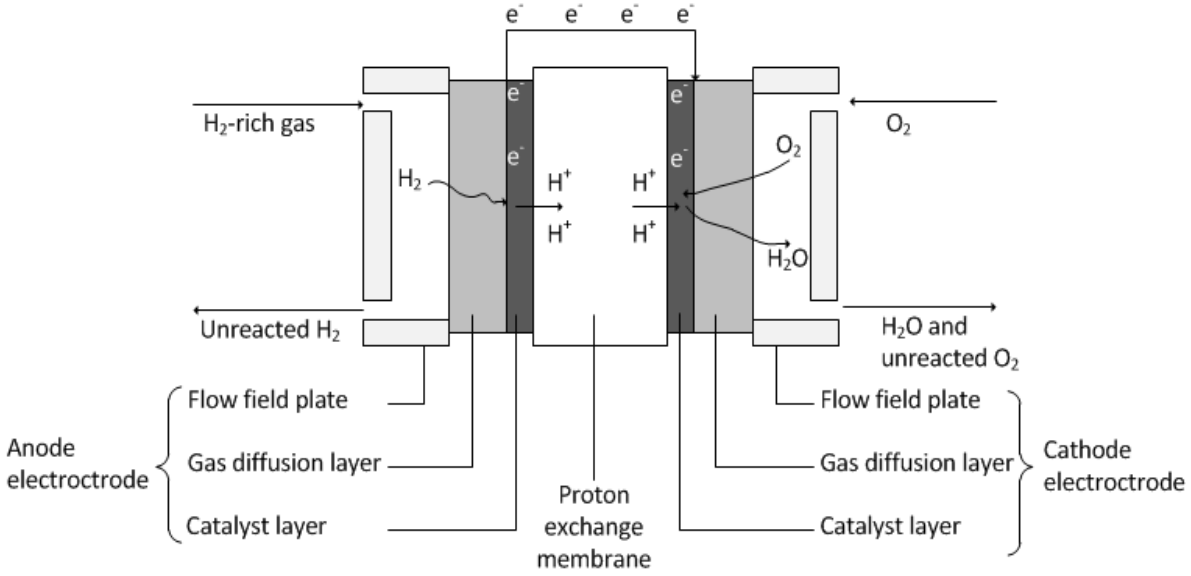

Figure 2-1: A simplified diagram of a PEMFC

A good electrolyte is proton conductive but electronic insulated. A H_2-rich gas (fuel) and O_2 or air (oxidant) are fed on the anode and cathode electrodes, respectively. Hydrogen oxidation reaction (HOR) (Eqn 2.1) and oxygen reduction reaction (ORR) (Eqn 2.2) take place on the anode and cathode electrodes, respectively.

Anode:	$H_2 \rightarrow 2H^+ + 2e^-$	Eqn 2.1
Cathode:	$0.5\ O_2 + 2H^+ + 2e^- \rightarrow H_2O$	Eqn 2.2
Overall:	$H_2 + 0.5\ O_2 \rightarrow H_2O$	Eqn 2.3

Via the HOR (Eqn 2.1), protons and electrons are generated at the anode electrode. Protons are drawn through the electrolyte to the cathode electrode while electrons are drawn via an external circuit to the cathode electrode thus generating direct current. On the cathode electrode O_2 (typically from air) is oxidised via the ORR (Eqn 2.2). The kinetics of both HOR and ORR reactions are facilitated by catalysts. The most commonly used electro-catalysts are Pt-based. Ideally, H_2 and O_2 do not mix anywhere in the cell, and thus there is no H_2 combustion in the cell. Therefore, unlike in combustion engines, chemical energy is directly converted to electrical energy, hence high efficiency are obtainable. As shown by the overall reaction (Eqn 2.3), water is the only by-product.

Hydrogen is the most abundant element on earth, however, the challenge is that H_2 does not occur naturally and must be produced from H_2-rich sources such as hydrocarbons. The

use of hydrocarbons to produce H_2 does not eliminate emission of CO_2 but it is the first step towards the hydrogen economy. Hydrogen can also be obtained by electrolysis of water using electricity, a process where water is split into H_2 and O_2. If electricity (in the case of electrolysis) is derived from renewable resources such as solar and wind, the use of fuel cells can provide energy storage mechanism for the renewable resources. However, electrolysis, due to the large amount of energy (i.e. electricity) required, is currently not economic feasible and is still under development (Palo *et al*., 2007).

Another key challenge is storing and distributing H_2 especially under the current infrastructure. While H_2 has high gravimetric energy density it has low volumetric energy density compared to hydrocarbons and alcohols (see Figure 2-2). For instance, at ambient conditions one gram of H_2 occupies ~ 12 litres of space. This is important to consider especially for the application of FCs for transport and portable power generation where volume and weight needs to be minimised. Hence H_2 is typically stored either as compressed gas or liquid, however, the increase in volumetric energy density in this case comes at a cost of parasitic energy loss required for compression. Hence hydrocarbons (e.g. diesel and gasoline) and alcohols (e.g. ethanol and methanol) are typically converted to produce H_2. The technique used to convert hydrocarbons or alcohols to H_2 is called fuel processing (refer to chapter 2.3).

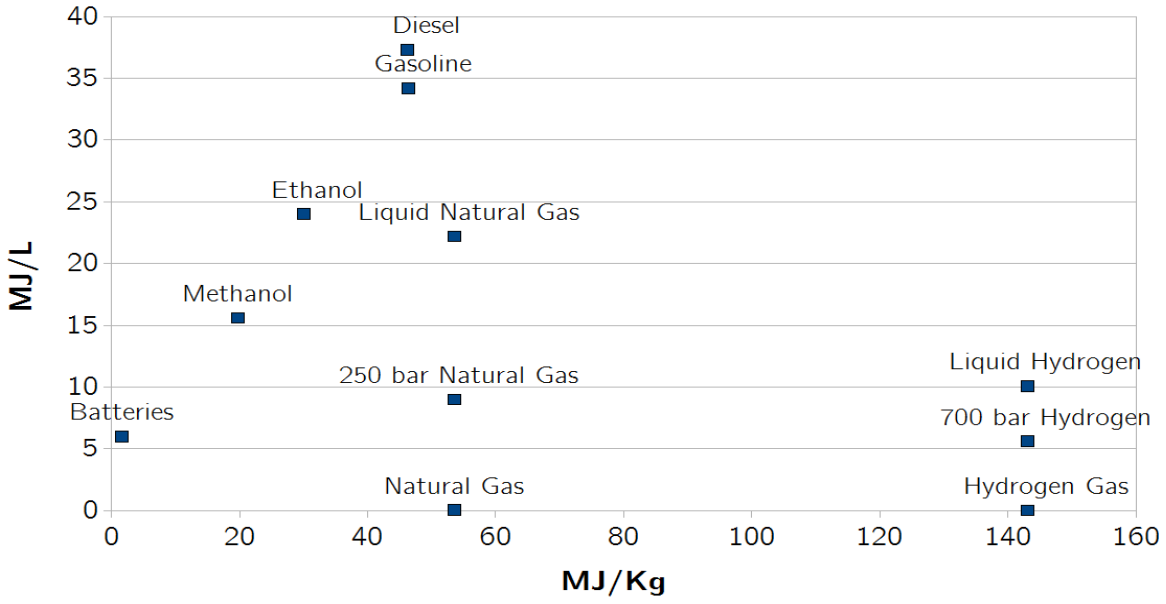

Figure 2-2: Volumetric and gravimetric energy densities of various fuels (after Carbon Transformers, 2014)

2.2. DMFC vs RMFC

Unlike reformed methanol fuel cell (RMFC) in which methanol is first 'reformed' to H_2 in a fuel processor, direct methanol fuel cell (DMFC) uses methanol directly as a fuel. DMFC like PEMFC (or RMFC) operates in the temperature range of 60-120°C. The reactions that take place on the anode and cathode of a DMFC are as per Eqn 2.4 and Eqn 2.5, respectively. The overall reaction (Eqn 2.6) shows that water and CO_2 are by-products. As already discussed, in PEMFC water is produced as an only by-product, however, CO_2 is produced in the fuel processing stage.

Anode: $CH_3OH + H_2O \rightarrow 6H^+ + 6e^- + CO_2$ Eqn 2.4

Cathode: $1.5\ O_2 + 6H^+ + 6e^- \rightarrow 3\ H_2O$ Eqn 2.5

Overall: $CH_3OH + 1.5\ O_2 \rightarrow 2\ H_2O + CO_2$ Eqn 2.6

Feeding methanol directly simplifies and reduce size and weight of DMFC system as auxiliary components (i.e. heat exchangers and pumps) are eliminated (Wang *et al*., 2015). In addition, methanol has a relatively higher energy density. Consequently, DMFC system has a high theoretical energy density hence it is attractive for portable power application.

However, there are a number of drawbacks with DMFC. The oxidation of methanol reaction (Eqn 2.4) on the cathode electrode is slower than hydrogen oxidation (Eqn 2.1) in the case of PEMFC. Also, the oxidation reaction (Eqn 2.4) requires at least one water molecule for every methanol molecule converted. In addition, to reduce methanol cross-over, methanol concentration in the feed is typically kept between 1 M and 3 M i.e. (~ 3 to 10 wt%) (Liu *et al*., 2006). Thus the energy density of DMFC system is reduced due to dilution of methanol fuel. By far literature considers methanol crossover (from the anode to the cathode) as most severe phenomena that compromise DMFC performance (Wang *et al*., 2015). Methanol cross-over leads to mixed potentials (i.e. oxidation of methanol on the cathode electrode) and consequently decrease in cell performance. According to (Kamarudin *et al*., 2009), less than 30% of chemical energy stored in methanol can be converted to electrical energy due to methanol crossover. The oxidation of methanol on the cathode electrode also competes for active sites and thus limit oxygen reduction reaction (Eqn 2.5) (Bello, 2011). Moreover, methanol and water crossover normally results in flooding of the cathode electrode and limit O_2 access to the active sites and consequently lowers the rate of reduction reaction

(Eqn 2.5). Most of the research and development as far DMFC is concerned is on improving the electrolyte membrane i.e. reducing the membrane methanol permeability (Houchins *et al*., 2012).

While DMFC have high theoretical energy density they can produce less energy over a long period of time and therefore are not suitable for transport purposes especially large vehicles. Hence they are typically used to power electronic devices (e.g. cellphones, laptops etc.). On the other hand, PEMFC has relatively higher power density than DMFC hence it is used for transport application. However, efficiency of RMFC depends on the efficiency of both the fuel processor and PEMFC. It is therefore crucial that not only the fuel cell (PEMFC) run efficiently but also the fuel processor.

2.3. Fuel Processing

This section provides an overview of a typical fuel processing system (section 2.3.1) and fuel processing techniques typically used for H_2 production (section 2.3.2).

2.3.1. Typical Fuel Processing System

Fuel processing is divided mainly into two stages i.e. H_2 production and CO removal. Figure 2-3 is a typical fuel processing system. The feedstock is a H_2-dense compound, typically, hydrocarbons and alcohols. Currently, methane is the main fuel that is used in industry for the production of H_2 (Balat and Kırtay, 2010). There are three main technologies that are used to convert H_2-dense compounds into H_2 i.e. steam reforming (SR), partial oxidation (POx) and auto-thermal reforming (ATR). Details for these technologies are given in section 2.3.2. Depending on the technique, reaction conditions and catalyst used, CO is often formed either as a product or a by-product. CO in the reformate is undesired as it poison the anodic catalyst of fuel cell downstream the fuel processor. Hence the CO removal is necessary (refer to section 2.3.2.4 for more details). WGS is normally the preliminary stage of CO removal. PEMFC requires CO concentrations to be less than 10 ppm (Kim *et al*., 2009) to avoid or minimize poisoning of anode catalyst. Hence additional CO removal step, i.e. preferential oxidation (PrOX) or selective methanation (SelMeth), is required.

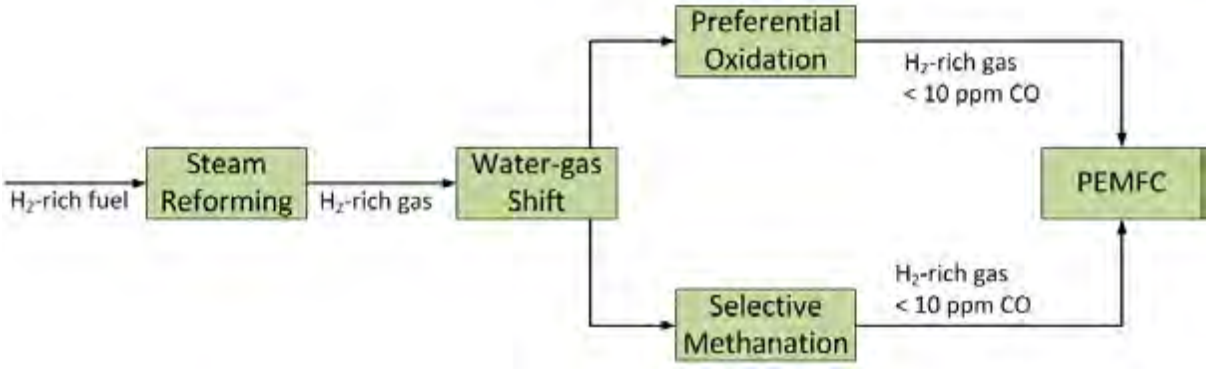

Figure 2-3: A typical fuel processing system with a fuel cell

2.3.2. Typical fuel processing techniques

Methane and methanol (i.e. a hydrocarbon and an alcohol feedstock, respectively) are used as examples to demonstrate the key reactions that take place for steam reforming (SR), partial oxidation (POx) and auto-thermal reforming (ATR) fuel processing techniques.

2.3.2.1. Steam Reforming

Steam reforming is the most commonly used fuel processing technique due to its H_2-rich reformate. Water is used as an oxidant to extract hydrogen from H_2-rich compound (Shoesmith, 1994). Methane is the main feedstock used in industry for the production of H_2. Steam reforming of fuels is a highly endothermic reaction (see Eqn 2.7 and Eqn 2.8), thus an external heat source is required to raise reaction temperature so as to obtain high conversions of feedstock. SR of methane typically takes place in the temperature range of 600 - 900°C while SR of methanol (which is relatively less endothermic) is typically carried out in the temperature range of 200 - 300°C. The relatively lower reforming temperature makes methanol SR attractive for PEMFC technology.

$CH_4 + H_2O \leftrightarrow CO + 3H_2$ $\quad \Delta_{rxn}H_{298K} = 198$ kJ/mol $\quad$ Eqn 2.7

$CH_3OH + H_2O \leftrightarrow CO_2 + 3H_2$ $\quad \Delta_{rxn}H_{298K} = 49$ kJ/mol $\quad$ Eqn 2.8

WGS reaction (Eqn 2.13) also takes place during SR. Consequently, while high reaction temperatures are desired for high SR conversions, high temperatures also lead to high CO concentrations in the reformate due to the exothermicity of the WGS reaction. In addition, methanol decomposition (MD, Eqn 2.9) also takes place during SR of methanol thus also contributing in production of CO.

$CH_3OH \leftrightarrow CO + 2H_2$ $\quad \Delta_{rxn}H_{298K} = 49$ kJ/mol $\quad$ Eqn 2.9

A feed steam to carbon ratio is another important parameter that affect composition of the reformate. As shown in Figure 2-4, when the steam to carbon ratio increases from 2 to 4 at the reaction conditions (700°C, 5 bar) methane equilibrium conversion also increases from 61 to 80%. However, the increase in the conversion comes at the expense of thermal duty i.e. more energy in the form of heat is required to vaporize water at higher steam to carbon ratio.

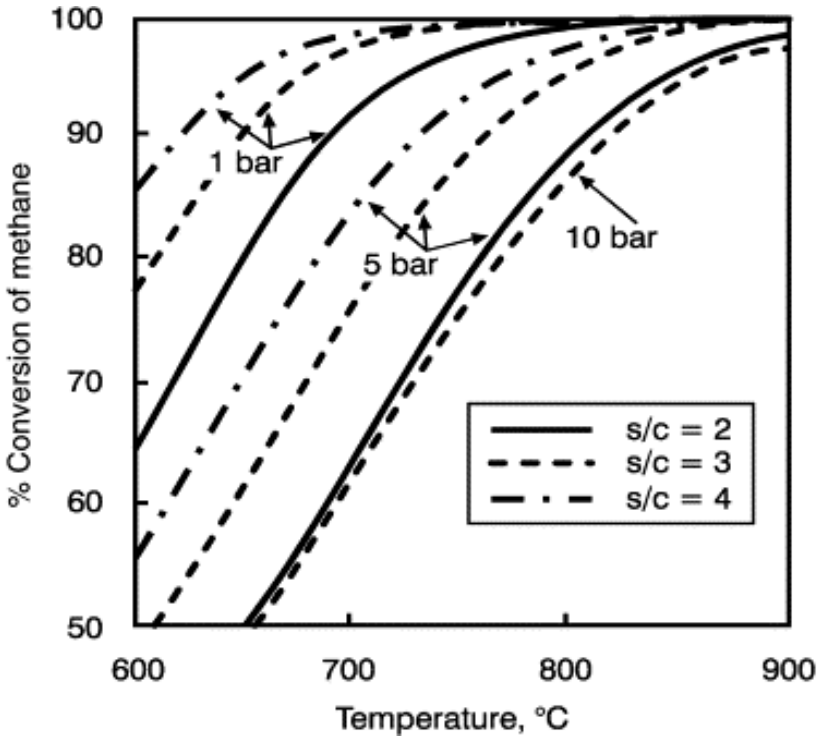

Figure 2-4: Effects of steam to carbon ratio on SR of methane equilibrium (after Joensen and Rostrup-Nielsen, 2002)

2.3.2.2. Partial Oxidation

In partial oxidation (POx) O_2 is used as an oxidant. As shown by Eqn 2.10 and Eqn 2.11, POx is an exothermic reaction and thus no external heat source is required. The exothermicity of POx makes the technique good for start-ups (Shoesmith, 1994). Typically air is used in the feed as it is expensive to produce and store pure O_2. However, the feeding of air leads to the dilution of the reformate by N_2 and thus make POx less attractive technique for fuel cell application.

$CH_4 + 0.5\ O_2 \leftrightarrow CO + 2H_2$ $\quad \Delta_{rxn}H_{298K} = -36$ kJ/mol Eqn 2.10

$CH_3OH + O_2 \leftrightarrow CO_2 + 2H_2$ $\quad \Delta_{rxn}H_{298K} = -193$ kJ/mol Eqn 2.11

2.3.2.3. Auto-thermal Reforming

Auto-thermal reforming is a combination of POx and SR such that heat produced by the exothermic POx reaction is used to facilitate the endothermic SR reaction. By controlling the fuel: steam: O_2 ratios it is possible to operate close to the 'auto-thermal' condition. Auto-thermal reforming has high thermal efficiency. However, as in the case of POx, the feeding of air leads to dilution of reformate. Eqn 2.12 is a general equation for ATR of hydrocarbons and alcohols (Kolb, 2008).

$$C_xH_yO_z + n(O_2 + 3.76N_2) + (x\text{-}2n\text{-}z)H_2O \leftrightarrow xCO + (x\text{-}2n\text{-}z\text{+}0.5y)H_2 + 3.7nN_2 \qquad \text{Eqn 2.12}$$

2.3.2.4. CO Removal

Water-gas Shift:

The preliminary stage of CO clean-up is typically the slightly exothermic reaction i.e. water gas shift (WGS, Eqn 2.13). WGS is advantageous in that for every mole of CO consumed a mole of H_2 is added. Typically, two WGS reactors in series are used i.e. high temperature shift (HTS) followed by low temperature shift (LTS).

$$CO + H_2O \leftrightarrow CO_2 + H_2 \qquad \Delta_{rxn}H_{298K} = -41 \text{ kJ/mol} \qquad \text{Eqn 2.13}$$

HTS is used for 'bulk' conversion of CO. Relatively higher temperatures are used for HTS in order to obtain faster reaction rates and consequently reduce the reactor size. However, due to equilibrium limitations, 'deep' conversion of CO cannot be achieved at high temperatures. Hence a LTS is used to achieve low CO concentrations. According to Meshkani and Rezaei (2015), HTS operates at 375 - 450°C and Fe-Cr-Cu based catalysts are used. Typically, HTS achieve ~ 3 vol% CO. On the other hand, LTS operates at 200 - 300°C and uses Cu-Zn-Al based catalysts. LTS reduce CO levels to ~ 0.1 vol%. If the feed fuel contains sulphur a ZnO 'guard' bed is typically used to adsorb sulphur as sulphur poisons Cu based catalysts (Smith *et al*., 2010).

Preferential Oxidation:

As already discussed, WGS can only achieve at best ~ 0.1 vol% CO due to thermodynamic limitations. On the other side, PEMFC requires a H_2-rich gas with less than 10 ppm of CO (Kim *et al*., 2009). Preferential oxidation (PrOx) is one of the methods that can be used to

achieve such low CO concentrations. As shown by Eqn 2.14, PrOx is the oxidation of CO and is a highly exothermic reaction.

$CO + 0.5\ O_2 \leftrightarrow CO_2$ $\Delta_{rxn}H_{298K} = -283$ kJ/mol Eqn 2.14

Mainly, noble metal based catalysts (i.e. supported Pt, Pd, Ru, Rh) are used for PrOx. As reported in the review on "Preferential Oxidation of Carbon Monoxide", conducted by Mishra and Prasad (2011), gold based and base metal oxide based catalysts (typically CuO-CeO_2) can be used. Base metal oxides based catalysts are economically attractive compared to noble metals. Due to high activities of the catalysts, PrOx can be carried out at low temperatures (80 - 177°C). Low temperature operation makes PrOx attractive for PEMFC, however, the narrow operation temperature range combined with the strong exothermic reaction is the downside of PrOX.

During PrOx other side reactions can take place such as the combustion of H_2 (Eqn 2.15), CO methanation (Eqn 2.16), CO_2 methanation (Eqn 2.17) and WGS (Eqn 2.13). It is therefore crucial that a catalyst is selective i.e. can eliminate or at least minimize side reactions, especially H_2 combustion and CO_2 methanation as these reactions results in H_2 consumption and do not consume CO.

$H_2 + 0.5\ O_2 \leftrightarrow H_2O$ $\Delta_{rxn}H_{298K} = -242$ kJ/mol Eqn 2.15

Selective Methanation:

Selective methanation (SelMeth) is an alternative CO removal method to PrOx. SelMeth is the hydrogenation of CO and is highly exothermic (see Eqn 2.16). Typically, noble metal based catalysts are used for SelMeth (Mishra and Prasad, 2011). Unlike PrOx, SelMeth does not require the addition of O_2 or air and thus can achieve relatively high H_2-rich gas.

$CO + 3\ H_2 \leftrightarrow CH_4 + H_2O$ $\Delta_{rxn}H_{298K} = -205$ kJ/mol Eqn 2.16

Unfortunately, the undesired reaction i.e. CO_2 methanation (Eqn 2.17), often occur along with CO methanation (Eqn 2.16), hence high catalyst selectivity is important. WGS (Eqn 2.13) is another potential side reaction during SelMeth.

$CO_2 + 4\ H_2 \leftrightarrow CH_4 + 2H_2O$ $\Delta_{rxn}H_{298K} = -165$ kJ/mol Eqn 2.17

2.4. Methanol Steam Reforming

Methanol steam reforming has received serious consideration over the past decade as a promising fuel processing option for the production of H_2 for PEMFCs (Mateos-Pedrero *et al*., 2015). This is because methanol has several advantages when compared to other fuels i.e. it is obtained sulphur-free, it is a hydrogen dense fuel (H/C = 4) and therefore produces a hydrogen-rich gas upon reforming, and can be reformed at low temperatures (200 - 300°C) compared to LPG, diesel, methane and ethanol. Moreover, methanol exists as liquid at ambient conditions and thus can be easily handled, distributed and stored (Sá *et al*., 2010; Chin *et al*., 2002). The challenge is that methanol is typically produced using syngas derived from fossil fuels such as natural gas and coal which result in emission of CO_2. However, although currently not economic feasible, the renewable source, biomass, is a considered future feedstock for the production of methanol (Shabangu *et al*., 2014; Martin and Wörner, 2011; Balat and Kırtay, 2010).

According to literature, methanol steam reforming takes place according to the following chemical equation (Eqn 2.18, SRM);

$$CH_3OH + H_2O \leftrightarrow CO_2 + 3H_2 \qquad \Delta_{rxn}H_{298K} = 49.7\ kJ/mol \qquad \text{Eqn 2.18}$$

However, there are also two side reactions that take place during methanol steam reforming i.e. methanol decomposition (MD) (Eqn 2.19) and water-gas shift (WGS) (Eqn 2.20) (Ghasemzadeh *et al*., 2015).

$$CH_3OH \leftrightarrow CO + 2H_2 \qquad \Delta_{rxn}H_{298K} = 90.2\ kJ/mol \qquad \text{Eqn 2.19}$$

$$CO + H_2O \leftrightarrow CO_2 + 2H_2 \qquad \Delta_{rxn}H_{298K} = -41.2\ kJ/mol \qquad \text{Eqn 2.20}$$

Due to the endothermicity of the SRM reaction, methanol steam reforming requires an external heat source in order to raise reaction temperature. However, as shown in Figure 2-5, elevated temperatures are also problematic in that they lead to high concentrations of CO in the reformate. This is due to high reaction rates at high temperatures of the endothermic reactions i.e. MD and reverse WGS reactions. Hence active catalysts are required so as to obtain high conversions at relatively low temperatures (ca. <= 250°C). In addition, low temperature reforming will reduce heat management challenges for an integrated fuel processor-fuel cell since PEMFC operates at relatively low temperatures (~ 60 – 120°C).

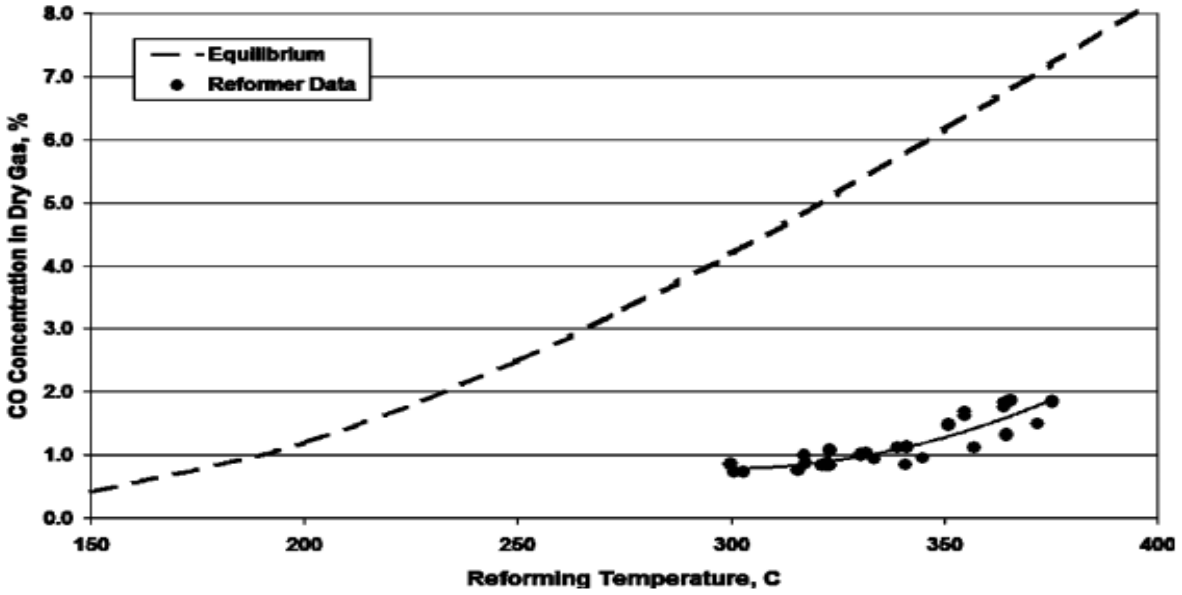

Figure 2-5: CO concentration in dry reformate as function of reaction temperature (after Dagle and Holladay, 2007)

Typically, the feed is set such that water to methanol molar ratio is close to the stoichiometric amount (~ 1-1.5) so as to minimize energy required to heat the reaction mixture and also to reduce the size of the reformer. A higher steam to carbon ratio results in less CO concentrations in the reformate due to abundance of steam for WGS reaction, however, this comes at the expense having high reactor load (i.e. heat duty) and a larger reformer. Thus optimization is required.

2.5. Typical Catalysts for Methanol Steam Reforming

Methanol steam reforming is a catalysed reaction and catalyst development plays a significant role in improving efficiency or performance of a reformer and consequently efficiency of a reformer-fuel cell integrated system. This section provides a literature review on catalysts typically used for methanol steam reforming i.e. Cu-based and Pd-based, and PdZn-based catalysts in sections 2.5.1 and 2.5.2, respectively.

2.5.1. Cu-based and Pd-based catalysts

The preferred products of methanol steam reforming are H_2 and CO_2. However, side reactions i.e. MD (Eqn 2.19) and reverse WGS (Eqn 2.20) as mentioned in the previous sections (i.e. sections 2.3.1 and 2.4), lead to formation of CO. Thus in addition to high activity (i.e. high H_2 production), it is crucial that a catalyst has a high selectivity towards CO_2. This is because low temperature PEMFCs can tolerate low concentrations of

CO (~ 10 ppm) due to poisoning effect or strong adsorption of CO on the anode catalyst (typically Pt-based) of the fuel cell which eventually leads to the deterioration of the cell performance (Nepel *et al*., 2013; Takeguchi *et al*., 2012).

Typical catalysts for methanol steam reforming are divided into two main categories i.e. Cu-based and Pd-based catalysts (Mateos-Pedrero *et al*., 2015). The review of the catalysts used for methanol steam reforming conducted by (Sá *et al*., 2010) shows that Cu-based catalysts are the most studied. This is due to the fact that Cu-based catalysts are cheaper and exhibit high activity (i.e. H_2 production) and selectivity towards CO_2 compared to group 8-10 metal-based catalysts. The most studied Cu-based catalyst is a family of $Cu/ZnO/ZrO_2/Al_2O_3$ catalysts which includes Cu/ZnO, Cu/ZrO_2, Cu/Al_2O_3, $Cu/ZnO/Al_2O_3$ etc. However, the use of Cu-based catalysts for methanol steam reforming has some downsides in that Cu-based catalysts are thermal unstable as the metal, Cu, suffer from sintering at high temperatures (> 250°C) (Zhang and Farrauto, 2011). This is important to consider as high temperatures might be required in the reformer so as to drive the endothermic methanol steam reforming reaction. In addition, Cu is pyrophoric (i.e. can ignite spontaneously when exposed to air) (Wang *et al*., 2014). This makes Cu-based catalysts unattractive especially for portable power and on-board fuel cell applications. In addition to thermal instability and pyrophoricity, according to (Ilinich *et al*., 2008), Cu-based catalysts also deactivates when exposed to condensing steam due to loss of mechanical integrity.

On the other hand, group 8-10 metal-based catalysts (including Pd-based ones) are stable in the typical methanol steam reforming conditions (i.e 200 - 300°C, 1 bar). However, the summary of studies in the review by (Sá *et al*., 2010) shows that Pd-based catalysts exhibits poor selectivity towards CO_2 compared to Cu-based ones, for instance, the catalysts i.e. unsupported Pd, Pd/SiO_2, Pd/Al_2O_3, Pd/La_2O_3, Pd/Nd_2O_3, Pd/Nb_2O_5, Pd/MgO, Pd/A.C. and Pd/Ta_2O_5 exhibited low CO_2 selectivities (< 10%). This makes Pd-based catalysts unattractive for methanol steam reforming.

2.5.2. PdZn catalysts

As already mentioned in section 2.5.1, Cu-based catalysts exhibit high activity (i.e. high H_2 production) and high selectivity towards CO_2, however, they are thermal unstable at high temperatures (> 250°C), sensitive to air and condensing steam. Although Pd-based catalysts are stable in the typical methanol steam reforming temperature range (200-300°C), they

also have a drawback in that they exhibit low selectivity towards CO_2. Recent literature reports an extensive research and development of PdZn catalysts because they exhibit comparable activity and selectivity as Cu-based ones and are thermally stable in the typical steam reforming conditions (Sá *et al*., 2010; Ilinich *et al*., 2008).

Pd when supported on metal oxides which are hard to reduce such as Al_2O_3, SiO_2, CeO_2, ZrO_2, La_2O_3 and Nb_2O_5 exhibit low selectivity towards CO_2 due to predominance of MD reaction (Eqn 2.19). Most literature attributes high CO_2 selectivity of Pd/ZnO catalysts to PdZn alloy which is formed when the catalyst is reduced at high temperatures (> 250°C) (Friedrich *et al*., 2013; Huang *et al*., 2011; Sá *et al*., 2010).

Recently, Arroyo-Ramírez *et al*. (2014) compared the methanol steam reforming performance of Al_2O_3 and ZnO supported Pd catalysts prepared by impregnation. Both catalysts were 1 wt% Pd and were pre-treated in 5 vol% H_2 at 250°C. When the reaction temperature was increased from 180°C to 250°C, CH_3OH conversion also increased for both Pd/Al_2O_3 and Pd/ZnO catalysts i.e. 31% to 92% and 28% to 78%, respectively. On the hand, CO_2 selectivity for the Pd/Al_2O_3 catalyst remained almost constant with increase in temperature i.e. 5% to 2% at 180°C to 250°C. However, for Pd/ZnO catalyst CO_2 selectivity increased with increase in temperature i.e. 21% to 50% at 180 to 250°C. The relatively higher selectivity towards CO_2 on the part of Pd/ZnO was ascribed to the formation of PdZn alloy while poor selectivity on the part Pd/Al_2O_3 catalyst was understood to be due to the predominance of the MD reaction (Eqn 2.19) over metallic Pd.

Iwasa *et al*. (1995) also obtained similar trends (see Figure 2-6). They tested a 10 wt% Pd/ZnO prepared by impregnation. Prior to testing the catalyst was reduced in H_2 at a desired temperature, however, the reaction temperature was 230°C for all the tests. As shown in Figure 2-6, when the reduction temperature was increased from the reduction temperature of ~ 220°C to 510°C both CH_3OH conversion and CO_2 selectivity increased i.e. from 36% to 55% and 65% to 98%, respectively. The increase in CH_3OH conversion and CO_2 selectivity was attributed to the formation of PdZn alloy.

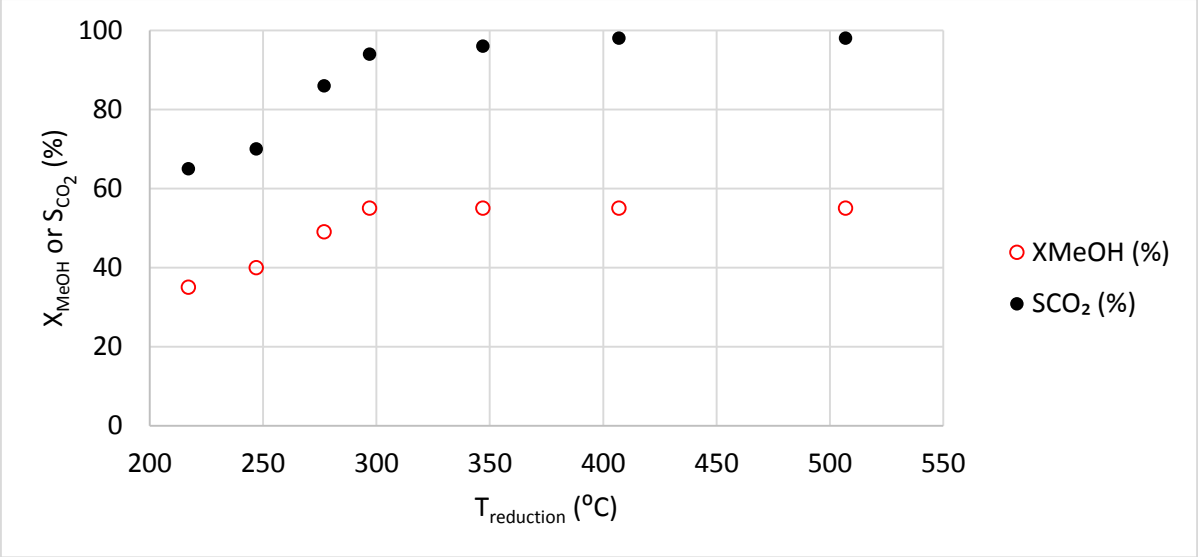

Figure 2-6: CH_3OH conversion and CO_2 selectivity over a 10 wt% Pd/ZnO catalyst reduced at different temperatures. S/C = 1, Feed diluent (N_2) = 80 vol%, T_{rxn} = 220 °C (after Iwasa *et al*., 1995).

Wang *et al*. (2006) studied a 15.9 wt% Pd/ZnO prepared by co-precipitation using characterisation techniques (including XRD, H_2-TPR and H_2-TPD) and proposed the following mechanism for the formation of the PdZn alloy:

PdO/ZnO → Pd/ZnO → $PdZnO_{1-x}$/ZnO → amorphous PdZn alloy/ZnO → crystallite PdZn alloy/ZnO

According to Wang *et al*. (2006), when the catalyst was treated in H_2 at elevated temperatures PdO was the first metal oxide to reduce. The hydrogen 'spill-over' from metallic Pd facilitated the reduction of ZnO in close vicinity to the metallic Pd. The XRD results suggest that an amorphous PdZn alloy was formed at first and eventually a crystallite PdZn alloy. However, the ZnO in the bulk remain unreduced. Although Iwasa *et al*. (2002) worked with slightly different catalysts, the H_2-TPR analysis suggests that the reduction mechanism proposed by Wang *et al*. (2006) is valid. Iwasa *et al*. (2002) conducted H_2-TPR experiments on Pd/ZnO/CeO_2 and Pd/ZnO/SiO_2 catalysts, both catalysts with a Pd loading of 10 wt% and a Pd to Zn atomic ratio of 1. Both catalysts exhibited a negative at ~ 40°C and two positive peaks at ~ 100°C and 450°C. The negative peak (~ 40°C) was ascribed to the decomposition of PdH_x. The low temperature and the high temperature positive peaks were understood to be due to the reduction of PdO and ZnO, respectively. However, the positive peaks for the Pd/ZnO/SiO_2 were relatively smaller and it was speculated that this is due to the effect of the support (i.e. SiO_2). The reduction of ZnO was understood to be facilitated by H_2 'spill-over' from the metallic Pd and that the reduction of ZnO is an indication that a

PdZn alloy was formed. A progressive formation of PdZn alloy (for a Pd/ZnO catalyst) with increase in reduction temperature was confirmed by the XRD studies.

Eswaramoorthi and Dalai (2009) characterised Pd-Zn/SBA-15 catalysts (prepared by impregnation of Pd and Zn on SBA-15). Five catalysts with a Pd loading of 0.5 to 5.5 wt% and a Zn to Pd mass ratio of 1.5 were characterised. The H_2-TPR analysis of the catalysts show a negative peak below 100°C and two positive peaks i.e. at 100-140°C and 300-400°C. The negative peak which occurred at low temperatures (< 100°C) was attributed to the decomposition of PdH_2 which formed in the presence of H_2. It was understood that a small fraction of PdO was reduced at room temperature, however, most of the Pd was reduced in the temperature range of 100°C - 140°C. The peak which occurred at the highest temperature (i.e. 300 - 400°C) was ascribed to reduction of ZnO and was understood to indicate formation of PdZn alloy. However, the negative peak which occurred at low temperature (i.e. < 100°C) was not observed by Chin *et al*. (2002) and Eblagon *et al*. (2014).

A surface sensitive technique, diffuse reflectance infrared fourier transform spectrometry (DRIFTS), was used by Gallagher *et al*. (2015) to characterise 2 wt% Pd - 12 wt% Zn/Al_2O_3 catalyst prepared by impregnation. The catalyst was reduced *in-situ* at different temperatures. DRIFTS spectra were taken at room temperature and CO was used as a probe molecule. The spectra for the catalyst show that CO was bound to surface Pd in two modes i.e. bridge and linear modes. For the bridge mode, one molecule of CO is bound onto two surface Pd sites. The band for this mode occurs in the region, 1800 - 2000 cm^{-1}. For the linear mode, one CO is bound onto one surface Pd site and the band for linear CO appears in the region, 2000 and 2200 cm^{-1}. It was noted that the ratio of linear to bridge bound CO increased with increase in reduction temperature i.e. 0.75 to 1.38 at 175 to 450°C (see Figure 2-7). This indicates that the surface of the catalyst was changing with increase in reduction temperature, in particular, relatively more linear CO sites were available at higher reduction temperature. The increase of linear to bridge sites with increase in reduction temperature was ascribed to the formation of PdZn alloy. It was understood that as the reduction temperature was increased more Zn was incorporated into the PdZn alloy structure thus reducing the ability of the surface to bound CO in a bridge fashion. On the contrary, the linear to bridge CO ratio was relativity low for the Pd/Al_2O_3 catalyst as there was no alloying even at a high reduction temperature (i.e. 450°C).

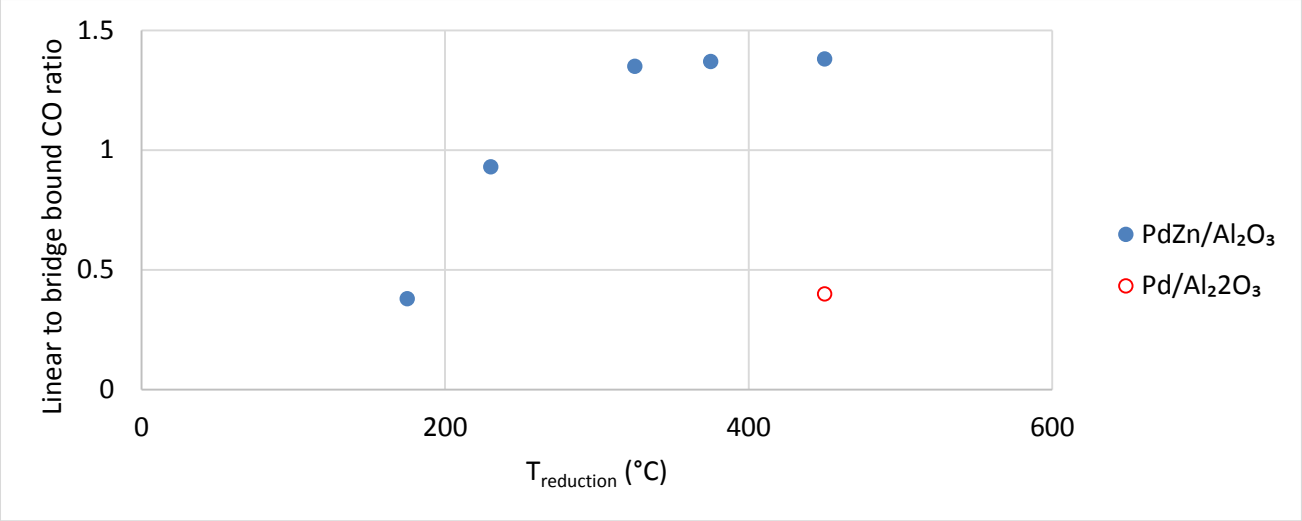

Figure 2-7: Effects of reduction temperature on linear to bridge bound CO (measured by DRIFTS) of 2 wt% Pd-12 wt% Zn/Al_2O_3 and Pd/Al_2O_3 catalysts (after gallagher *et al.*, 2015).

These results are in agreement with the work conducted by Föttinger (2013) on a 5 wt% Pd/ZnO catalyst prepared by impregnation. Upon reducing the catalysts at 30°C, the DRIFTS spectra exhibited two bands i.e. at ~ 1900 - 2000 cm^{-1} (attributed to bridge CO) and at ~ 2000 - 2100 cm^{-1} (attributed to linear CO). However, when the catalyst was reduced at 400°C the band attributed to bridge CO disappeared (refer to Figure 2-8). This was understood to be as a result of PdZn alloy formation. Long exposure (~ 1 hour) of the catalyst to pure CO resulted in re-appearance of the bridge CO band and decrease in the linear CO band. Thus it was understood that CO degrades the PdZn alloy structure. It was speculated that this is due to the strong Pd-CO bond which led to the enrichment of Pd on the surface. These results suggest that under methanol steam reforming conditions (where both CO and H_2 are formed) PdZn alloy is not stable as it would be degraded by CO while it is concurrently re-formed due to reduction of the catalyst in the presence of H_2.

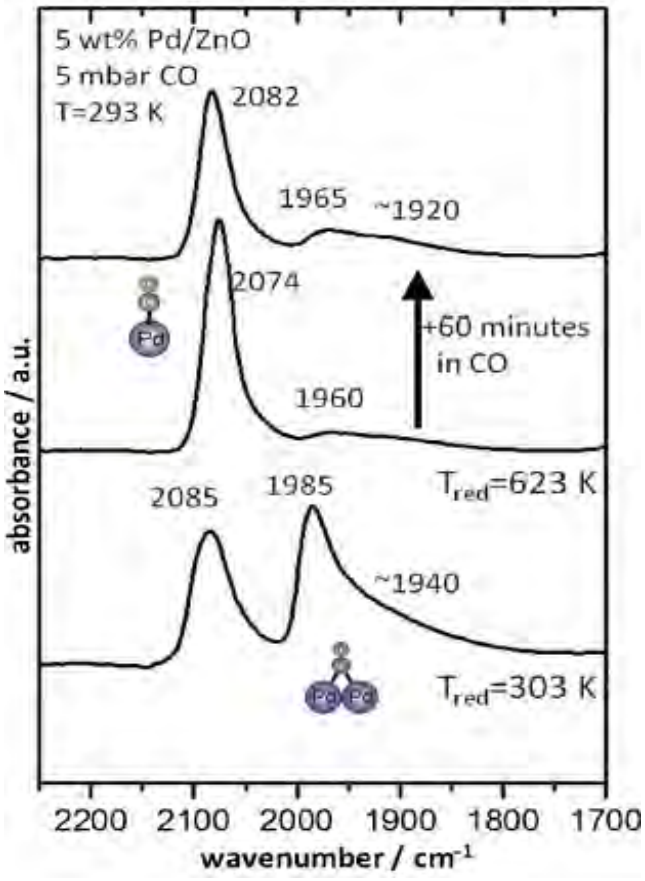

Figure 2-8: Effect of reduction temperature on CO adsorption for a 5 wt% Pd/ZnO (after Föttinger, 2013)

Bollmann *et al*. (2008) studied the effect of Zn addition on 2wt% Pd-x wt% Zn/Al_2O_3 catalysts (with x = 0, 2, 6, 10, 14, 19) for a WGS reaction. DRITFS spectra were taken under WGS reaction conditions (i.e. 280°C, 6.8% CO, 8.5% CO_2, 11% H_2O, and balance N_2). Similarly to the previous studies, linear CO and bridge CO bands were observed in the regions 2075 - 2000 cm^{-1} and 1980 -1880 cm^{-1}, respectively. Using the adsorption co-efficients for linear and bridge CO, the number of moles bound in linear and bridge modes were calculated. As shown in Figure 2-9, increase in Zn loading resulted in increase in the fraction of CO bound in linear mode.

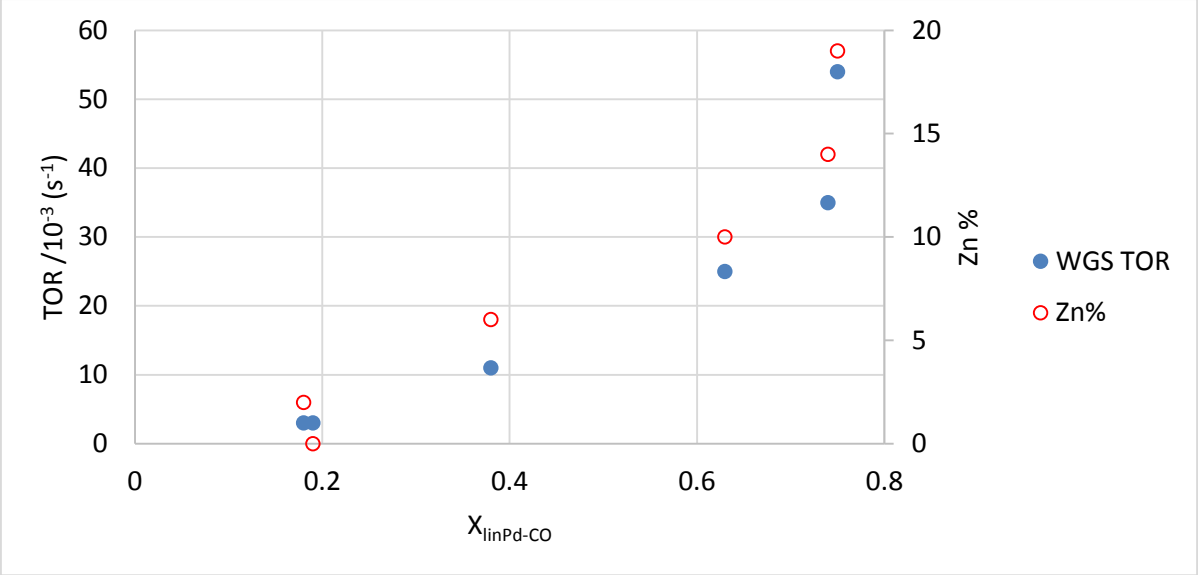

Figure 2-9: Effect of surface Pd that binds linear with CO on WGS TOR. Rates are expressed per exposed mol of Pd and measured under WGS reaction condition (280°C and 1 atm: 6.8% CO, 8.5% CO_2, 37% H_2O, balance Ar) (after Bollmann *et al.*, 2008)

Furthermore, increase in the fraction of linear CO lead to high turnover rates (TOR) for the WGS reaction i.e. 3 X 10^{-3} to 54 X 10^{-3} s^{-1} at 0.18 to 0.75. Thus it was understood that as more Zn is incorporated into the PdZn structure the surface changes such that more linear CO sites are formed as was also suggested by Gallagher *et al*. (2015). On the other hand, this work shows that the formation of PdZn alloy favours the WGS and further suggests that high selectivity towards CO_2 during methanol steam reforming on the part of PdZn catalysts is due to the formation of PdZn alloy.

While there are controversies in literature regarding reaction mechanism of methanol steam reforming it is generally agreed that there are three reactions that take place i.e. SRM (Eqn 2.18), MD (Eqn 2.19) and WGS (Eqn 2.20) (Sá *et al.*, 2010). In the case of PdZn catalysts, as already shown, most researchers attribute high selectivity towards CO_2 of PdZn catalysts to PdZn alloy which is formed upon reducing the PdZn catalysts at high temperatures. In addition, equilibrium effects can mask effects of reducing the catalysts.

Chapter 3 Objectives of the Study

3.1. Aims

The aims of this study are:

- To prepare ZnO supported Pd catalysts by incipient wetness impregnation and co-precipitation methods.
- To characterize the catalysts and to conduct performance tests of the catalysts for methanol steam reforming.

3.2. Objectives

The objectives of this study are:

- To investigate whether reduction of Pd/ZnO catalysts at high temperatures results in formation of PdZn alloy.
- To investigate whether 'PdO and ZnO' reduced catalysts have higher selectivities towards CO_2 compared to 'PdO only' reduced catalysts.

3.3. Hypothesis

Based on literature it is hypothesized that:

- An increase in reduction temperature of Pd/ZnO catalysts results in reduction of PdO to metallic Pd. A further increase in reduction temperature (below 600°C) results in reduction of ZnO in close vicinity to metallic Pd due to H_2 spill-over from metallic Pd. However, ZnO in the bulk remains unreduced below 600°C.
- The formation of PdZn alloy result in high selectivity towards CO_2 during methanol steam reforming.

3.4. Key Questions

The key questions are as follows:

- Does reduction of Pd/ZnO catalysts at high temperatures leads to formation of PdZn alloy?
- Does selectivity towards CO_2 increase with an increase in reduction temperature?

Chapter 4 Experimental Procedures

4.1. Catalyst Preparation

ZnO supported Pd catalysts were prepared via two methods i.e. incipient wetness impregnation and co-precipitation. The impregnation and co-precipitation methods are described in sections 4.1.1 and 4.1.2, respectively. Details for catalyst nomenclature are provided in section 4.1.3.

4.1.1. Incipient Wetness Impregnation Method

Firstly, the pore volume of the commercial ZnO support (99.999 wt%, Sigma-Aldrich) was determined and the support was found take up to 0.96 ml-water/g-support (refer to Appendix A.1). Figure 4-1 is a schematic representation of the catalyst preparation procedure.

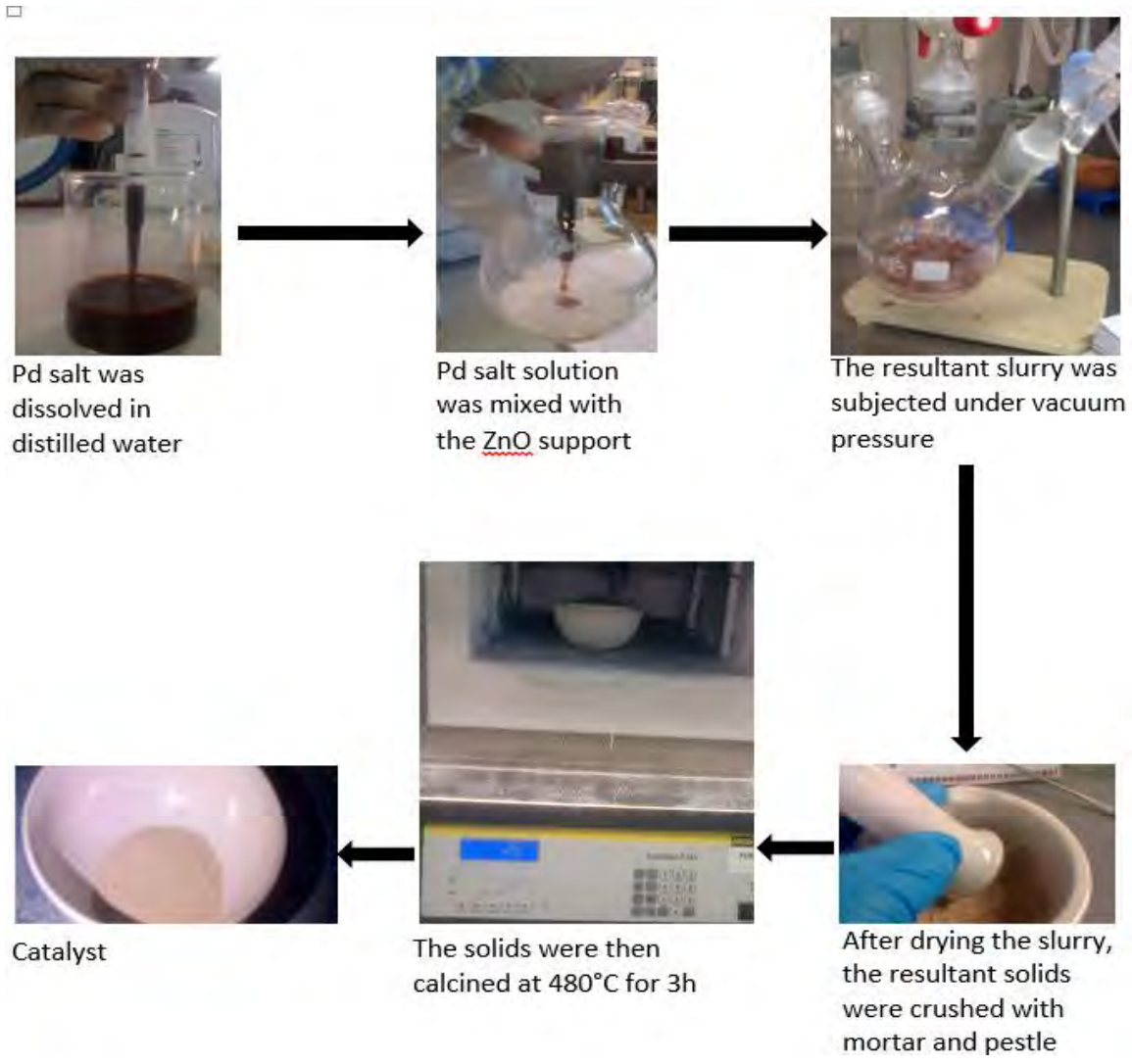

Figure 4-1: Catalyst preparation procedure: incipient wetness impregnation method

The Pd salt, $Pd(NO_3)_2.xH_2O$ (37.0-42.0 wt% Pd, Sigma-Aldrich) (1.8660 g) was dissolved in distilled water (26.6000 g). The Pd salt solution was introduced dropwise into the ZnO support (28.0300 g). Using a vacuum pump, a resultant slurry was subjected under vacuum (~ - 90 kPa) for 10 minutes to ensure that precursor solution got into the pores of the support. The slurry was then subjected under ultrasonic sound for 10 minutes while it was still under vacuum. This was done so as to facilitate mixing or homogeneity. The sample was then dried, firstly, at 60°C for 3 hours, and then at 120°C for 20 hours. The resultant solids were crushed with mortar and pestle and then calcined as follows: heat from room temperature to 480°C at a heating rate of 5°C/min, hold the temperature at 480°C for 3 hours, and then cool the solids back to room temperature. During calcination ZnO support remained unchanged while $Pd(NO_3)_2$ was decomposed to PdO (see Eqn 4.1).

$$Pd(NO_3)_2 \rightarrow PdO \qquad \text{Eqn 4.1}$$

Note: The catalyst was aimed at 2.5 wt% Pd on ZnO support. Amounts of materials used to prepare a duplicate catalyst are provided in Appendices A.2.

4.1.2. Co-precipitation Method

The Pd salt, $Pd(NO_3)_2.xH_2O$ (supplied by Sigma-Aldrich) 1.0000g (Pd eq. 0.42 g, 3.95 mmol) and the zinc salt, $Zn(NO_3)_2.6H_2O$ (also supplied by Sigma-Aldrich) 49.39 g (Zn eq. 10.86 g, 166.04 mmol) were dissolved in 30 ml of distilled water. Using a magnetic stirrer the solution was stirred for 10 minutes, after which the pH was 0.65. While still stirring the solution, aqueous NH_4OH (70.19 ml, 5 M) was added drop-wise to the solution. Aqueous NH_4OH was used to adjust the pH of the mixture in order to precipitate metal hydroxides, i.e. $Pd(OH)_2$ and $Zn(OH)_2$. The precipitation reactions proceed as per Eqn 4.2 and Eqn 4.3 and the amount of NH_4OH added was 3 mol% more than stoichiometric amount.

$$Pd(NO_3)_2 + 2NH_4OH \rightarrow Pd(OH)_2 + 2NH_4NO_3 \qquad \text{Eqn 4.2}$$

$$Zn(NO_3)_2 + 2NH_4OH \rightarrow Zn(OH)_2 + 2NH_4NO_3 \qquad \text{Eqn 4.3}$$

After adding NH_4OH (70.19 ml, 5 M), the pH of the mixture was 7.10. The mixture was then stirred for a further 1.5 hours after which the pH was 6.85. The mixture was then suction filtered and the precipitates were washed with small amount of distilled water (~ 20 ml). The slurry was dried firstly at 60°C for an hour, and then at 120°C for 16 hours. The resultant

solids were crushed with mortar and pestle and then calcined as per impregnation method (refer to section 4.1.1). During the calcination the metal hydroxides decompose to their respective metal oxides as shown in Eqn 4.4 and Eqn 4.5.

$$Pd(OH)_2 \rightarrow PdO \qquad \text{Eqn 4.4}$$

$$Zn(OH)_2 \rightarrow ZnO \qquad \text{Eqn 4.5}$$

4.1.3. Catalyst Nomenclature

The catalyst or test nomenclature indicates catalyst preparation method, pre-testing reduction temperature, and a reaction temperature (refer to Figure 4-2).

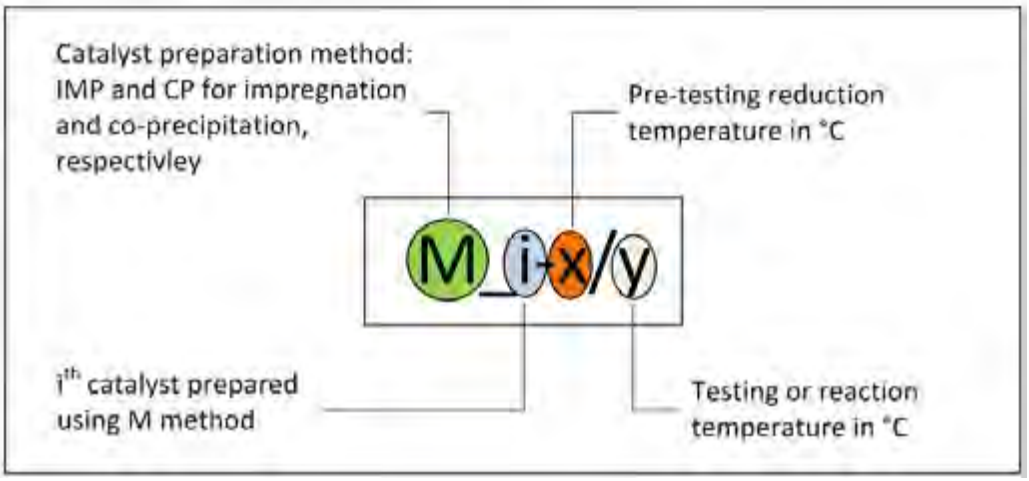

Figure 4-2: A catalyst nomenclature and its description.

For instance, IMP_1-200/180 means that a catalyst was prepared via incipient wetness impregnation method (described section 4.1.1), then treated with 10 vol% H_2/Ar at 200°C and subsequently tested at a reaction temperature of 180°C. The impregnation and co-precipitation catalysts 'as prepared' are referred to as IMP and CP, respectively.

4.2. Catalyst Characterisation

Catalysts were characterised using the following techniques; inductively coupled plasma-optical emission spectroscopy (ICP-OES), temperature programmed reduction (H_2-TPR), Brunauer-Emmett-Teller surface area (BET) and transmission electron microscopy (TEM) and thermogravimetric analysis (TGA).

4.2.1. Inductively Coupled Plasma-Optical Emission Spectroscopy

Elemental analysis of catalysts, with Pd and Zn being elements of interest, was performed using a Varian 730 ICP-OES spectrometer (supplied by Varian Inc.). Prior to the analysis the solid samples were digested in aqua regia, a mixture of hydrochloric and nitric acid.

4.2.2. Temperature Programed Reduction

H_2-TPR experiments were conducted using a AutoChem 2950 instrument (supplied by Micromeritics). A sample was placed in a (quartz glass) U-tube as shown Figure 4-3. Quartz wool was packed downstream the sample to prevent the sample from being carried away by a gas stream.

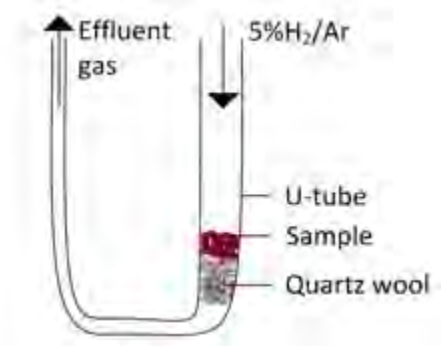

Figure 4-3: Sample loading on a U-tube quartz glass, and gas flow during H_2-TPR experiment

The (glass) U-tube was placed in a furnace of the AutoChem instrument and was connected to a gas line. A mass flow controller was used to control gas flowrate through the gas line. H_2-TPR experiment consisted of mainly three stages, i.e. sample drying, analysis, and cooling. During the drying stage, the sample was dried under Ar flow (10 ml/min) at 120°C for one hour. The sample was then cooled to 60°C while still under Ar flow. During the analysis stage, the sample was ramped at 10°C/min up to 600°C under H_2 flow (5 vol% H_2/Ar) at 50 ml/min.

Typically, metals are not reduced at low temperatures, however, as a sample temperature increases H_2 starts to react with the metal atoms (M) in the sample. The following chemical reaction (Eqn 4.6) is a general reduction reaction;

$$MO_{X(s)} + H_{2(g)} \rightarrow M^0_{(s)} + H_2O_{(g)} \qquad \text{Eqn 4.6}$$

The composition of the tube effluent gas is the same as that of the inlet gas when there is no reduction taking place, however, the composition differs when reduction reaction occurs since H_2 is consumed. A thermal conductivity detector (TCD) was used to determine the amount of H_2 consumed by measuring the difference in thermal conductivity of the inlet and effluent stream. Figure 4-4 is a typical H_2-TPR profile;

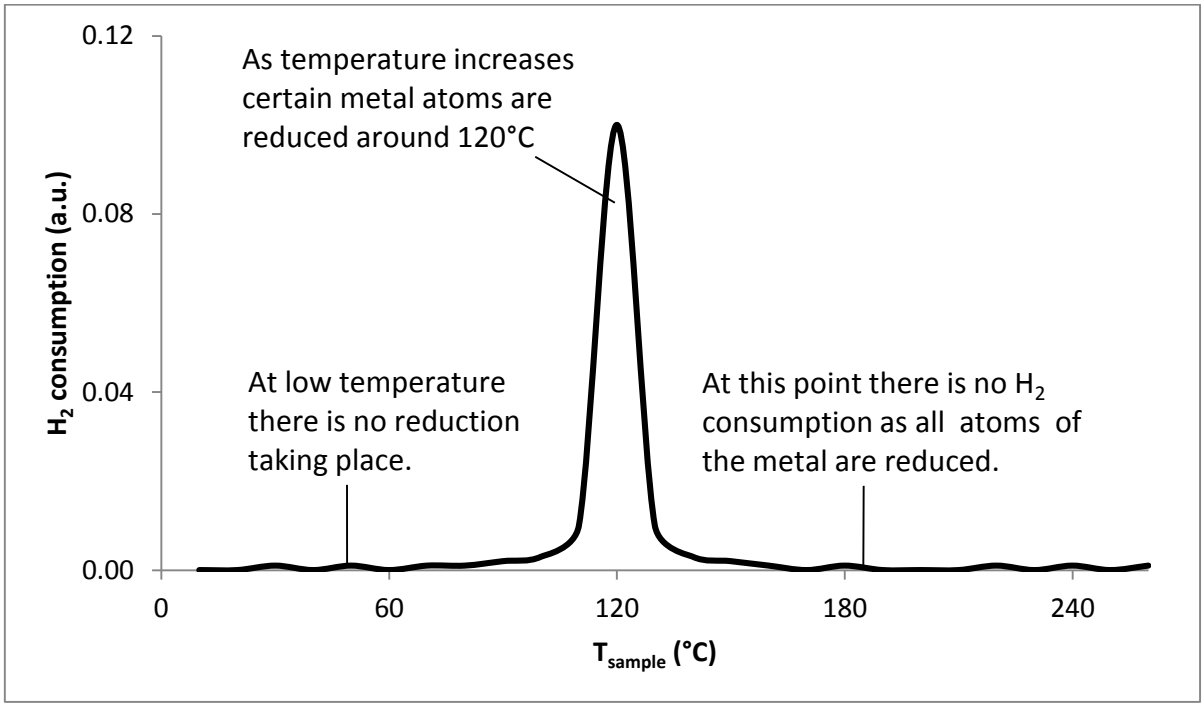

Figure 4-4: A typical H_2-TPR profile

Water produced during reduction was 'cold trapped' before the effluent gas reached the TCD detector. The cold trap, operating at approximately 0°C, ensured that the detector was not damaged by water. It also minimizes the error due to changes in conductivity contributed by water.

4.2.3. Brunauer-Emett-Teller Surface Area

BET surface area analyses of powder samples were determined by using an ASAP 2020 instrument (supplied by Micromeritics). The standard N_2 absorption method was used.

4.2.4. Transmission Electron Microscopy

The images (nano-range) of powder samples were generated using the FEI Tecnai™ T20 transmission electron microscope (TEM) instrument. The instrument was equipped with an electron gun that can generate an electron beam of 80 to 200 kV. The images were analysed using ImageJ1 software so as to obtain crystallite size distribution.

4.2.5. Thermogravimetric Analysis

TGA analyses of powder samples were conducted using a TGA/SDTA 851^e instrument (supplied by Mettler Toledo Inc.). The instrument was equipped with an ultra-micro balance (maximal sample weight: 1 g; resolution: 1 µg). About 25 mg of a powder sample was loaded on the microbalance. The sample temperature was ramped at 10°C/min up to 800°C/min.

4.3. Fixed Bed Catalyst Testing Apparatus

4.3.1. Overview of the Testing Apparatus

Catalyst performance tests were performed using a stainless steel tubular packed bed reactor (length = 50 cm, I.D = 1.6 cm). Figure 4-5 is a simplified schematic diagram of the testing apparatus.

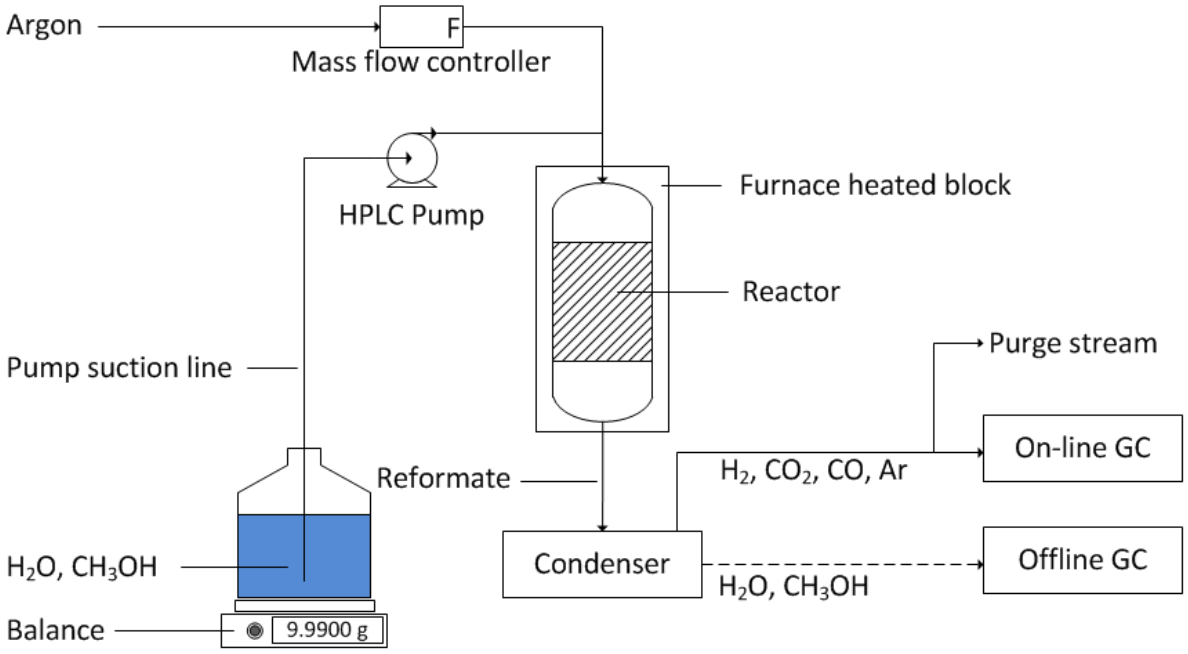

Figure 4-5: A simplified schematic diagram of the testing unit.

An HPLC pump was used to feed a water-methanol liquid mixture into the reactor. The feed bottle was placed on a balance so as to record the mass of liquid fed to the reactor over time. Also, Ar which was used as an internal standard was fed via a mass flow controller (MFC). A catalyst was placed in an isothermal zone of the reactor. The reaction temperature was controlled electronically by controlling the temperature of the furnace heated block surrounding the reactor. Unreacted CH_3OH and H_2O in the reactor effluent stream (i.e. reformate) was trapped in a condenser operating at ~ 3°C. After a time interval, Δt, the liquid was collected, weighed, and analysed by an off-line GC-FID. The gases which pass through the condenser were analysed by an online GC-TCD. The analyses of liquid and gases was done for the same time interval, Δt, so that CH_3OH conversion and CO_2 selectivity could be determined concurrently. Refer to Figure 4-6. for a detailed process flow diagram of the testing apparatus.

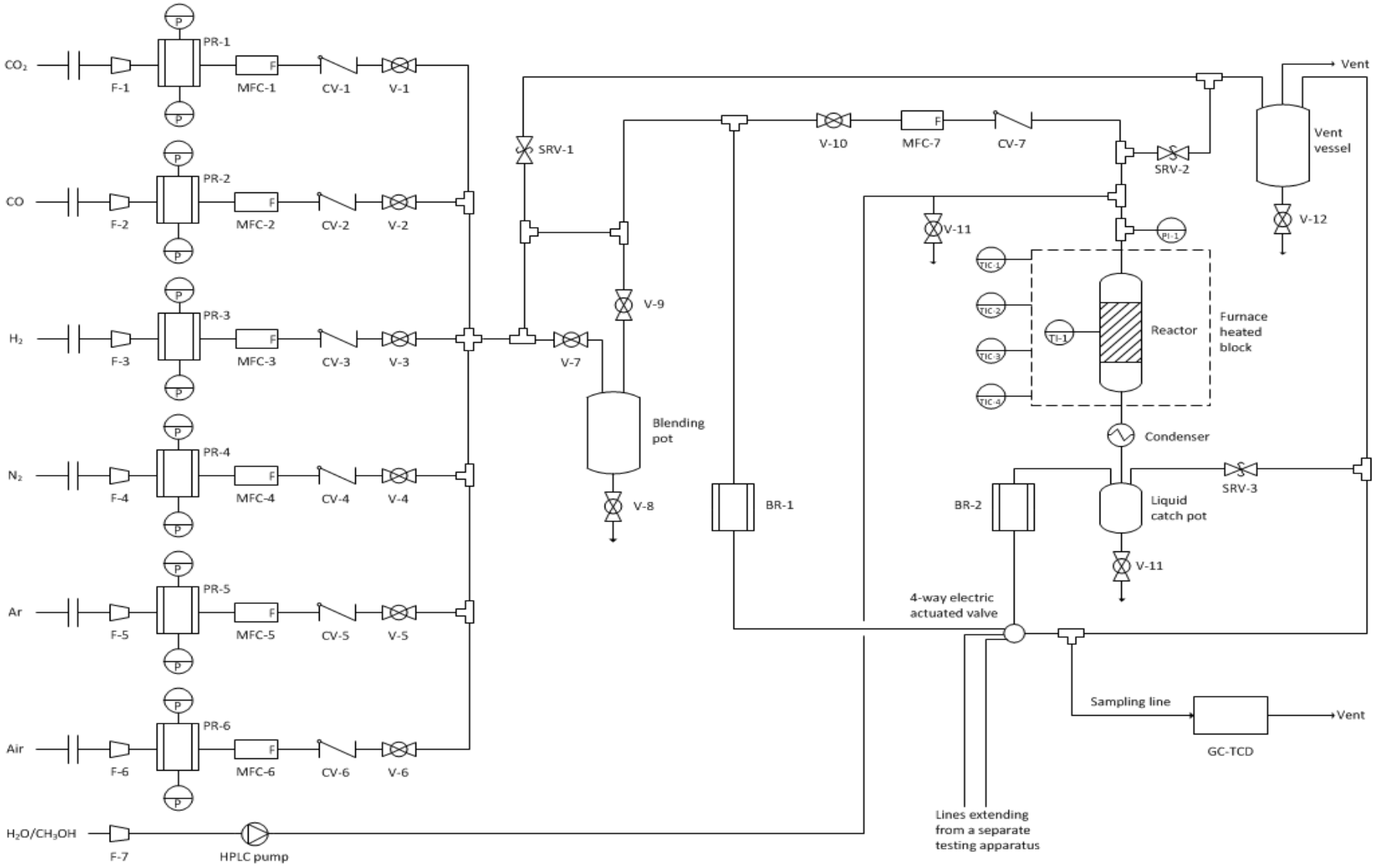

Figure 4-6: The process flow diagram of the testing apparatus

4.3.2. Sections of the Testing Apparatus

The testing apparatus consisted of three sections i.e. feed, reactor and reformate. Details for these sections are provided on sections 4.3.2.1, 4.3.2.2 and 4.3.2.3, respectively. Refer to the process flow diagram in Figure 4-6.

4.3.2.1. Feed Section

This section consisted of six mass flow controllers (MFCs) supplied by Brooks Instruments LLC. The MFCs were used to control flowrates of various gases from their respective sources. However, only four MFCs (i.e. CO_2, CO, H_2 and Ar) were used in this work. The gases, CO_2, CO, H_2 and Ar, were supplied by Afrox and were at least 99.7% pure. The gases were used for calibration and in addition Ar was used as an internal standard. Downstream of each MFC was fitted a filter (F) and a pressure regulator (PR). The aim of the filter was to prevent particles from entering the MFC while a PR was used to control the pressure downstream of MFC.

During methanol steam reforming, water-methanol liquid mixture was fed into a reactor by means of an HPLC pump (supplied by Scientific Systems, Inc.). The liquid feed was made of distilled H_2O and CH_3OH (LC-MS CHROMASOLV grade, >= 99.9% purity, supplied by Sigma-Aldrich). The liquid feed was such that molar steam to carbon ratio is approximately 1.1 (~ 60 wt% CH_3OH), unless stated otherwise. Argon which was used as an internal standard was fed into the reactor via MFC-5 (see Figure 4-6).

4.3.2.2. Reactor Section

The reaction temperature was controlled by controlling (electronically) the temperature of the furnace heated block which surrounded the reactor. This was achieved by using the temperature controllers, TIC-1, TIC-2, TIC-3 and TIC-4. The reactor was fitted with a thermo-well. Thus temperature at any position inside the reactor was monitored using a thermocouple which could be adjusted to be at any position in the thermo-well inside the reactor. A temperature profile and or isothermal zone inside the reactor was thus generated (see Figure 4-7). A spring loaded back pressure regulator (BR-2, see Figure 4-6) was used to hold the reactor and or system at a set pressure.

4.3.2.3. Reformate Section

In addition to Ar (used as an internal standard) and product gases (H_2, CO_2, CO), the reactor effluent stream also consisted of unreacted H_2O and CH_3OH in the vapour form. The vapour was condensed and trapped in a liquid catch pot. The liquid trapped in the catch pot was

collected by slowly opening valve, V-11, thus forcing liquid out. The liquid collected was weighed and analysed using off-line GC-FID (see section 4.5.2). A sample of the reformate gas was analysed by an on-line GC-TCD (see sections 4.5.1 and 4.5.3) while the rest of reformate gas was vented out of the system.

4.4. Catalyst Testing Procedure

4.4.1. Catalyst Loading

Catalyst testing was performed using a tubular stainless reactor (Length = 50 cm, I.D. = 1.6 cm) (Refer to Figure 4-7). Reactor loading was as follows;

i. Catalyst of the desired amount was mixed with 20 g of silicon carbide (SiC) with an average PSD of 300 μm before loading.
ii. The bottom half of the reactor was filled with SiC particles (with PSD ~ 300 μm). The reactor was then tapped so as to ensure that the SiC was tightly packed. This relatively fine SiC was used to ensure that a catalyst powder does not sieve down the reactor
iii. The catalyst mixed with SiC (as described in i.) was then loaded into the reactor (in isothermal zone). The isothermal zone was sufficiently long (> 20 cm) as can be seen in Figure 4-7 and catalyst bed was less than 7 cm for all tests conducted.
iv. A relatively coarser SiC (mean PSD ~ 1 mm) was then used to fill the top half of the reactor. This section of the reactor was where water-methanol liquid mixture evaporated before reaching the catalyst bed. The temperature increased from feed entrance until the isothermal zone. The coarser SiC ensured that liquid was not trapped at the reactor feed entrance (which was at relatively lower temperature) and thus resulting in a longer period of time before a steady state operation was reached.
v. To confirm that the system was leak-free, a leak tests was conducted before catalyst reduction or testing. This was done by pressurizing the system to 3 barg (under Ar gas), and monitoring pressure drop with time.

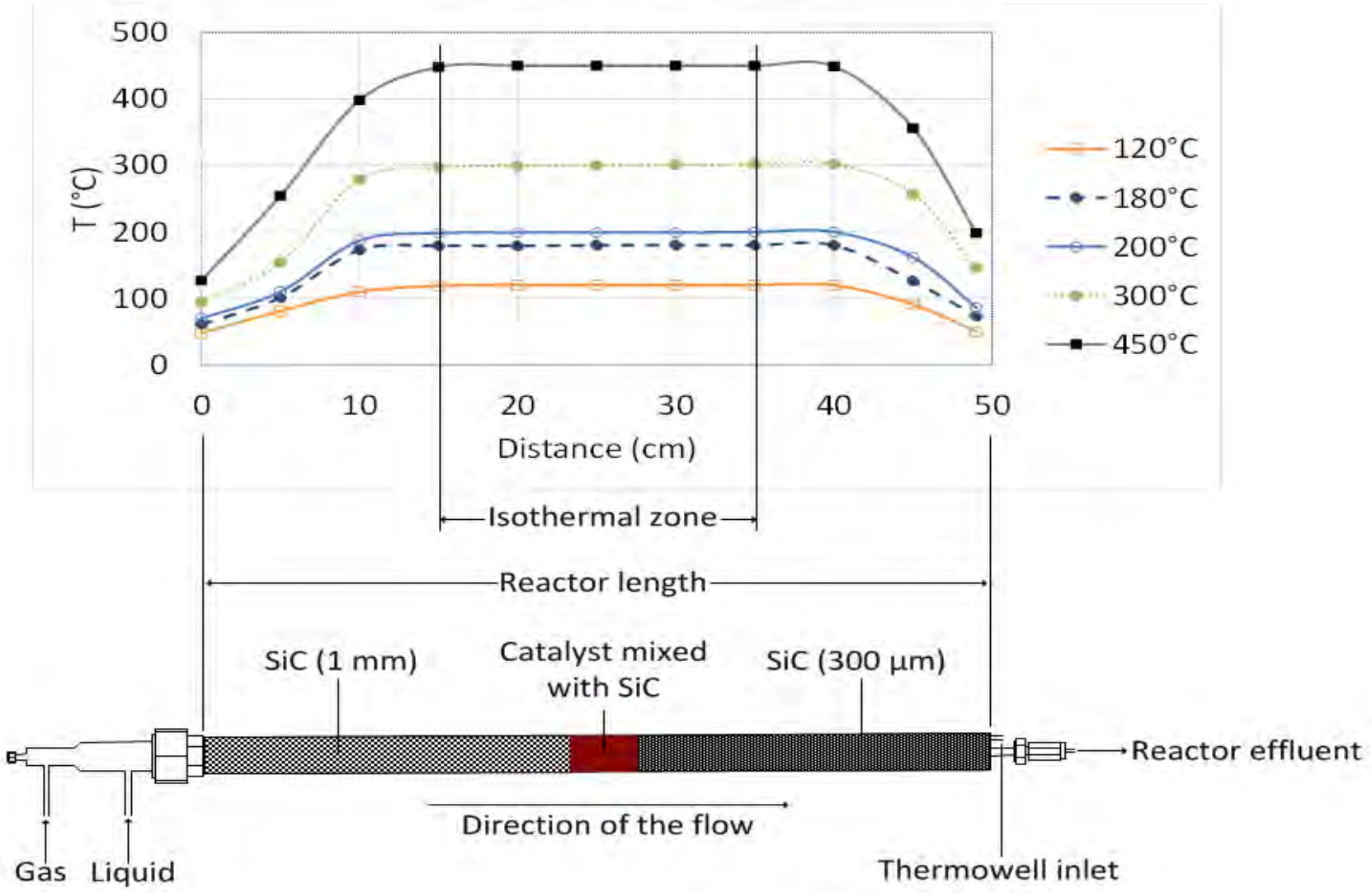

Figure 4-7: The schematic diagram of the reactor showing feed and effluent flows, catalyst position, and reactor isothermal zone

4.4.2. Catalyst Reduction

After catalyst loading (described in section 4.4.1), a catalyst was reduced at 1 barg in 10 vol% H_2/Ar at a desired temperature (here referred to as reduction temperature). The gas mixture, 10 vol% H_2/Ar, was achieved by controlling flowrates of H_2 and Ar via MFC-3 and MFC-5 (see Figure 4-6). The reactor temperature was ramped at 7°C/min up to the reduction temperature. The temperature was then held at the reduction temperature for two hours. The flow of H_2 was then stopped for at least 30 minutes while Ar was still flowing through the reactor (at 28 ml/min). Thus H_2 was purged out of the reactor before a catalyst performance test was conducted.

4.4.3. Catalyst Performance Test

All catalyst performance tests were conducted at 1 barg. Reactor feed was such that molar steam to carbon ratio was approximately 1.1 unless stated otherwise. The tests were conducted as follows;

Start-up stage:

i. Immediately after catalyst reduction (described in section 4.4.2) and when H_2 had been purged out of the reactor, the reactor temperature was ramped to the desired reaction temperature. (In special cases where the reaction temperature was higher than the reduction temperature, it was ensured that H_2 was purged out of the reactor before ramping the reactor temperature so as to avoid further reduction of a catalyst).
ii. When the desired reaction temperature was reached, water-methanol liquid mixture was fed into the reactor using the HPLC pump (see Figure 4-6). The feed bottle was placed on a balance and thus the mass of liquid pumped into the reactor was measured. Argon, which was used as an internal standard, was also fed into the reactor via the mass flow controller, MFC-5.
iii. When the feed was stable (~ 1 hour on stream depending on the feed rate) the catch pot was emptied by opening the valve, V-11.

Testing stage:

iv. After a time interval, Δt, unreacted water-methanol liquid was collected from the catch pot. This liquid was weighed and the mass was recorded. Also the mass of liquid pumped into the reactor during the same time interval, Δt, was recorded.

v. The liquid samples were analysed using a Varian 3900 GC (described in section 4.5.2) while reformate gases were analysed by an online Micro GC (described in section 4.5.3).

4.4.4. Reactor Shutdown Procedure

4.4.4.1. Normal Shutdown Procedure

A normal shutdown procedure of the testing apparatus was as follows (refer to Figure 4-6);

i. Set the HPLC pump flow to zero
ii. Turn off the pump
iii. Turn off the cooling bath (i.e. condenser)
iv. Turn off the heating block furnace supplying heat to the reactor
v. Pressurise the reactor system by feeding Ar.
vi. Empty the catch pot by slowly opening valve, V-11
vii. Set the gas mass flow controllers (MFC-1, MFC-2, MFC-3, MFC-4 and MFC-6) to zero
viii. Close the valves (V1, V2, V3, V4 and V6) downstream of their respective MFCs
ix. Close the main gas supply valves for all the gases (not necessary for short term shutdown)
x. Finally, when the reactor temperature is close to ambient temperature, set Ar flow (MFC-5) to zero and close V-5.

4.4.4.2. Emergency Shutdown Procedure

An emergency shutdown procedure of the testing apparatus was as follows;

i. Turn off the gas supply to the testing unit
ii. Turn off the pump
iii. Turn off the main switch (electricity supply) of the testing apparatus

4.5. Reformate Analysis and Data Work-up

This section provides details on sample analyses during and after catalyst performance tests. Section 4.5.1 provides an overview of reformate analysis. Unreacted water-methanol vapour in the reformate was condensed, collected and analysed using an off-line GC-FID system (described on section 4.5.2) while reformate gases were analysed using an on-line GC-TCD system (described in section 4.5.3).

4.5.1. Overview of Reformate Analysis

Reformate consisted of a gas (Ar, H_2, CO_2 and CO) and unreacted H_2O and CH_3OH in vapour form. Online GC columns operated below the boiling point of water (see Table 4-3) and therefore water vapour would condense in the columns, resulting in flooding which would render the columns inoperable. To avoid the flooding, water vapour was trapped in a condenser or catch pot (see Figure 4-6) operating at ~ 3°C. Unfortunately, CH_3OH also condensed upon condensing H_2O. Therefore in order to determine CH_3OH conversion liquid samples were collected from the condenser and analysed using an off-line GC-FID system (details in section 4.5.2).

The reformate gas, on the other hand, was analysed using an online GC-TCD system (details in section 4.5.3). The reformate gas line, extending from the condenser through the back pressure regulator (BPR-2) and 4-port valve to the online GC system, was kept at 55°C to avoid condensation of small amounts of water vapour still remaining. Once the gas reaches the sampling line, it was drawn by a vacuum pump to a sample-loop which is 10 µL. The rest of the reformate gas was vented out of the system. The sampling time was 30 ms. Thes stabilisation time (a time to allow a sample in the gas-loop to stabilise) was 30 ms. The gas sample in the sample-loop was pressurised until its pressure was the same as the column head pressure. It should be noted that this process was the same for the 3 channels (see Table 4-3) and that it was taking place simultaneously in the 3 channels. Sample pressurisation took 120 ms. The gas sample in the sample-loop was then transported by a carrier gas during injection step. The injection time was 40 ms for all the channels. The run time and or data acquisition started immediately after injection, and was 10 minutes. This run time was sufficient for analysis of all the gas components mentioned in Table 4-3.

The 4-port electric actuated valve (supplied by Valco Instruments Co. Inc.) was installed so as to allow analysis of multi-streams. The valve was used to select a gas line to be analysed

at a time since the GC-TCD system could not analyse more than one gas stream at a time. The gas lines that were connected to the 4-port valve and therefore could be used to analyse reactor feed ('by-pass'), reactor effluent gas, and two other lines extending from a separate testing apparatus (see Figure 4-6).

4.5.2. Off-line GC

4.5.2.1. Off-line GC-FID System

The off-line GC-FID system (i.e. Varian 3900 GC, autosampler, supplied by Varian Inc.) was used to analyse unreacted water-methanol liquid samples collected during catalyst performance tests. The system consisted of 3 main parts i.e. injector, column and a detector as shown in Figure 4-8. Samples prepared for analysis were automatically injected into the column as predefined by a method (see Table 4-1). A fused Capillary Column (supplied by Supelco, a member of the Sigma-Aldrich group) was used. This column is 30 m long with 0.25 mm i.d., and is coated with 0.25 µm fused silica.

Nitrogen was used as a carrier gas (mobile phase). The compounds in the sample interacted with the fused silica (stationery phase) as they flow with nitrogen through the column, and depending on their nature (i.e. polarity, mass and size), compounds spent different periods of time (here referred to as retention times) in the column, and thus were separated.

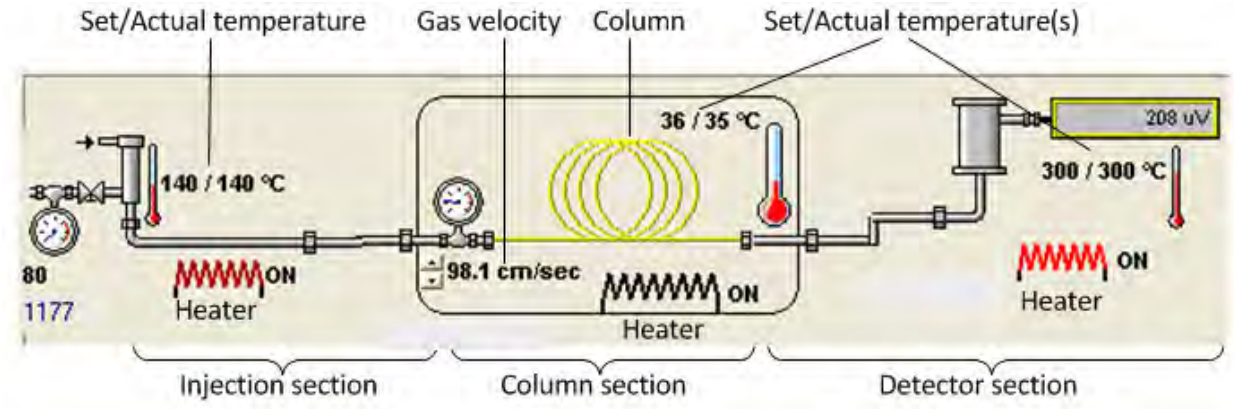

Figure 4-8: Varian 3900 GC system PC display

As gas exit the column it entered the Flame Ionization Detector (FID). Hydrogen (fuel gas) and air (oxidant) were mixed with eluent as shown in Figure 4-9. At the tip of the column, flame was ignited, and therefore organic eluent was combusted. Reduced carbon ions caused by combustion of an eluent were collected by collector plates. A sensitive ammeter

attached to the collector plates detected the ions hitting the plate. The signal was then sent to an amplifier, integrator, and finally to a display screen. The quantity of ions produced during combustion was proportional to the concentration of an eluent in the carrier gas and thus the concentration of an eluent could be determined.

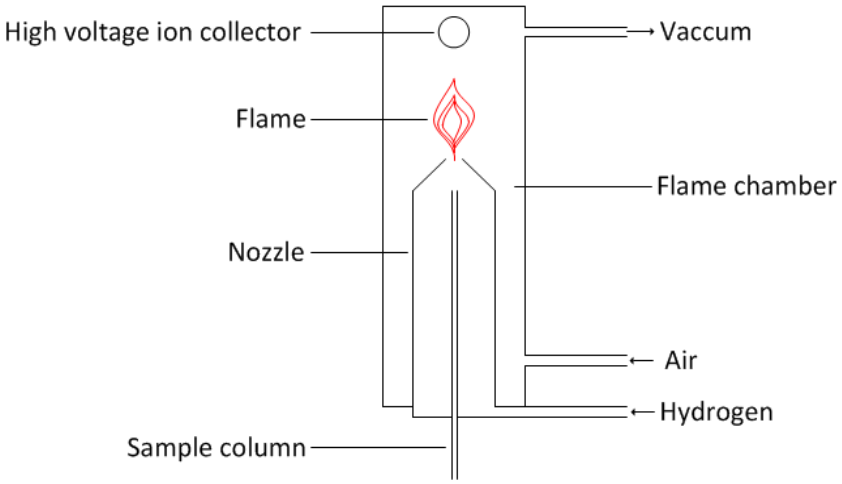

Figure 4-9: Schematic diagram of a typical Flame Ionization Detector (FID)

4.5.2.2. Peak Identification

The retention time of components were determined by analysing samples of single components. As an example, Figure 4-10 show a chromatogram of methanol (LC-MS CHROMASOLV grade, >= 99.9% purity). The details of sampling method used to obtain chromatograms are in section 4.5.2.3.

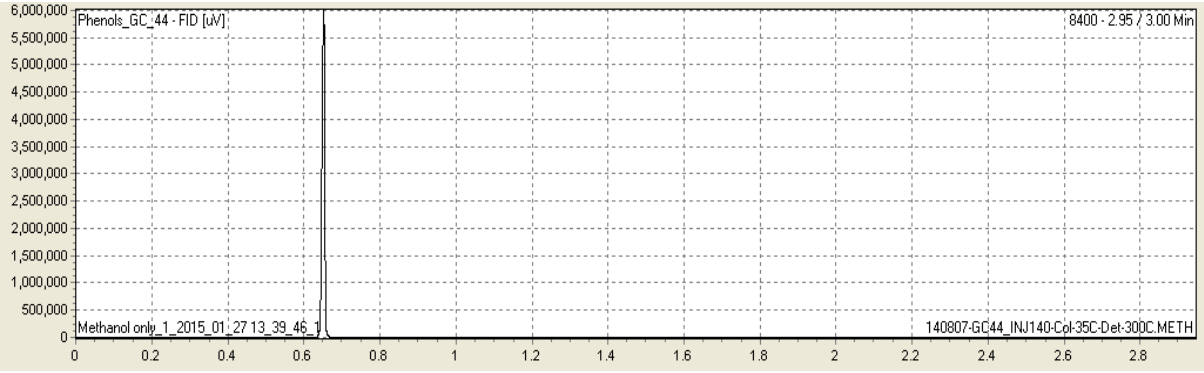

Figure 4-10: The chromatogram of pure methanol

Both acetone and ethanol were 99.9% pure and were supplied by Kimix. The retention times of the components of interest are summarised in Table 4-1.

Table 4-1: The retention times of components

Component	Acetone	Ethanol	Methanol
Retention time, min	0.77	0.73	0.64

4.5.2.3. Sampling Method

The off-line GC-FID system (Varian 3900 GC) is an autosampler/autoinjector GC. Sampling and injection procedure were programmed via the galaxie software (also supplied by Varian Inc.). Table 4-2 gives a summary of key variable inputs.

Table 4-2: The autosampler GC sampling method settings.

Category	**Sub-category**	**Settings**
Injection		
Injector cleaning	Fill volume	5 µL
	Draw-up speed	5 µL/s
	Strokes	1
	Cleaning solvent	Acetone
	Pre-injection solvent flushes	3
	Pre-injection sample flushes	2
	Post-injection solvent flushes	3
Injection (oven) temperature	-	140°C
Injection volume	-	0.2 µL
Split ratio = split vent flow/column flow	-	100
Column		
Column oven program	Heater mode	ON
	Column Temperature	35°C (kept constant)
Detector		
Detector temperature	-	300°C
Electronic Flow Control (EFC)	Nitrogen flow	25.0 ml/min
	H_2 flow	30.0 ml/min
	Air flow	300.0 ml/min

See Appendix D for the off-line GC-FID system calibration, sample preparation and CH_3OH conversion calculations.

4.5.3. Online GC

4.5.3.1. The Online GC-TCD System

A Micro GC system (CP-4900, supplied Varian, Inc.) was used to analyse the gas stream. The system comprised of 3 channels, each with a column and a TCD detector. The type of column installed on channels 1 and 2 was Molsieve 5Å, and 5CB on channel 3. Table 4-3 shows specifications and operating conditions of the 3 columns.

Table 4-3: Varian CP-4900 GC system column specifications and operating conditions

Category/Channel	1	2	3
Column type	Molsieve 5Å	Molsieve 5Å	5CB
Column length (m)	10	20	8
Injection temperature (°C)	55	55	50
Column temperature (°C)	50	50	40
Column pressure (kPa)	150	150	70
Detector type	TCD	TCD	TCD
Carrier gas	Ar	H_2	H_2
Gases analysed	H_2	Ar, CO, *CH_4	CO_2

*CH_4 was not detected in all the performance tests conducted

The Micro GC system was connected to a PC via galaxie software (also supplied by Varian Inc.). Via this interface the sampling method was programmed and data acquisition was performed. As shown in Table 4-3, each channel of the Micro GC was equipped with a TCD detector. A TCD detector uses a difference in thermal conductivity of a reference gas (pure carrier gas) and the carrier gas which transports the sample through the column. Hence a carrier gas for each channel was chosen such that there is a relatively higher difference in thermal conductivity between a carrier gas and a gas to be analysed in a respective column. The higher the concentration of an analyte in a carrier gas the higher the difference in thermal conductivity between the reference gas and a gas which transport the sample. Thus after calibrating the GC system a concentration of an analyte could be quantified.

4.5.3.2. Peak Identification

The retention times of components were determined in a similar way as was done for the off-line GC-FID, that is, by analysing samples of single components. The retention times of the components of interest are summarised in Table 4-4.

Table 4-4: The retention time of gas components in the respective channels

Gas analysed	Channel	Retention time (min)
H_2	1	0.56
Ar	2	0.91
CO	2	3.2
***CH_4**	2	2.21
CO_2	3	0.34

The calibration of the online GC-TCD and the calculation of selectivity towards CO_2 are provided in Appendix E.

Chapter 5 Results

This section reports on reproducibility of the experiments and results of the catalyst characterisations, equilibrium calculations and catalyst performance tests.

5.1. Reproducibility

For the impregnation catalyst in this work, weight loading of Pd on ZnO was aimed at 2.5 wt%. ICP-OES analysis of the impregnation catalyst, IMP_1, showed that the actual Pd loading was 2.8 wt% (see Table 5-2). This increase in Pd loading was due to the actual Pd content in the Pd salt being 42 wt% (see the TGA results in section 5.2.5), whereas 38 wt% Pd content of the salt was assumed for catalyst preparation (see Table A-2) . The assumption was based on the supplier specification, i.e. 37.0 - 42.0 wt% Pd. Likewise, when reproducing the impregnation catalyst, using the same preparation procedure, IMP_2 resulted in a similar Pd weight loading of 2.7 wt% (confirmed by ICP-OES). This shows that the impregnation method (described in section 4.1.1) is reproducible with a relative standard deviation 2.6% Pd loading.

The co-precipitation method (described in section 4.1.2) resulted in a Pd weight loading of 1.1 wt%, whereas the target Pd loading for the CP catalyst was 3.0 wt%. The significant loss of Pd was due to partial precipitation Pd and with the fraction which did not precipitated discarded during filtration. This unpredictable Pd loading in co-precipitation method makes it irreproducible.

During the catalyst activity (and selectivity) tests of methanol steam reforming, each condition was measured several times and the standard deviation was calculated. Table 5-1 shows the average conversion and the corresponding standard deviation per condition (refer to section 4.1.3 for details on test or catalyst nomenclature). These standard deviations (SD) are also expressed as a percentage of the average (i.e. relative standard deviation, RSD). As can be seen on Table 5-1, during the first ~ 50 hours on stream, RSD is higher and this was due to lining-in of the catalysts during this period. However, RSD was lower than 7% for all the tests after the catalyst line-in period.

Table 5-1: Relative standard deviations per condition for for the catalyst performance tests

Test Nomenclature	ToS (h)	GHSV (h^{-1})	X_{MeOH} (%)	SD (-)	RSD (%)
IMP_1-120/180	0 - 50	1100	16.1	2.9	17.8[a]
	120 - 160	1100	11.1	0.1	1.0
IMP_2-120/180	0 - 35	1060	12.8	1.7	13.0[b]
	35 - 121	240	24.7	1.4	5.5
	120 - 150	1060	12.0	0.5	3.9
IMP_1-200/180	0 - 50	1100	14.8	2.1	13.8[c]
IMP_1-450/180	90 - 150	1100	10.4	0.5	4.8
CP-250/225	0 - 60	920	36.2	1.6	4.5[d]
	60 - 121	480	46.5	0.7	1.5
	121 - 168	760	37.7	0.4	0.9
	168 - 218	920	29.3	0.8	2.6
CP-450/225	218 - 295	920	23.8	1.1	4.6
	295 - 360	410	36.5	0.8	2.3
	360 - 400	1270	16.4	0.5	2.9
	460 - 490	920	19.9	1.2	6.2

[a, b, c, d] RSD during catalyst line-in period

Catalyst IMP_2 was tested under similar conditions as per IMP_1 to calculate the overall reproducibility from catalyst preparation to testing. Both, IMP_1 and IMP_2, were reduced at 120°C and subsequently tested at 180°C and at a similar GHSV of 1100 and 1060 h^{-1}, respectively. Both catalysts showed similar trends during the first ~ 120 hours on stream where the catalysts slowly lined-in. During those times CH_3OH conversion decreased gradually from around 18% to approximately 10% hence a significant higher standard deviation (see Table 5-1). After the line-in period (~ 120 to 160 hours on stream) both catalysts were tested under similar conditions and the conversions for IMP_1 was 11.1 ± 1.0% (average conversion ± RSD). A similar conversion of 12.0 ± 3.9% was obtained for IMP_2 (refer to Table 5-1 and Figure 5-1).

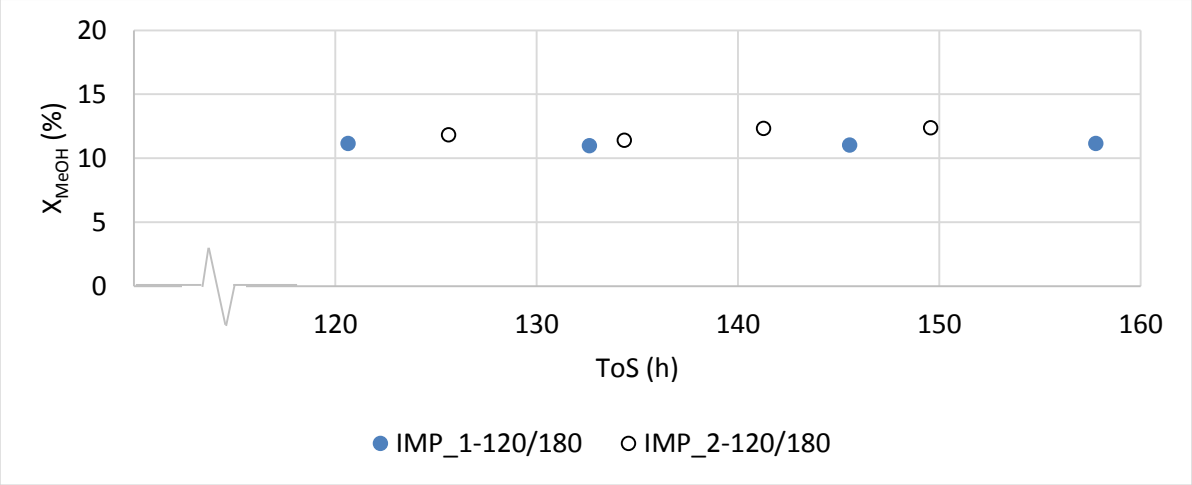

Figure 5-1: CH_3OH conversion as a function of time on stream for the catalysts IMP_1 and IMP_2 under similar conditions. $T_{reduction}$ = 120°C (in 10 vol% H_2/Ar for 2h), T_{rxn} = 180°C, S/C = 1.1, IMP_1 GHSV = 1100 h^{-1} and IMP_2 = 1060 h^{-1}, P=1 barg

The selectivities towards CO_2 were in both experiments > 99% and thus no standard deviation was calculated for this. The conversions reported throughout this thesis are expressed as the average conversion of the condition ± the relative standard deviation unless stated otherwise. For instance the conversion for the test IMP_1-120/180 from 120 to 160 hours on stream was 11.1 ± 1.0% (refer to Table 5-1 and Figure 5-1).

5.2. Catalyst Characterisation

To give a better understanding of the prepared catalysts, some characterisation techniques were used. The types of characterisation performed on the catalysts are inductively coupled plasma-optical emission spectroscopy (ICP-OES), temperature programmed reduction (TPR), Brunauer-Emmett-Teller surface area (BET), transmission electron microscope (TEM) and thermogravimetric analysis (TGA). Refer to section 4.2 for more details on the characterisation techniques and conditions at which the characterisations were conducted.

5.2.1. Inductively Coupled Plasma-Optical Emission Spectroscopy

Impregnation catalysts (i.e. IMP_1 and IMP_2) were aimed at 2.5 wt% metallic Pd on ZnO support. According to the ICP-OES results, Pd weight loadings of IMP_1 and IMP_2 were 2.8 and 2.7 wt%, respectively (see Table 5-2). The loadings were both similar and show that the incipient wetness impregnation method (described in section 4.1.1) was reproducible. However, the loadings were slightly higher than the aimed loading. This was due to underestimation of amount of Pd in the Pd salt used in the catalyst preparation. According to the supplier (Sigma-Aldrich) specifications, the Pd content of the salt is 37.0 - 42.0 wt%. For the catalyst incipient wetness impregnation it was assumed (see Appendix A.3) that the salt was 38 wt% Pd (within the specification range). However, the TGA results (discussed in section 5.2.5) shows that the Pd content of the salt is 42 wt%.

During the calcination step of the impregnation catalyst preparation (see section 4.1), $Pd(NO_3)_2$ was decomposed to PdO (see Eqn 4.1) while ZnO support remained unchanged. For the co-precipitation (CP) catalyst, during calcination the precipitates, i.e. $Pd(OH)_2$ and $Zn(OH)_2$, were decomposed to PdO and ZnO, respectively (see Eqn 4.2 and Eqn 4.3). Therefore for both impregnation and co-precipitation catalysts, Pd and Zn were present in the form of their respective oxides, i.e. PdO and ZnO, respectively. Knowing this, the Zn content of the catalysts was calculated based on the Pd loadings (i.e. ICP-OES results). The calculated Zn content of the catalysts (see Table 5-2) was close to the results obtained via ICP-OES analysis.

The intended Pd weight loading for CP catalyst was 3.0 wt%, however, according to the ICP-OES analysis the loading was only 1.1 wt% (see Table 5-2). This shows that the co-precipitation method (described in section 4.1.2) is not optimal, as much of the Pd will be wasted due to partial precipitation of Pd. For this reason, the method will not be

reproducible as the extent of precipitation of Pd will vary from one batch to another. In the case of the bulk Zn precipitation, the calculated Zn content of CP was similar to the one obtained by ICP-OES analysis.

Table 5-2: The ICP-OES analysis results of the catalyst

Catalyst	Pd (wt%)		Zn (wt%)	
	ICP-OES analysis	Aimed loading	ICP-OES results	Calculated content
IMP_1	2.8	2.5	78.9	77.7
IMP_2	2.7	2.5	77.3	77.8
CP	1.1	3.0	79.9	79.3

5.2.2. Temperature Programmed Reduction

H_2-TPR experiments of the three prepared catalysts, IMP_1, IMP_2 and CP, were conducted. As reference analyses, H_2-TPR experiments of an empty tube and pure ZnO (99.999 wt%, Sigma-Aldrich) were also conducted prior to that of each catalyst. During analysis, a sample was ramped at 10°C/min up to 600°C under H_2 flow (5 vol% H_2/Ar) at a flowrate of 50 ml/min. More details on the experiment are provided in section 4.2.2.

The TPR analysis of IMP_1 (see Figure 5-2) exhibits a sharp peak at 87°C. In addition, the analysis shows a second reduction which is much broader than the initial peak. The second peak starts around 260°C, and reaches its maximum at 348°C, ending around 385°C.

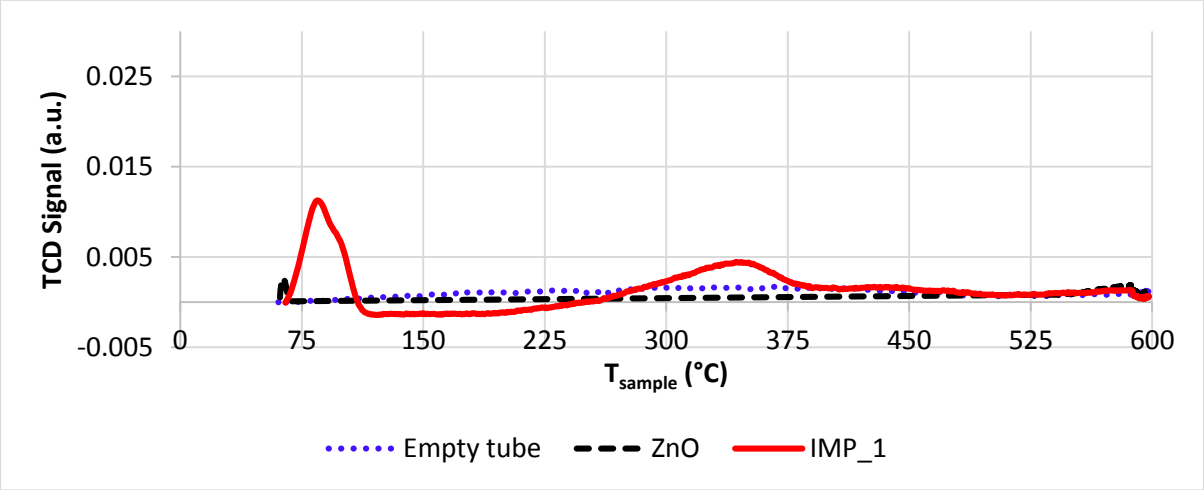

Figure 5-2: The TPR profiles of an empty tube, ZnO (99.999 wt%, Sigma-Aldrich), and IMP_1

A similar H_2-TPR analysis was obtained for IMP_2. The analysis of IMP_2 (see Figure 5-3) also exhibits a sharp peak with a maximum at 91°C. The second peak is broader and starts at a slightly lower temperature than IMP_1; around 243°C, reaching its maximum at 316°C, ending around 360°C.

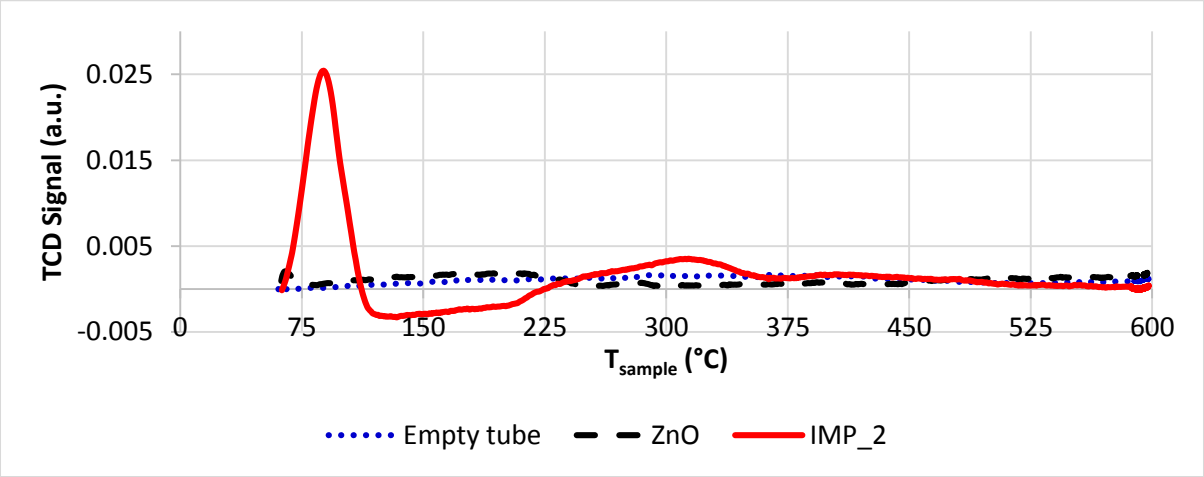

Figure 5-3: The TPR profiles of an empty tube, ZnO (99.999 wt%, Sigma-Aldrich), and IMP_2

Iwasa *et al*. (1995) obtained similar results when performing a H_2-TPR experiment over a 10 wt% Pd/ZnO catalyst prepared by impregnation. In their work the TPR profile shows a peak at 104°C and a relative larger and broader peak with a maximum at 425°C.

All the H_2-TPR analyses of an empty tube and pure ZnO do not show any peak below 600°C. As discussed in more details in section 6.4, for the impregnation catalysts, the peak which occurs at lower and higher temperatures are due to reduction of PdO and ZnO, respectively. The H_2-TPR analysis of ZnO shows that ZnO is not reduced in the absence of Pd. This proves that the reduction of ZnO in the case of IMP catalysts is facilitated by H_2 spill-over from metallic Pd.

It should be noted that the TPR analysis of ZnO and CP catalyst (see Figure 5-4) were obtained using a different TPR instrument than those reported in Figure 5-2 and Figure 5-3. The TPR profile of CP catalyst exhibits a sharp peak at 80°C. The peak is understood to be due to reduction of PdO. The apparent difference in reduction temperature of PdO for the CP and IMP catalysts is probably due to a systematic error (in gas flow and temperature calibrations) of the two TPR instruments. Another possible reason is that there are different

Pd-Zn interactions due to different catalyst preparation methods and that PdO in CP catalyst was easily reduced (i.e. reducible at lower temperatures).

The CP analysis does not show a peak at higher temperature (due to ZnO reduction) as expected. There are two possible reasons for this, i.e. the systematic error of the instruments and difference in Pd loadings from catalyst preparation methods. The CP catalyst has about 2.5 times less Pd loadings compared to the IMP catalysts.

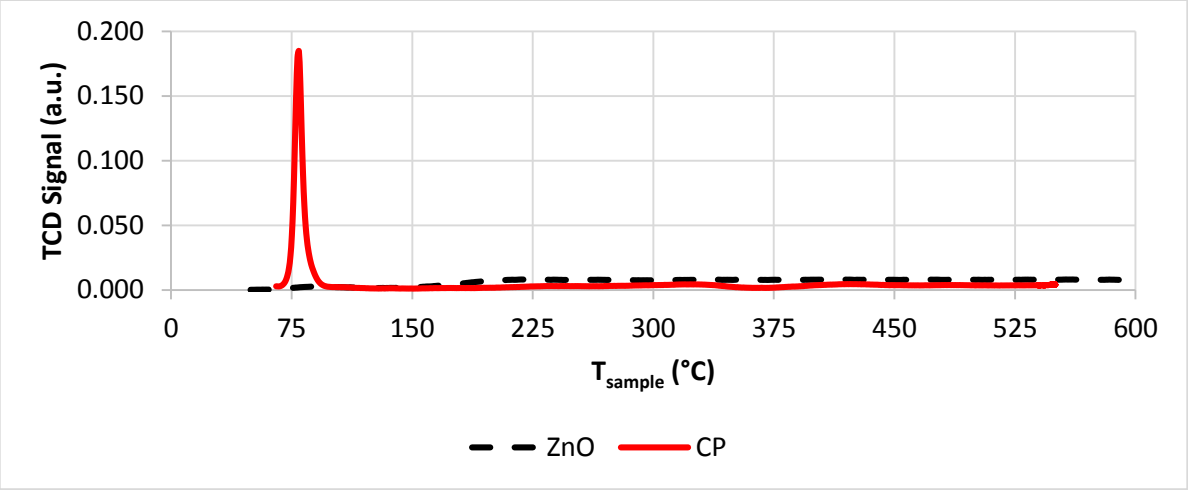

Figure 5-4: The TPR profiles of ZnO (99.999 wt%, Sigma-Aldrich), and CP

Unfortunately, for comparison, H_2-TPR analyses of impregnation catalysts could not be conducted on the other TPR instrument as this equipment was no longer operable. In addition, CP catalyst was depleted and therefore H_2-TPR experiments of the CP samples using the earlier TPR instrument could not be conducted.

5.2.3. Brunauer-Emmett-Teller Surface Area

The BET surface areas of powder materials were determined using Micrometrics ASAP 2020 instrument (refer to section 4.2.3). The BET surface areas of IMP_1 and IMP_2 are 3.3 and 3.2 m^2/g, respectively (see Table 5-3). It was expected that the surface areas of these catalysts would be similar as they were prepared using the same method. However, the BET surface area of the commercial ZnO (i.e. 2.8 m^2/g) used to prepare the impregnation catalysts was slightly lower than that of the catalysts. Sá *et al*. (2010) and Chin *et al*. (2003) reported that ZnO support is modified by the acidic aqueous solution of $Pd(NO_3)_2$. When exposed to acidic aqueous $Pd(NO_3)_2$ solution, ZnO support leach out in the form of Zn^{2+} ions from the ZnO matrix into the pores modifying structure of ZnO support. Chin *et al*. (2003) showed that below 9 wt% Pd loading the BET surface area of Pd/ZnO catalyst increases from

3.4 m^2/g for pure ZnO support to 10.5 m^2/g at 9 wt% Pd. This was understood to be due to leaching of ZnO from the ZnO matrix. However, beyond 9 wt% Pd loading the BET surface area decreased from 10.5 m^2/g at 9 wt% Pd to 7.2 m^2/g at 16.7 wt% Pd. This was understood to be as a result of collapse of the ZnO matrix due to excessive leaching. Thus for the case under consideration, the slight increase of the BET surface area from 2.8 m^2/g (for pure ZnO support) to 3.2 and 3.3 m^2/g (for IMP_1 and IMP_2, respectively) is due to milder leaching of the ZnO support. On the other hand, the BET surface area of the CP catalyst (i.e. 5.3 m^2/g) was higher than that of the impregnation catalysts.

Table 5-3: The BET and Chemisorption analysis results

Sample	BET surface area (m^2/g)
ZnO (99.999 wt%, Sigma-Aldrich)	2.8
IMP_1	3.3
IMP_2	3.2
CP	5.3

5.2.4. Transmission Electron Microscope

The transmission electron microscope (TEM) image of IMP_1 shows PdO crystallites (darker spots) on ZnO support (refer to Figure 5-5A). Using ImgaeJ1 software, the crystallite size distribution of the PdO crystallites was determined (see Figure 5-5B). The average PdO crystallite size was found to be 6.7 ± 2.4 nm.

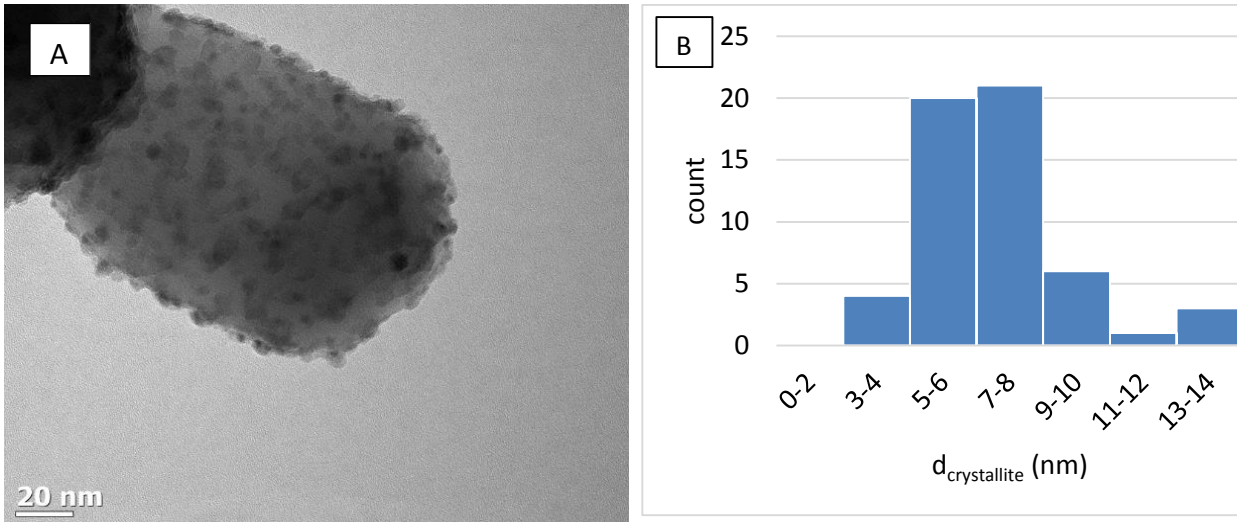

Figure 5-5: (A) TEM image of IMP_1 and (B) Pd crystallite size distribution of IMP_1

A similar PdO crystallite size distribution was obtained for IMP_2. The average crystallite size was 6.3 ± 1.9 nm (refer to Figure 5-6).

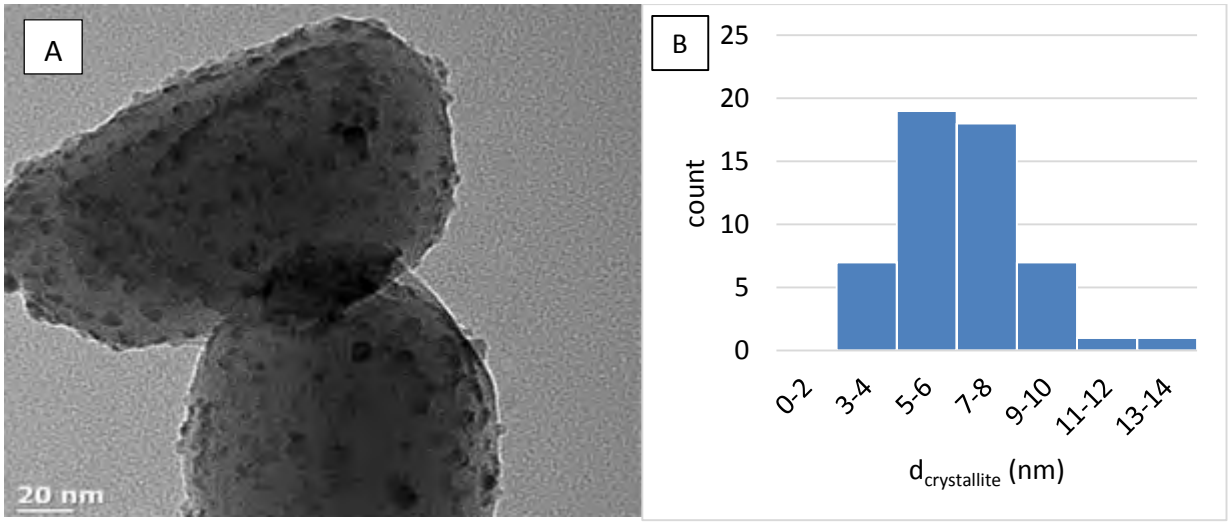

Figure 5-6: (A) TEM image of IMP_2 and (B) Pd crystallite size distribution of IMP_2

The TEM image of IMP_1 (Figure 5-7A) when compared to that of the ZnO support (Figure 5-7B) suggests that the ZnO support crystallite size distribution did not change significantly during catalyst preparation. This is in agreement with the BET surface areas of the IMP catalysts and ZnO (see section 5.2.3).

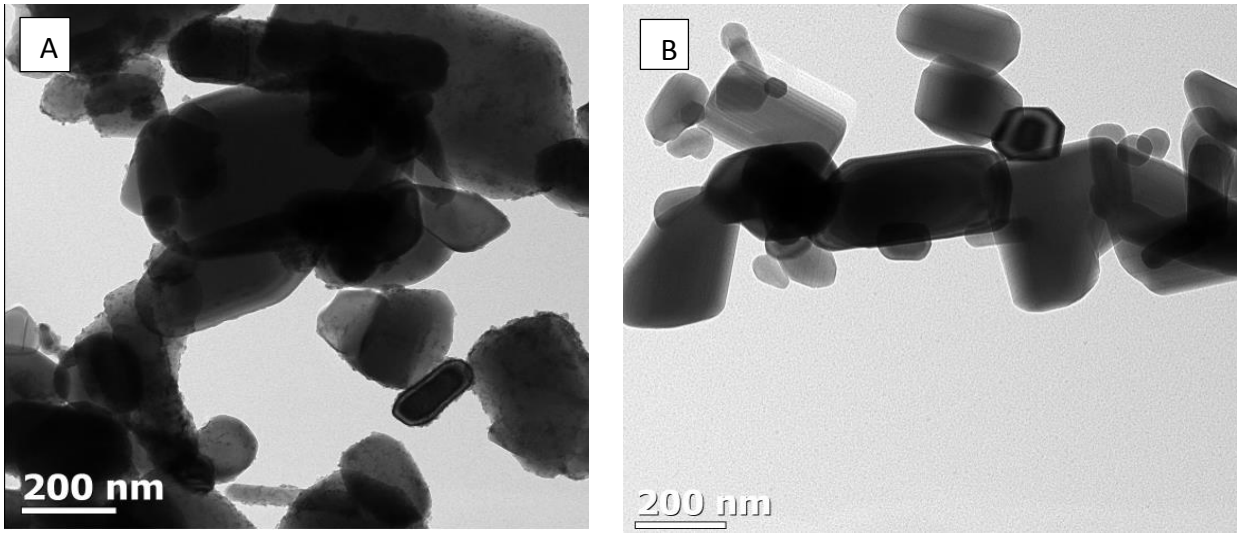

Figure 5-7: TEM images of (A) IMP_1 and (B) ZnO (99.999 wt%, Sigma-Aldrich)

Unfortunately, the TEM images of the CP catalyst could not be taken as the catalyst was depleted.

5.2.5. Thermogravimetric Analysis

The thermogravimetric analysis (TGA) results of the Pd salt (Figure 5-8) shows that the mass of the salt decreased to 95 wt% of the original mass as the temperature reaches 100°C. This decrease in mass was as a result of evaporation of water absorbed by the salt. The mass then decreased rapidly to approximately 50 wt% of the initial mass when temperature reaches 150°C. This is understood to be due to a combination of water evaporation and decomposition of $Pd(NO_3)_2$. Finally, the mass decreased to about 42 wt% of the initial mass as the temperature reached 250°C. This shows that the Pd content of the salt was 42 wt%. The experiment was reproducible as both run 1 and 2 show similar trends (see Figure 5-8).

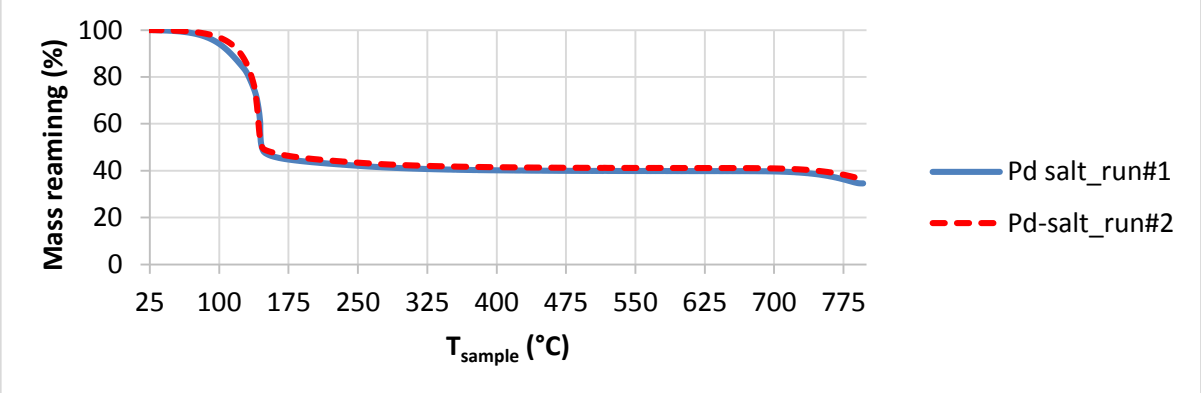

Figure 5-8 : The TGA analysis results of the Pd salt, $Pd(NO_3)_2.xH_2O$ (37.0 - 42.0 wt% Pd, Sigma-Aldrich)

The TGA results of IMP_1 show that the change in mass was less than 1 wt% of the initial mass (see Figure 5-9). This shows that IMP_1 did not absorb significant amount of moisture from the atmosphere.

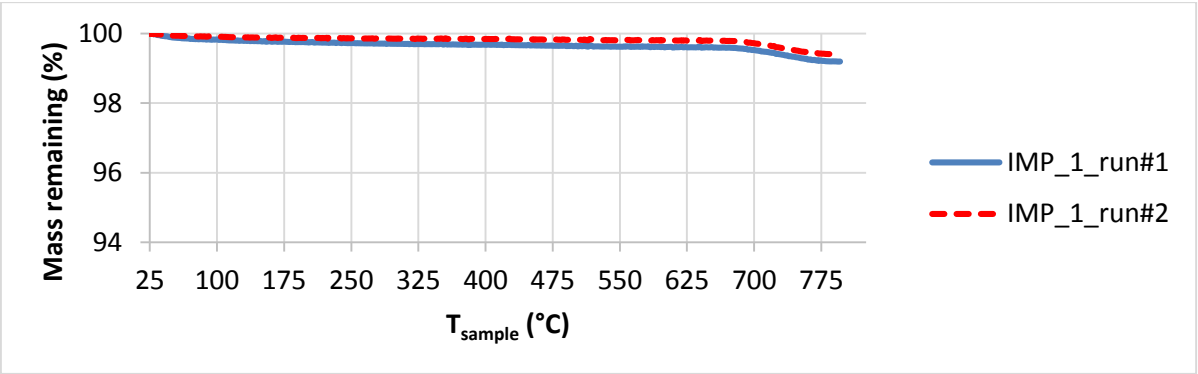

Figure 5-9: The TGA analysis results of IMP_1

Similar results as per IMP_1 were obtained for IMP_2 (refer to Figure 5-10).

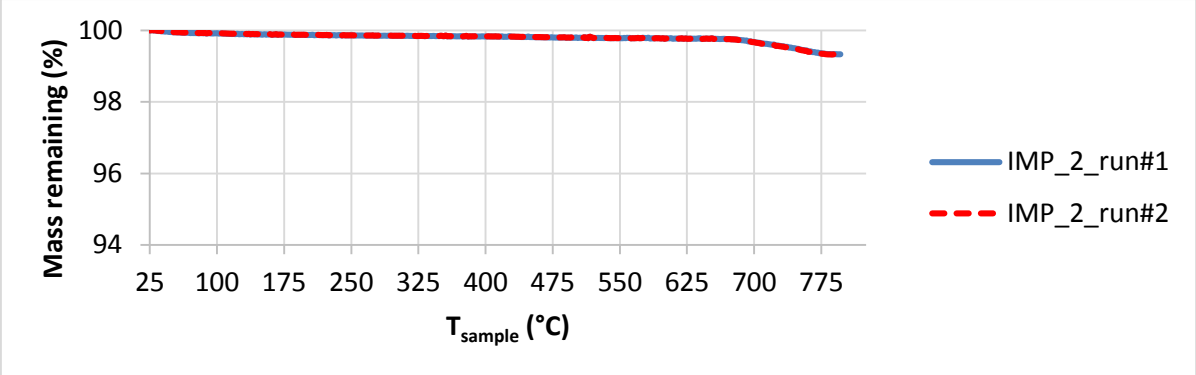

Figure 5-10: The TGA analysis results of IMP_2

5.3. Fixed Bed Catalyst Testing

This section presents the results of the equilibrium calculations, reference tests and catalyst performance tests for both the impregnation (IMP) and co-precipitation (CP) catalysts.

5.3.1. Equilibrium Calculations

The equilibrium calculations were obtained via Aspen Plus v8.6 simulation software. The simulations were conducted such that they cover the conditions of the catalyst performance tests for this work (i.e. T_{rxn} = 180 - 200°C, S/C = 1.1, Ar_{feed} = 5 - 15 mol%, P = 1 barg). Refer to Appendix C for more details on the simulations.

For the simulation of methanol steam reforming, three chemical equilibrium reactions i.e. steam reforming of methanol (SRM) (Eqn 2.18), methanol decomposition (MD) (Eqn 2.19) and water-gas shift (WGS) (Eqn 2.20) were taken into account. The results of the simulation are shown in Figure 5-11. As shown in the figure, CH_3OH conversion is high and increases with increase in temperature i.e. 98.8% at 150 °C, reaching higher than 99.9% conversion for temperatures above 250 °C. This increase in conversion with increase in temperature is expected since SRM and MD are endothermic reactions. However, the selectivity towards CO_2 decreases with increasing temperature i.e from 98.4% at 150 °C to 69.7% at 400 °C due to the exothermicity of the WGS equilibrium reaction.

The simulation result show that at the conditions of the catalyst performance tests (i.e. T_{rxn} = 180 - 200°C, S/C = 1.1, Ar_{feed} = 5 - 15 mol%, P = 1 barg) CH_3OH equilibrium conversion is over 99% and therefore the catalyst performance tests in this work were conducted far from the methanol steam reforming equilibrium since CH_3OH conversion for the tests was less than 50%.

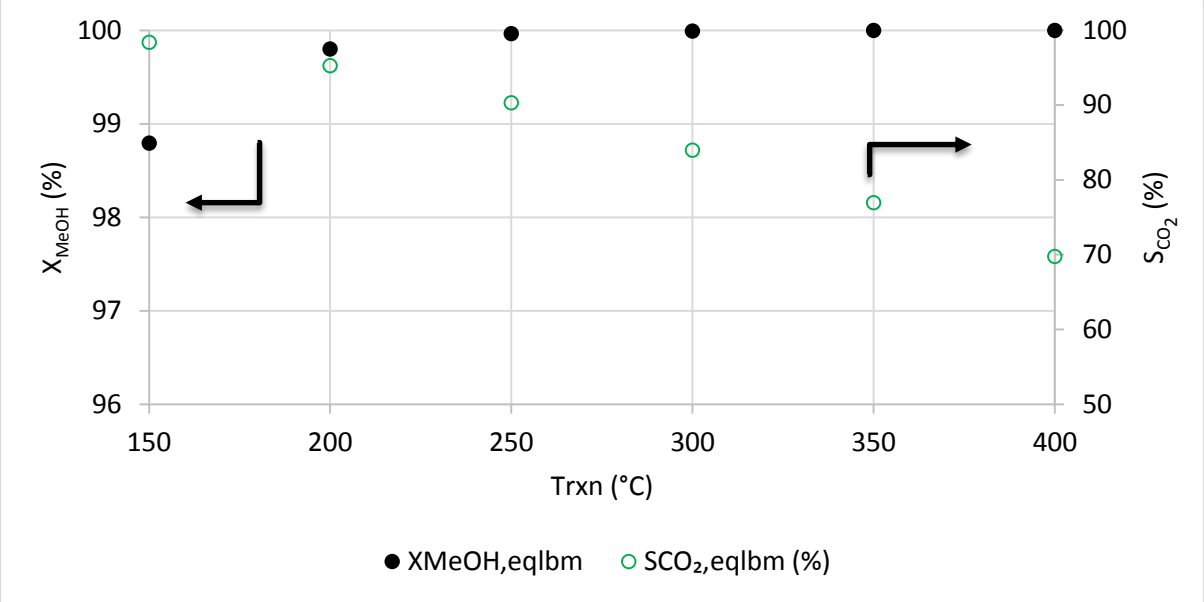

Figure 5-11 : Steam reforming of CH_3OH equilibrium conversion and CO_2 selectivity. Conditions: S/C = 1.1, Ar_{feed} = 5 mol%, P = 1 barg

However, the CO_2 equilibrium selectivity (shown Figure 5-11) is based on CH_3OH equilibrium conversion > 98%. Thus the simulation does not provide information on CO_2 selectivity at low CH_3OH conversions (i.e. < 50%). To address this challenge, a WGS equilibrium was simulated at low CH_3OH conversions (i.e. < 50%). A hypothetical feed composition for the WGS equilibrium reactor was calculated assuming that a CH_3OH was converted to CO and H_2 via MD (see Appendix C for more details).

The results of the second simulation are shown in Figure 5-12. As shown in the figure, CO_2 equilibrium selectivity decreases with an increase in CH_3OH conversion i.e. 99.9% at 5.0% reaching less than 97.0% selectivity at a conversion of 80.0% (for T_{rxn} = 180°C). In addition, high temperatures do not favour CO_2 selectivity i.e. (for a CH_3OH conversion of 80%) CO_2 selectivity is 98.0% at 180°C and 87.7% at 300°C. This is due to the exothermicity of the WGS. The formation of CO_2 is still favourable over CO especially at the lower temperatures and lower CH_3OH conversions.

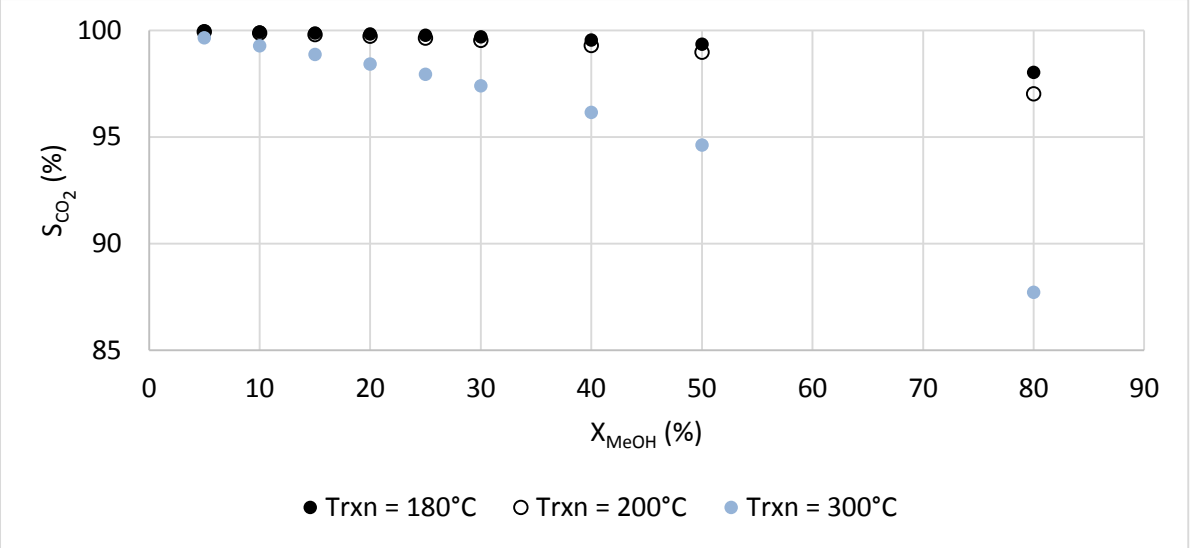

Figure 5-12: CO_2 equilibrium selectivity as a function of CH_3OH conversion at P = 1 barg.

5.3.2. Reference Tests

A reactor filled only with silicon carbibe (SiC), referred to as a blank reactor, and a reactor loaded with ZnO support (99.999 wt%, Sigma-Aldrich) were tested to assess "background" performance (e.g. reactivity of stainless steel reactor wall or the ZnO). For the blank test, the reactor was packed with SiC with a particle size distribution (PSD) of ~ 3 mm (no catalyst was added). The reaction temperature was set at 300°C to increase potential reactivity. A water-methanol liquid mixture (S/C = 3.0) was fed to the reactor at 5.91 ± 0.08 g/h (average ± absolute standard deviation). Argon was set at 5.83 sccm, making up 5.4 mol% of the total feed.

Six liquid samples were collected from the catch pot over 70 hours on stream (see Figure 5-13). The average CH_3OH conversion was 2.2 ± 1.4% (average ± absolute standard deviation). In the absence of an active catalyst no significant reaction can be observed and the apparent CH_3OH conversion (i.e. 2.2%) was due to experimental error. In addition, the blank test was conducted at a significant higher reaction temperature (i.e. 300°C) and higher steam to carbon ratio (i.e. 3) compared to the catalyst tests condition in this work (i.e. T_{rxn} = 180 - 200°C, S/C = 1.1). Both high temperature and high steam to carbon ratio favour CH_3OH conversion and were aimed at facilitating any potential activity.

For the ZnO support test, the ZnO was packed in the isothermal zone of the reactor as described in section 4.4.1. Prior to testing, the ZnO was treated in 10 vol% H_2/Ar at 450°C for three hours. The reaction temperature was then set to 250°C. A water-methanol liquid

mixture (S/C =1.1) and Ar were fed such that the total GHSV was 960 h^{-1} with Ar making up 6.4 mol% of the feed.

Five liquid samples were collected over ~ 50 hours on stream (see Figure 5-13). The average CH_3OH conversion was - 0.1 ± 2.7% (average ± absolute standard deviation). According to the TPR analysis (see Figure 5-2, Figure 5-3 and Figure 5-4), in the absence of Pd, ZnO is not reduced below 600°C and therefore ZnO was not active for methanol steam reforming in this test.

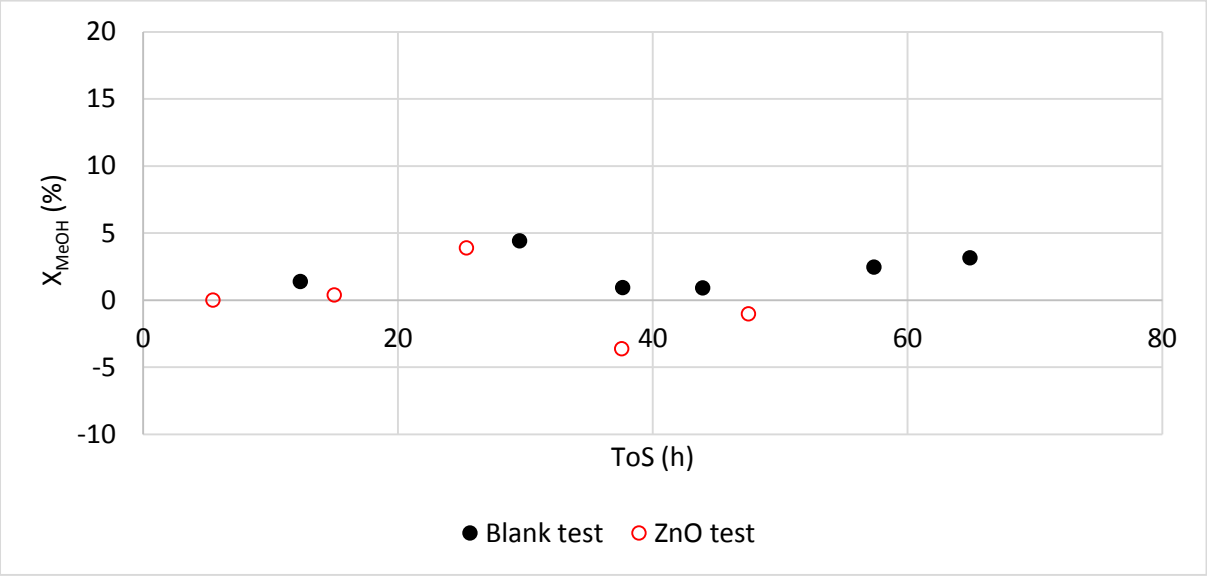

Figure 5-13 :CH_3OH conversion as a function of time on steam for reference tests. Blank test conditions: T_{rxn} = 300°C, Liquid flow = 5.91 ± 0.08 g/h, S/C = 3.0, Ar_{feed} = 5.4 mole%, P = 1 barg. ZnO test conditions: $T_{reduction}$ = 450°C (10 vol% H_2/Ar, 3h), T_{rxn} = 250°C, S/C = 1.1 - 1.2, GHSV = 920/h, P = 1 barg

Both, the blank and ZnO support tests, have negligible CH_3OH conversion. The high standard deviations are due to the very low conversions and reflect the experimental error.

5.3.3. Tests with impregnation catalysts

This section reports results of the performance tests of the impregnation catalyst, IMP_1, pre-treated in H_2 at different temperatures for different reductions.

5.3.3.1. IMP_1-120/180

A fresh catalyst, IMP_1 (refer to section 4.1.3 for details on test nomenclature) 'as prepared', was treated in 10 vol% H_2/Ar at 120°C for two hours. At this treatment temperature PdO of the catalyst reduce (see the H_2-TPR analysis in Figure 5-2), however, ZnO remain unreduced as it only start to reduce at temperatures above 260°C.

After the reduction, H_2 was purged out of the reactor and reaction temperature was set to 180°C. A water-methanol liquid mixture (S/C = 1.1) and Ar (6.4 mol% of the feed) were fed such that the total GHSV was 1100 h^{-1}. During the first 70 hours on stream, CH_3OH conversion decreased from approximately 22% to 11%. This was due to the lining-in (i.e. initial deactivation) of the catalyst. However, from 120 to 160 hours on stream, the catalyst was stable and the conversion remained constant at 11.1 ± 1.0% (see Figure 5-14). Selectivity towards CO_2 remained greater than 99%.

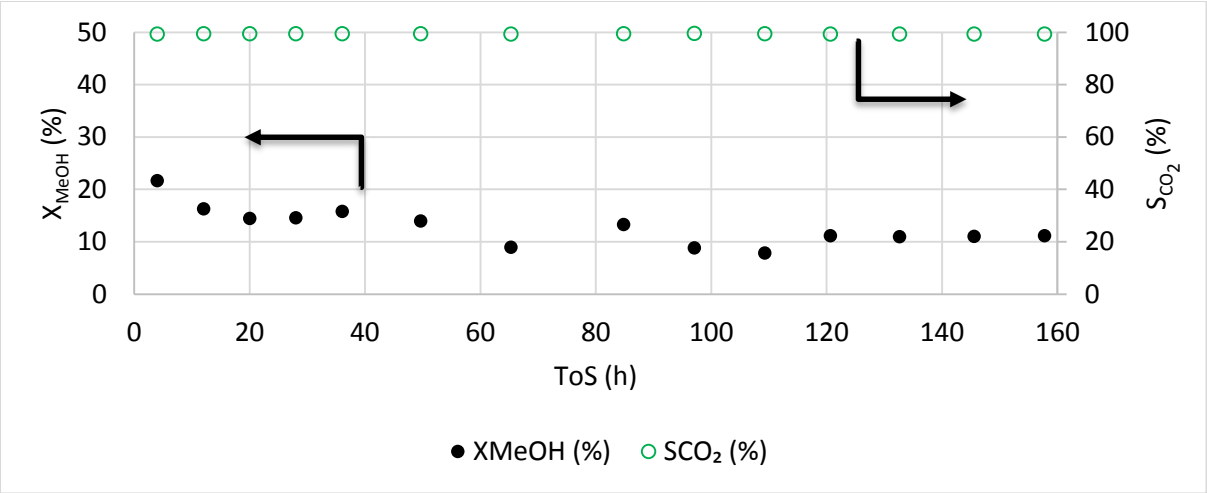

Figure 5-14: CH_3OH conversion and CO_2 selectivity as a function of time on stream (ToS) for IMP_1. $T_{reduction}$ = 120°C (in 10 vol% H_2/Ar for 2h), T_{rxn} = 180°C, S/C = 1.0 - 1.2, GHSV = 1100h^{-1}, P = 1 barg

5.3.3.2. IMP_1-200/180

Similar to IMP_1-120/180 test, a fresh IMP_1 catalyst was treated for two hours in 10 vol% H_2/Ar. However, the reduction temperature (200°C) for the current test was slightly higher than the reaction temperature (180°C) to limit *in-situ* reduction during the activity tests. Also, the reduction temperature was significantly lower than 260°C, a temperature where ZnO of the catalyst begins to reduce. From the H_2-TPR analysis it is expected that during the treatment PdO reduced to metallic Pd while ZnO remained unreduced (see the TPR profile in Figure 5-2).

Similar to IMP_1-120/180 test, during the first 50 hours on stream, CH_3OH conversion dropped from 17% to 12%. This was due to initial deactivation of the catalyst. Unfortunately, the test was interrupted by several of power cuts (due to load shedding) from the 63 hours on stream. During the test the selectivity towards CO_2 was greater than 99%.

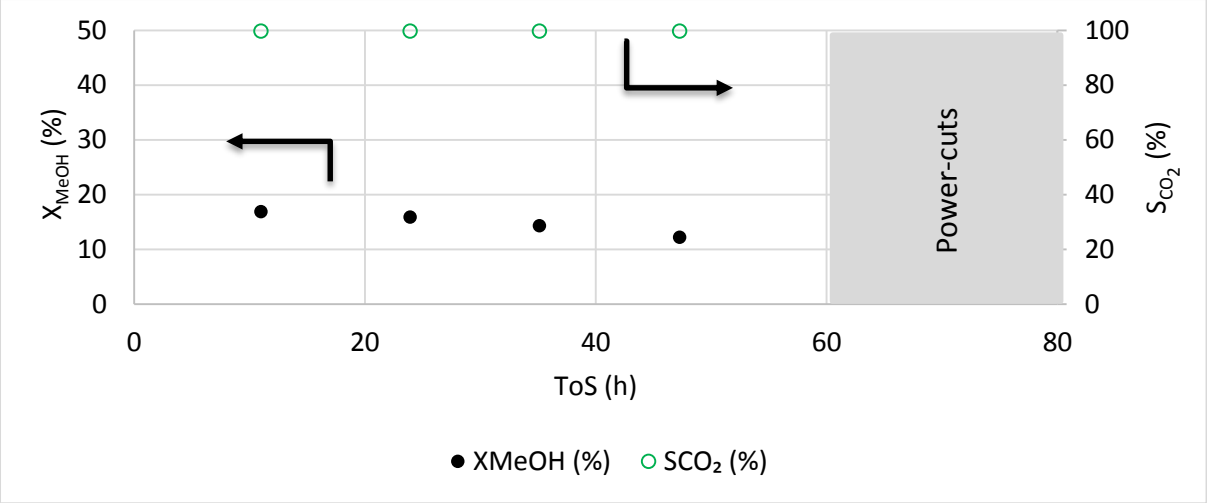

Figure 5-15: CH_3OH conversion and CO_2 selectivity as a function of time on stream (ToS) for IMP_1. $T_{reduction}$ = 200°C (in 10 vol% H_2/Ar for 2h), T_{rxn} = 180°C, S/C = 1.1 - 1.2, GHSV = 1100h^{-1}, Ar = 6.4 mol%, P=1 barg

5.3.3.3. IMP_1-450/180

After the test IMP_1-200/280, and the power-cut period, the catalyst was used for the 450°C reduction temperature experiments. It should be noted that during the power-cut the reactor was maintained at a temperature of 180°C while Ar flow kept the catalyst inert.

After the power-cut period, the catalyst was treated in 10 vol% H_2/Ar at 450°C for 2 hours. Consequently, not only PdO reduced but also ZnO in the near vicinity of metallic Pd (see the H_2-TPR analysis in Figure 5-2). After reduction, the reactor temperature was set at 180°C. A feed (GHSV = 1100 h^{-1}, S/C = 1.1) was then introduced into the reactor.

Over the period, 90 to 150 hours on stream, CH_3OH conversion remained constant at 10.4 ± 4.8%. No lining-in of the catalyst was expected as the catalyst has been running for ~ 90 hours. In addition, the selectivity towards CO_2 remained > 99% throughout the test, at equilibrium similarly to the tests at lower reduction temperatures.

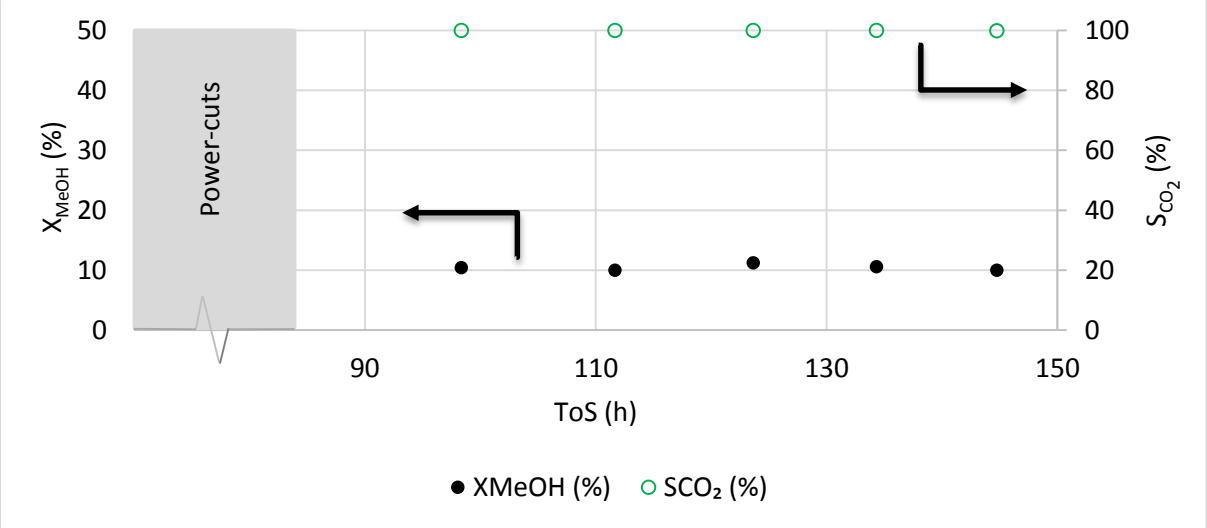

Figure 5-16: CH_3OH conversion and CO_2 selectivity as a function of time on stream (ToS) for IMP_1. $T_{reduction}$ = 450°C (in 10 vol% H_2/Ar for 2h) , T_{rxn} = 180°C, S/C = 1.1 - 1.2, GHSV = 1110/h, P = 1 barg

5.3.4. Tests with co-precipitation Catalyst

This section presents the result of the performance tests of the co-precipitation (CP) catalyst reduced at 250 and 450°C.

5.3.4.1. CP-250/225

A fresh CP catalyst was reduced in 10 vol% H_2 at 250°C for 2 hours. The H_2-TPR analysis of the catalyst (see Figure 5-4) show that PdO (and possibly ZnO in the near vicinity of Pd as well) reduce at this reduction temperature. The reaction temperature was set to 225°C and the feed (S/C = 1.1, Ar = 6.3 vol%) was such that the GHSV was 920 h^{-1}. During the next 60 hours on stream CH_3OH conversion decreased from ~ 39% to 34% (see Figure 5-17). This decline in conversion was due to conditioning of the catalyst (i.e. lining-in). Thereafter, the decline in conversion was slower as the catalyst was reaching stable activities. Once the catalyst was stable three space velocities were tested and the conversions are presented in Table 5-4.

Table 5-4: Conversions and their standard deviations for each GHSV

ToS (h)	GHSV (h^{-1})	X_{MeOH} (%)	SD (-)	RSD (%)
0 - 60	920	36.2	1.6	4.5[a]
60 - 121	480	46.5	0.7	1.5
121 - 168	760	37.7	0.4	0.9
168 - 218	920	29.3	0.8	2.6

[a] RSD during catalyst lining-in period. SD and RSD are absolute and standard deviation, respectively.

The test was conducted again at a GHSV of 920 h^{-1} from 168 to 218 hours on stream as was done in the first 60 hours on stream and the conversion decreased nearly 1/5 from the initial conversion at 55 hours (i.e. from 36.2% to 29.3%). During the complete experiment the selectivity towards CO_2 remained constant (> 99%).

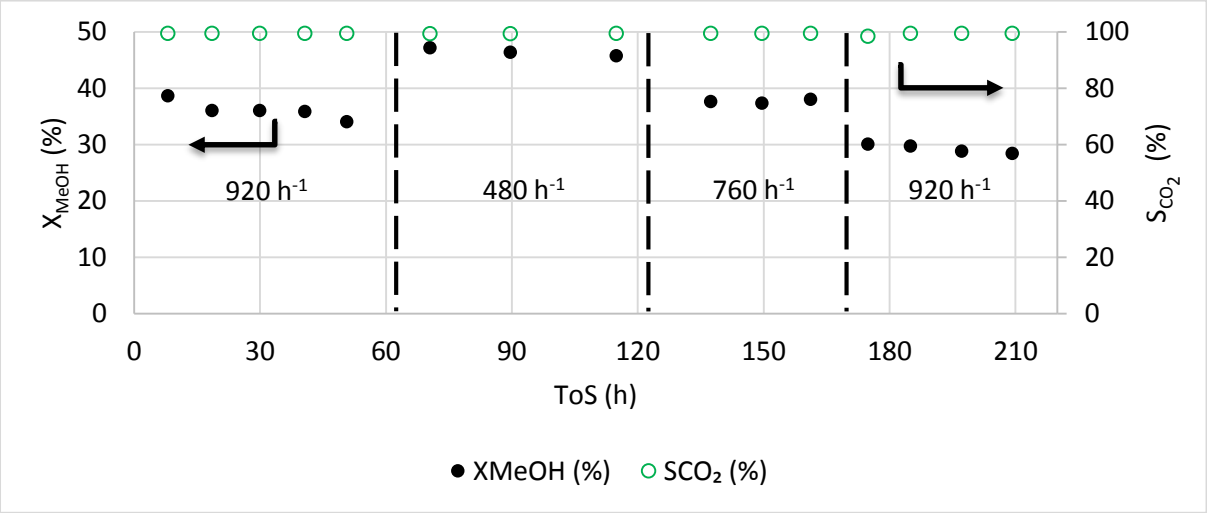

Figure 5-17: CH_3OH conversion and CO_2 selectivity as a function of time on stream (ToS) for CP. $T_{reduction}$ = 250°C (in 10 vol% H_2/Ar for 2h), T_{rxn} = 225°C, S/C = 1.1 - 1.2, P = 1 barg

5.3.4.2. CP-450/225

This test extended from the test, CP-250/225. Immediately after collecting the last sample of IMP-250/225 at 209 hours on stream, the catalyst was reduced at 450°C for two hours. After reduction, a water-methanol mixture (S/C = 1.1) was fed to the reactor. Three space velocities were tested and the conversions are presented in Table 5-5.

Table 5-5: Conversions and their standard deviations for the tested GHSVs of the CP catalyst reduced at 450°C.

ToS (h)	GHSV (h^{-1})	X_{MeOH} (%)	SD (-)	RSD (%)
218 - 295	920	23.8	1.1	4.6
295 - 360	410	36.5	0.8	2.3
360 - 400	1270	16.4	0.5	2.9
460 - 490	920	19.9	1.2	6.2

The catalyst was already lined-in (see Figure 5-18) hence CH_3OH conversion as a function of time on stream was relatively constant for each GHSV. From ~ 460 to 490 hours on stream, the test was again conducted at 920 h^{-1} as was done during the first ~ 60 hours on stream of the test and the conversion dropped by nearly 1/6 from the initial conversion (from ~ 218 to 295 hours on stream).

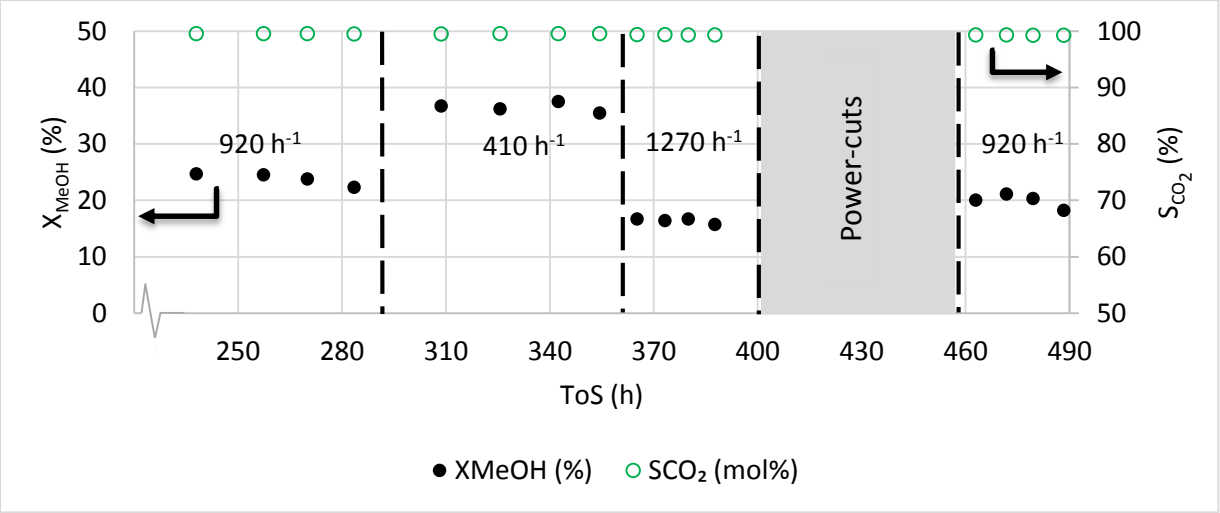

Figure 5-18: CH_3OH conversion and selectivity towards CO_2 as a function of time on stream for CP. $T_{reduction}$ = 450°C (10 vol% H_2/Ar for 2h), T_{rxn} = 200°C, S/C = 1.1 - 1.2, P = 1 barg

Chapter 6 Discussion

6.1. Reproducibility

The ICP-OES analysis of the impregnation catalysts, i.e. IMP_1 and IMP_2, show that the impregnation preparation method is reproducible with a relative standard deviation of 2.6% Pd loading (refer to section 5.2.1). In addition, for both IMP_1 and IMP_2 catalysts PdO crystallite size distribution on ZnO support was found to be similar, i.e. 6.7 ± 2.4 nm and 6.3 ± 1.9 nm, respectively (refer to section 5.2.4). The performance of IMP_1 and IMP_2 catalysts after similar pre-treatment and reaction conditions (see IMP_1-120/180 and IMP_2-120/180 in section 5.1) were similar with CH_3OH conversion remaining at ~ 11% at a GHSV of 1100 h^{-1} after lining in. The selectivity towards CO_2 for both catalysts was greater than 99%. However, the co-precipitation method was not reproducible. The CP catalyst was aimed at 3 wt% Pd but according to the ICP-OES results it was found to be only 1.1 wt% Pd (see Table 5-2). The loss of Pd was likely due to partial precipitation of Pd as result of lower pH level (< 7) during the precipitation step of the preparation. Thus co-precipitation (CP) was not successful and hence more focus was on the impregnation (IMP) catalyst rather.

6.2. Reference Tests

For the blank test only silicon carbide (SiC) was added into the reactor (refer to chapter 5.3.2). SiC is highly thermally and chemically stable (Verrall *et al.*, 1999) and it was confirmed that SiC did not contribute to chemical reactions at the reaction conditions. The test was conducted at a relative higher reaction temperature (i.e. 300°C) compared to the catalyst performance tests (i.e. 180 and 200°C) so as to enhance any potential reactivity especially from the stainless steel walls of the reactor. The measured average CH_3OH conversion over ~ 70 hours on stream was 2.23 ± 1.41% (i.e. conversion ± absolute error). In the absence of a catalyst it is expected that no conversion occurs and therefore the apparent conversion (i.e. 2.23%) was due to experimental error. The potential cause of the error is evaporation of CH_3OH (either to the gas stream, to the atmosphere during liquid sample collection from the catch pot, or during sample preparation and analysis of liquid samples). However, the error due evaporation of CH_3OH to the gas stream was negligible as the partial pressure of CH_3OH in the catch pot (operating at ~ 3°C) was less than 1% (see the calculations in Appendix B).

Steam reforming activity of methanol was determined over commercial ZnO. Prior to performance test at 250°C and 960 h^{-1}, the ZnO was treated (*in-situ*) in 10 vol% H_2/Ar at 450°C for 3 hours. During methanol steam reforming test the feed composition (i.e. S/C = 1.1, Ar = 6.4 mol%) was similar to most of the catalyst performance tests. The ZnO support was tested at slightly higher reaction temperature (i.e. 250°C instead of 180 - 200°C) so as to confirm its activity. Over about 50 hours on stream, the average CH_3OH conversion was -0.06 ± 2.71% (i.e. average ± absolute SD). This indicates that the support had no activity for CH_3OH conversion at the reaction conditions. This is in agreement with the H_2-TPR analysis (see Figure 5-2, Figure 5-3 and Figure 5-4) which shows that ZnO (in the absence of Pd) does not reduce below 600°C.

6.3. Methanol Steam Reforming and Water-gas Shift Equilibrium

The equilibrium calculations were obtained via Aspen Tech simulation (refer to chapter 5.3.1 and Appendix C). According to most literature (Lebarbier *et al*., 2010; Sá *et al*., 2010), it is understood that the reactions steam reforming of methanol (SRM) (Eqn 2.18) and its side reactions methanol decomposition (MD) (Eqn 2.19) and water-gas shift (WGS) (Eqn 2.20) take place during methanol steam reforming. Hence, these reactions were taken into account for the simulation of methanol steam reforming equilibrium. Equilibrium conversion for the testing conditions (i.e. T_{rxn} = 180 - 200°C, P = 1 barg, S/C = 1.1, Ar_{feed} = 5 - 15 mol%) is > 98% (as shown in Figure 5-11), however, to avoid further reduction of the catalysts during testing (as H_2 is the main product of steam reforming), the catalysts were tested at relatively low temperatures and this resulted in low CH_3OH conversions.

The equilibrium selectivity towards CO_2 (> 99%) obtained (Figure 5-11) was calculated at equilibrium conversion (> 98%). Hence it became necessary to simulate equilibrium selectivity towards CO_2 (WGS equilibrium) at lower CH_3OH conversions (i.e. < 50%) (refer to chapter 5.3.1). As shown in Figure 5-12, at the catalysts testing conditions (i.e. T_{rxn} = 180 - 200°C, X_{MeOH} < 50%) CO_2 selectivity is still high (> 98%).

6.4. CO_2 Selectivity and PdZn Alloy Formation

The catalyst performance tests were conducted at low reaction temperatures to avoid *in-situ* reduction of the metals due to H_2 produced by steam reforming of methanol. Figure 6-1 shows selectivity towards CO_2 as a function of CH_3OH conversion for all the catalyst performance tests reported in section 5.3.3 and 5.3.4. As shown on the figure, CH_3OH conversion ranges from 10.4% to 46.5%. The highest CH_3OH conversion reached for IMP and CP catalysts were 24.7% and 46.5%, respectively. Selectivity towards CO_2 remained higher than 99% irrespective of the change in CH_3OH conversion for both the IMP as well as for the CP catalysts as already mentioned in sections 5.3.3 and 5.3.4.

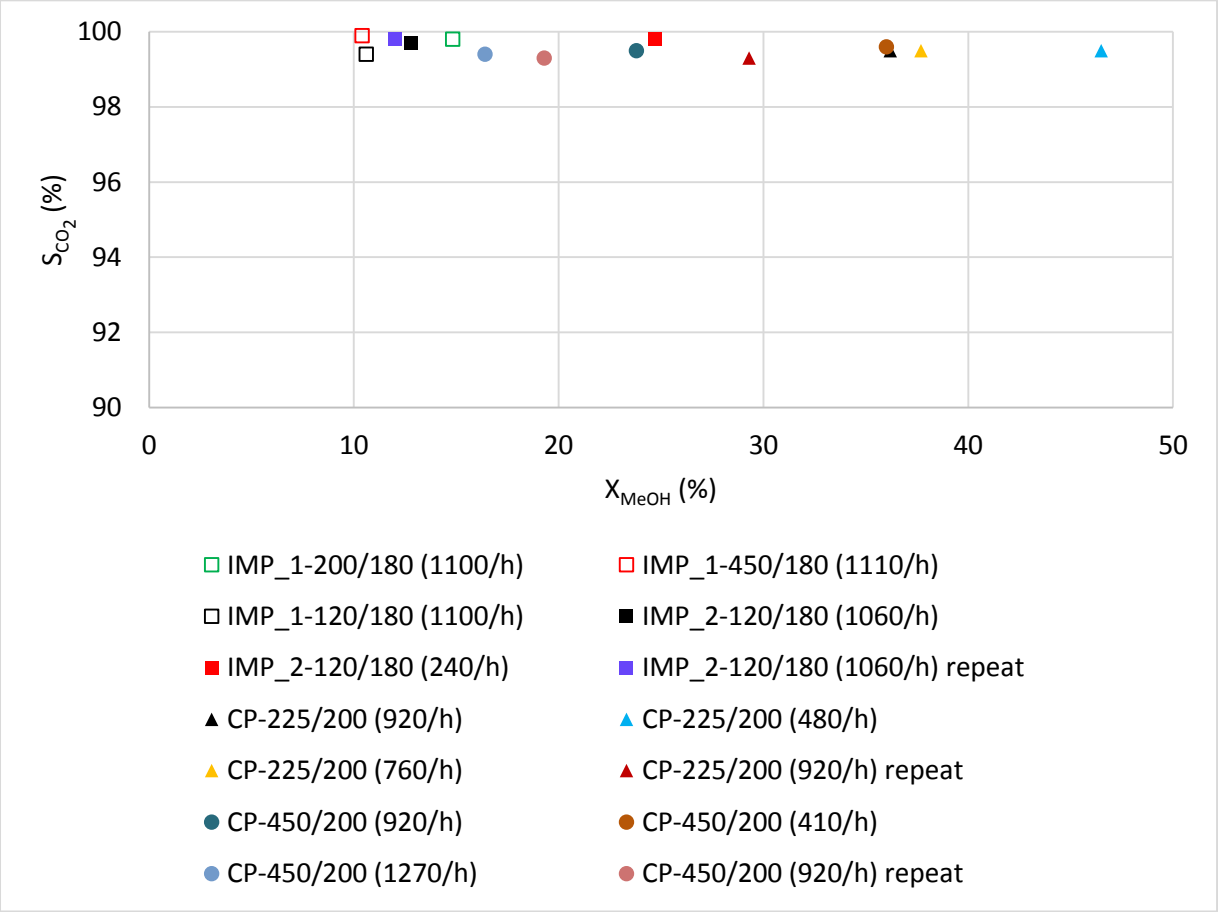

Figure 6-1: CO_2 selectivity as function of methanol conversion. Test index: Open squares = IMP_1, Filled squares = IMP_2, Triangles = CP ($T_{reduction}$=225°C) and Filled circles = CP ($T_{reduction}$=450°C)

Prior to methanol steam reforming, the catalysts were treated in 10 vol% H_2/Ar at a specified temperature (here referred to as reduction temperature) for two hours. As already shown in section 5.2.2, IMP_1 and IMP_2 showed similar H_2-TPR analyses. The analyses show a sharp peak at lower temperature around 90°C and a broader peak at higher

temperatures between 245 and 385°C (with maximum at 348 and 316°C for IMP_1 and IMP_2, respectively). However, the H_2-TPR analyses of the ZnO support without the presence of Pd does not show any peak below 600°C. Chin *et al*. (2002) obtained similar results when conducting H_2-TPR experiments over 9.0 and 16.7 wt% Pd/ZnO catalysts prepared by incipient wetness impregnation. The catalyst samples were ramped at 8°C/min up to 600°C. Each of the catalyst analysis showed two peaks; one at a lower temperature (i.e. 91 and 101°C for 9.0 and 16.7 wt% Pd/ZnO, respectively) and another at a higher temperature (i.e. 350 and 420°C for 9.0 and 16.7 wt% Pd/ZnO, respectively). The peak which occurs at lower temperature was ascribed to reduction of PdO while the one at the high temperature to the partial reduction of ZnO. The higher temperature peak was understood to be an indication for the formation of PdZn alloy. The areas of the peaks increased with increase in Pd weight loading. The increase in peak areas was attributed to increased amount of PdO reduced which further resulted in an increased amount of ZnO reduced.

Similar results were obtained by Eswaramoorthi and Dalai (2009) although they worked with a slightly different material i.e. SBA-15 supported Pd and Zn catalysts prepared by impregnation. In these experiments the Pd to Zn mass ratio of the catalysts was fixed at 0.67 while the Pd loadings were 0.5 - 5.5 wt% and Zn loadings 0.75 - 8.25 wt%. The H_2-TPR analyses of the catalysts exhibited two positive peaks i.e. one at low temperatures (~ 120°C) ascribed to the reduction of PdO and another at high temperatures (~ 300 - 400°C) ascribed to the reduction of ZnO. After studying a ZnO supported Pd catalyst (15.9 wt% Pd) via H_2-TPR and XRD, Wang *et al*. (2006) proposed the following mechanism for reduction:

$$PdO/ZnO \rightarrow Pd/ZnO \rightarrow PdZnO_{1-x}/ZnO \rightarrow \text{amorphous PdZn alloy/ZnO} \rightarrow \text{crystallite PdZn alloy/ZnO}$$

Wang *et al*. (2006) suggest that PdO is the first metal oxide to reduce as the temperature is increased from room temperature. Due to H_2 spill-over from metallic Pd, ZnO in close vicinity to the metallic Pd then reduce. From the XRD analysis they understood that at first amorphous and eventually crystallite PdZn alloy was formed. However, the ZnO in the bulk does not reduce. Thus for the TPR analyses of IMP_1 and IMP_2, the low temperature peak (i.e. at 87 and 90°C, respectively) is clear to be reduction of PdO and the partial reduction of ZnO at higher temperature was facilitated by H_2 spill-over from metallic Pd.

Most literature suggest that MD reaction (Eqn 2.19) is favoured over metallic Pd resulting in a high CO selectivity and attribute high selectivity towards CO_2 to the presence of PdZn alloy which is formed upon reducing PdZn catalysts at high temperatures (typically > 250°C) (Föttinger, 2013; Sá *et al*., 2010; Conant *et al*., 2008; Dagle *et al*., 2007; Karim, Conant *et al*., 2006; Wang *et al*., 2006; Chin *et al*., 2002; Iwasa *et al*., 1995). Thus it was expected that upon reducing IMP_1 in 10 vol% H_2/Ar at 200°C (i.e. IMP_1-200/180) that selectivity towards CO_2 would be low since no PdZn alloy but metallic Pd was formed as also suggested by the H_2-TPR (see Figure 5-2). However, selectivity towards CO_2 was already high (> 99%). The reduction temperature was then decreased to 120°C for the tests, IMP_1-120/180 and IMP_2-120/180 (see Figure 5-1), however, it was impractical to decrease reaction temperature since CH_3OH conversion was already low (< 15%) at a reaction temperature of 180°C. The H_2-TPR results indicates that PdO only reduce at a reduction temperature of 120°C. Although the reaction temperature (i.e. 180°C) was higher than the reduction temperature (i.e. 120°C) ZnO did not reduce during the reaction as ZnO only starts to reduce at higher temperature (~ 260°C) according to the H_2-TPR analysis of the catalyst. To account for the high CO_2 selectivity at the low reduction temperatures (i.e. 120 and 180°C), the following explanation is proposed;

> At the low reduction temperatures PdO reduced to metallic Pd while ZnO remained unreduced. Firstly, CH_3OH was converted to CO via the MD reaction (Eqn 2.19) over metallic Pd. CO was then converted to CO_2 via the WGS reaction (Eqn 2.20). It should be noted that the steam to carbon ratio in the feed was 1.1 and because CH_3OH conversion was low (< 30%), there was excess amount of steam (compared to CO and CO_2) in the reactor and this drove the WGS reaction to equilibrium i.e. CO_2 selectivity of ~ 99% (refer to section 6.3).

When the catalyst was reduced at 450°C in the case of IMP_1-450/180, CO_2 selectivity remained high (> 99%). However, since the selectivity towards CO_2 was already at equilibrium (> 99%) for the low reduction temperatures (i.e. 120 and 180°C) the contribution of high temperature reduction or PdZn alloy (if any) towards CO_2 selectivity could not be observed.

As discussed in section 5.2.2, the H_2-TPR analysis of the CP catalyst shows a sharp peak at 80°C. This is understood to be as a result of reduction of PdO. The relatively lower reduction temperature compared to that of IMP catalysts was likely to be due to systematic error (i.e. gas flow and temperature calibrations of the TPR equipments used for CP and IMP catalysts). Surprisingly, there was no peak at a higher temperature as in the case of IMP catalyst (see Figure 5-4). This was probably due to low Pd weight loading (i.e. 1.1 wt%, ~ 2.5 times less than IMP catalyst) which resulted in low H_2 spill-over from metallic Pd and consequently in small amount of ZnO reduced. The activity (and selectivity) tests of the CP catalysts, i.e. CP-250/225 and CP-450/225, were also conducted at the WGS equilibrium as the selectivity to CO_2 was high (> 99%). Relatively higher conversions in the case of CP catalyst tests were due to higher reaction temperatures.

Chapter 7 Concluding Remarks

ZnO supported Pd catalyst aimed at 2.5 wt% Pd was successfully prepared via incipient wetness impregnation and the duplicate preparation of the catalyst was successful. Both impregnation catalysts were confirmed by ICP-OES to contain similar weight Pd loadings i.e. 2.8 and 2.7 wt%, respectively. The actual Pd loading (ICP-OES) was slightly higher than the aimed loading due to underestimation of Pd content of the Pd salt used in the catalyst preparation. Furthermore, the PdO crystallite size distribution on ZnO support was similar (i.e. 6.7 ± 2.4 nm and 6.3 ± 1.9 nm) for the catalyst duplicates. Thus incipient wetness impregnation method is reproducible.

The H_2-TPR analysis of the impregnation catalyst shows two peaks, i.e. a narrow peak at lower temperature (87°C), and a broader peak at a higher temperature starting at approximately 260°C with a maximum at 348°C and ending around 385°C. The peak that occurs at lower temperature was due to reduction of PdO to metallic Pd. The H_2-TPR analysis of ZnO support showed no peak below 600°C and thus ZnO did not reduce below 600°C. Therefore the peak which occurs at the higher temperature in the case of impregnation catalyst was due to reduction of ZnO and was facilitated by H_2 spill-over from the metallic Pd. This peak is an indication of formation of PdZn alloy according to most literature. However, selectivity towards CO_2 selectivity was high (> 99%) for both 'only PdO reduced' and 'PdO and ZnO reduced' catalysts. The catalyst performance tests were conducted at low reaction temperatures to avoid further *in-situ* reduction of the catalyst during the reaction tests. Consequently, low CH_3OH conversions (< 30%) were obtained. In addition, feed molar steam to carbon ratio of 1.1, slightly higher than the stoichiometric ratio, resulted at low CH_3OH conversions in excess steam in the effluent. Low CH_3OH conversions and consequently excess steam in the effluent compared to CO and CO_2 drives the water-gas shift reaction to a high selectivity towards CO_2.

The co-precipitation method was not successful as the CP catalyst aimed at 3 wt% Pd was only 1 wt% according to the ICP-OES analysis. A large fraction of Pd was discarded due to partial precipitation of Pd. Hence less focus was paid on the CP catalyst.

Chapter 8 Recommendations

The following are recommendations for further studies:

- The co-precipitation method might be successful or reproducible if the final pH level of the Pd-and-Zn nitrate solution is adjusted (using aqueous NH_4OH) to greater than 7.
- In order to investigate the activity of water-gas shift further, testing off over ZnO treated in H_2 would confirm whether the bulk ZnO of the catalyst contribute to selectivity towards CO_2.
- *In situ* characterisation techniques such as FTIR and XRD can provide valuable insights as to changes (if any) the catalyst undergoes not only during pre-test treatment in H_2 but also under methanol steam reforming reaction conditions. Such characterisations can be insightful even at water-gas shift equilibrium where CO_2 selectivity can be misleading as to the state of a catalyst.
- As a reference, it would be helpful to characterize and conduct performance tests of Pd supported on 'hard to reduce support' such as Al_2O_3 and CeO_2 where only metallic Pd would form upon reducing the catalyst.

Chapter 9 References

Arroyo-Ramírez, L., Chen, C., Cargnello, M., Murray, C., B., Fornasiero, P. & gorte Raymond, J. 2014. Supported platinum–zinc oxide core–shell nanoparticle catalysts for methanol steam reforming. *J. Mater. Chem. A.* 2:19509-19514. DOI:10.1039/C4TA04790G.

Balat, H. & Kırtay, E. 2010. Hydrogen from biomass – Present scenario and future prospects. *International Journal of Hydrogen Energy.* 35(14):7416-7426. DOI:http://dx.doi.org/10.1016/j.ijhydene.2010.04.137.

Ball, M. & Weeda, M. 2015. The hydrogen economy – Vision or reality?1. *International Journal of Hydrogen Energy.* 40(25):7903-7919. DOI:http://dx.doi.org/10.1016/j.ijhydene.2015.04.032.

Bello, M. 2011. Assessment of Electrochemical Methods for Methanol Crossover Measurement through PEM of Direct Methanol Fuel Cell. *International Journal of Engineering & Technology.* 11(4):92-111. DOI:http://citeseerx.ist.psu.edu/viewdoc/download?doi=10.1.1.419.1416&rep=rep1&type=pdf.

Bollmann, L., Ratts, J.L., Joshi, A.M., Williams, W.D., Pazmino, J., Joshi, Y.V., Miller, J.T., Kropf, A.J. *et al*. 2008. Effect of Zn addition on the water–gas shift reaction over supported palladium catalysts. *Journal of Catalysis.* 257(1):43-54. DOI:http://dx.doi.org/10.1016/j.jcat.2008.04.005.

Cabtree, g.W., Dresselhauls, M.S. & Buchanan, M.V. 2004. The Hydrogen Economy. *Physics Today.* 57(12):39-45. DOI:http://dx.doi.org/10.1063/1.1878333.

Carbon Transformers 2014. *CO2 as a feedstock for producing fuels and chemical commodities.* Available: http://www.carbontransformers.com/commodity.html [01 September 2015].

Chianese, S., Loipersböck, J., Malits, M., Rauch, R., Hofbauer, H., Molino, A. & Musmarra, D. 2015. Hydrogen from the high temperature water gas shift reaction with an industrial Fe/Cr catalyst using biomass gasification tar rich synthesis gas. *Fuel Processing Technology.* 132:39-48. DOI:http://dx.doi.org/10.1016/j.fuproc.2014.12.034.

Chin, Y., Dagle, R., Hu, J., Dohnalkova, A.C. & Wang, Y. 2002. Steam reforming of methanol over highly active Pd/ZnO catalyst. *Catalysis Today.* 77(1–2):79-88. DOI:http://dx.doi.org/10.1016/S0920-5861(02)00234-1.

Chin, Y., Wang, Y., Dagle, R.A. & Shari Li, X. 2003. Methanol steam reforming over Pd/ZnO: Catalyst preparation and pretreatment studies. *Fuel Processing Technology.* 83(1–3):193-201. DOI:http://dx.doi.org/10.1016/S0378-3820(03)00067-5.

Cipriani, g., Di Dio, V., genduso, F., La Cascia, D., Liga, R., Miceli, R. & Ricco galluzzo, g. 2014. Perspective on hydrogen energy carrier and its automotive applications. *International Journal of Hydrogen Energy.* 39(16):8482-8494. DOI:http://dx.doi.org/10.1016/j.ijhydene.2014.03.174.

Conant, T., Karim, A.M., Lebarbier, V., Wang, Y., girgsdies, F., Schlögl, R. & Datye, A. 2008. Stability of bimetallic Pd–Zn catalysts for the steam reforming of methanol. *Journal of Catalysis.* 257(1):64-70. DOI:http://dx.doi.org/10.1016/j.jcat.2008.04.018.

Dagle, R.A. & Holladay, J.D. 2007. Methanol Steam Reforming for Hydrogen Production. *Chemical Reviews.* 107:3992−4021. DOI:http://pubs.acs.org/doi/pdf/10.1021/cr050198b.

Dagle, R.A., Ya-Huei Chin & Wang, Y. 2007. The Effects of PdZn Crystallite Size on Methanol Steam Reforming. *Topics in Catalysis.* 46(3):358-362. DOI:10.1007/s11244-007-9009-4.

Eblagon, K.M., Concepción, P.H., Silva, H. & Mendes, A. 2014. Ultraselective low temperature steam reforming of methanol over PdZn/ZnO catalysts—Influence of induced support defects on catalytic performance. *Applied Catalysis B: Environmental.* 154–155(0):316-328. DOI:http://dx.doi.org/10.1016/j.apcatb.2014.02.032.

Eswaramoorthi, I. & Dalai, A.K. 2009. A comparative study on the performance of mesoporous SBA-15 supported Pd–Zn catalysts in partial oxidation and steam reforming of methanol for hydrogen production. *International Journal of Hydrogen Energy.* 34(6):2580-2590. DOI:http://dx.doi.org/10.1016/j.ijhydene.2009.01.029.

Föttinger, K. 2013. The effect of CO on intermetallic PdZn/ZnO and Pd2Ga/Ga2O3 methanol steam reforming catalysts: A comparative study. *Catalysis Today.* 208(0):106-112. DOI:http://dx.doi.org/10.1016/j.cattod.2012.12.004.

Friedrich, M., Penner, S., Heggen, M. & Armbrüster, M. 2013. High CO2 Selectivity in Methanol Steam Reforming through ZnPd/ZnO Teamwork. *Angewandte Chemie International Edition.* 52(16):4389-4392. DOI:10.1002/anie.201209587.

FuelCell Energy 2013. *Types of Fuel Cells.* Available: http://www.fuelcellenergy.com/why-fuelcell-energy/types-of-fuel-cells/ [15 August 2015].

Gallagher, J.R., Childers, D.J., Zhao, H., Winans, R.E., Meyer, R.J. & Miller, J.T. 2015. Structural evolution of an intermetallic Pd–Zn catalyst selective for propane dehydrogenation. DOI:10.1039/C5CP00222B.

Ghasemzadeh, K., Morrone, P., Babalou, A.A. & Basile, A. 2015. A simulation study on methanol steam reforming in the silica membrane reactor for hydrogen production. *International Journal of Hydrogen Energy.* 40(10):3909-3918. DOI:http://dx.doi.org/10.1016/j.ijhydene.2014.04.010.

Houchins, C., Kleen, g.J., Spendelow, J.S., Kopasz, J., Peterson, D., garland, N.L., Donna Lee Ho, J., Kathi Epping Martin, M. *et al*. 2012. U.S. DOE Progress Towards Developing Low-Cost, High Performance, Durable Polymer Electrolyte Membranes for Fuel Cell Applications. *Membranes.* 2(4):855-878. DOI:10.3390/membranes2040855.

Huang, Y., He, X. & Chen, Z. 2011. First-principles study towards the reactivity of the Pd(111) surface with low Zn deposition. *Journal of Chemical Physics.* (184702):134. DOI:http://dx.doi.org/10.1063/1.3587136.

Ilinich, O., Liu, Y., Castellano, C., Koermer, g., Moini, A. & Farrauto, R. 2008. A new palladium-based catalyst for methanol steam reforming in a miniature fuel cell power source. *Platinum Metals Review.* 52(3):134-143. DOI:10.1595/147106708x324403.

Iwasa, N., Yoshikawa, M. & Arai, M. 2002. Selective hydrogenation of acetonitrile to ethylamine using palladium-based alloy catalysts. 4:5414-5420. DOI:10.1039/B206916B.

Iwasa, N., Masuda, S., Ogawa, N. & Takezawa, N. 1995. Steam reforming of methanol over Pd/ZnO: Effect of the formation of PdZn alloys upon the reaction. *Applied Catalysis A: general.* 125(1):145-157. DOI:http://dx.doi.org/10.1016/0926-860X(95)00004-6.

Joensen, F. & Rostrup-Nielsen, J.R. 2002. Conversion of hydrocarbons and alcohols for fuel cells. *Journal of Power Sources.* 105(2):195-201. DOI:http://dx.doi.org/10.1016/S0378-7753(01)00939-9.

Kamarudin, S.K., Achmad, F. & Daud, W.R.W. 2009. Overview on the application of direct methanol fuel cell (DMFC) for portable electronic devices. *International Journal of Hydrogen Energy.* 34(16):6902-6916. DOI:http://dx.doi.org/10.1016/j.ijhydene.2009.06.013.

Karim, A., Conant, T. & Datye, A. 2006. The role of PdZn alloy formation and particle size on the selectivity for steam reforming of methanol. *Journal of Catalysis.* 243(2):420-427. DOI:http://dx.doi.org/10.1016/j.jcat.2006.07.024.

Kim, Y.H., Park, E.D., Lee, H.C., Lee, D. & Lee, K.H. 2009. Preferential CO oxidation over supported noble metal catalysts. *Catalysis Today.* 146(1–2):253-259. DOI:http://dx.doi.org/10.1016/j.cattod.2009.01.045.

Kolb, g. 2008. *Fuel Processing for Fuel Cells.* Wiley-VCH.

Lebarbier, V., Dagle, R., Datye, A. & Wang, Y. 2010. The effect of PdZn particle size on reverse-water–gas-shift reaction. *Applied Catalysis A: general.* 379(1–2):3-6. DOI:http://dx.doi.org/10.1016/j.apcata.2010.02.008.

Liu, F., Lu, g. & Wanga, C. 2006. Low Crossover of Methanol and Water Through Thin Membranes in Direct Methanol Fuel Cells. *Journal of the Electrochemical Society.* 153(3):A543-A553. DOI:http://ecec.mne.psu.edu/Pubs/2006-Liu-JES.pdf.

Martin, S. & Wörner, A. 2011. On-board reforming of biodiesel and bioethanol for high temperature PEM fuel cells: Comparison of autothermal reforming and steam reforming. *Journal of Power Sources.* 196(6):3163-3171. DOI:http://dx.doi.org/10.1016/j.jpowsour.2010.11.100.

Mateos-Pedrero, C., Silva, H., Pacheco Tanaka, D.A., Liguori, S., Iulianelli, A., Basile, A. & Mendes, A. 2015. CuO/ZnO catalysts for methanol steam reforming: The role of the support polarity ratio and surface area. *Applied Catalysis B: Environmental.* 174–175:67-76. DOI:http://dx.doi.org/10.1016/j.apcatb.2015.02.039.

Mekhilef, S., Saidur, R. & Safari, A. 2012. Comparative study of different fuel cell technologies. *Renewable and Sustainable Energy Reviews.* 16(1):981-989. DOI:http://dx.doi.org/10.1016/j.rser.2011.09.020.

Meshkani, F. & Rezaei, M. 2015. Preparation of mesoporous nanocrystalline iron based catalysts for high temperature water gas shift reaction: Effect of preparation factors. *Chemical Engineering Journal.* 260:107-116. DOI:http://dx.doi.org/10.1016/j.cej.2014.08.080.

Mishra, A. & Prasad, R. 2011. A review on preferential oxidation of carbon monoxide in hydrogen rich gases. *Bulletin of Chemical Reaction Engineering and Catalysis.* 6(1):1-14.

Mondal, K.C. & Ramesh Chandran, S. 2014. Evaluation of the economic impact of hydrogen production by methane decomposition with steam reforming of methane process. *International Journal of Hydrogen Energy.* 39(18):9670-9674. DOI:http://dx.doi.org/10.1016/j.ijhydene.2014.04.087.

Nepel, T.C.M., Lopes, P.P., Paganin, V.A. & Ticianelli, E.A. 2013. CO tolerance of proton exchange membrane fuel cells with Pt/C and PtMo/C anodes operating at high temperatures: A mass spectrometry investigation. *Electrochimica Acta.* 88:217-224. DOI:http://dx.doi.org/10.1016/j.electacta.2012.10.039.

Pachauri, R.K., Allen, M.R., barros, V.R., Broome, J., Cramer, W., Christ, R., Church, J.A., Clarke, L. *et al*. 2014. *Climate Change 2014: Synthesis Report. Contribution of Working groups I, II and III to the Fifth Assessment Report of the Intergovernmental Panel on Climate Change.* (AR5). geneva, Switzerland: Intergovernmental Panel on Climate Change.

Palo, D.R., Dagle, R.A. & Holladay, J.D. 2007. Methanol Steam Reforming for Hydrogen Production. *Chemical Reviews.* 107(10):3992–4021. DOI:10.1021/cr050198b.

Roh, H., Eum, I. & Jeong, D. 2012. Low temperature steam reforming of methane over Ni–Ce(1−x)Zr(x)O2 catalysts under severe conditions. *Renewable Energy.* 42:212-216. DOI:http://dx.doi.org/10.1016/j.renene.2011.08.013.

Sá, S., Silva, H., Brandão, L., Sousa, J.M. & Mendes, A. 2010. Catalysts for methanol steam reforming—A review. *Applied Catalysis B: Environmental.* 99(1–2):43-57. DOI:http://dx.doi.org/10.1016/j.apcatb.2010.06.015.

Shabangu, S., Woolf, D., Fisher, E.M., Angenent, L.T. & Lehmann, J. 2014. Techno-economic assessment of biomass slow pyrolysis into different biochar and methanol concepts. *Fuel.* 117, Part A:742-748. DOI:http://dx.doi.org/10.1016/j.fuel.2013.08.053.

Sharaf, O.Z. & Orhan, M.F. 2014. An overview of fuel cell technology: Fundamentals and applications. *Renewable and Sustainable Energy Reviews.* 32:810-853. DOI:http://dx.doi.org/10.1016/j.rser.2014.01.012.

Smith R J, B., Loganathan, M. & Shekhar Shantha, M. 2010. A Review of the Water gas Shift Reaction Kinetics. *International Journal of Chemical Reactor Engineering.* 8(R4) DOI:10.2202/1542-6580.2238.

Takeguchi, T., Yamanaka, T., Asakura, K., Muhamad, E.N., Uosaki, K. & Ueda, W. 2012. Evidence of Nonelectrochemical Shift Reaction on a CO-Tolerant High-Entropy State Pt–Ru Anode Catalyst for Reliable and Efficient Residential Fuel Cell Systems. 134(35):14508–14512. DOI:3510.1021/ja304939q.

Verrall, R.A., Vlajic, M.D. & Krstic, V.D. 1999. Silicon carbide as an inert-matrix for a thermal reactor fuel. *Journal of Nuclear Materials.* 274(1–2):54-60. DOI:http://dx.doi.org/10.1016/S0022-3115(99)00089-6.

Wang, C. 2004. Fundamental Models for Fuel Cell Engineering. *Chemical Reviews.* 10(104):4727−4766. DOI:10.1021/cr020718s.

Wang, Q., Wang, g., Lu, X., Chen, C., Li, Z. & Sun, g. 2015. Investigation of Methanol Crossover and Water Flux in an Air-Breathing Direct Methanol Fuel Cell. *International Journal of Electrochemical Science.* 10:2939 - 2949. DOI:http://www.electrochemsci.org/papers/vol10/100402939.pdf.

Wang, C., Boucher, M., Yang, M., Saltsburg, H. & Flytzani-Stephanopoulos, M. 2014. ZnO-modified zirconia as gold catalyst support for the low-temperature methanol steam reforming reaction. *Applied Catalysis B: Environmental.* 154–155:142-152. DOI:http://dx.doi.org/10.1016/j.apcatb.2014.02.008.

WANG, Y., ZHANG, J. & XU, H. 2006. Interaction between Pd and ZnO during Reduction of Pd/ZnO Catalyst for Steam Reforming of Methanol to Hydrogen. *Chinese Journal of Catalysis.* 27(3):217-222. DOI:http://dx.doi.org/10.1016/S1872-2067(06)60015-6.

Wang, Y., Chen, K.S., Mishler, J., Cho, S.C. & Adroher, X.C. 2011. A review of polymer electrolyte membrane fuel cells: Technology, applications, and needs on fundamental research. *Applied Energy.* 88(4):981-1007. DOI:http://dx.doi.org/10.1016/j.apenergy.2010.09.030.

Yang, C. 2009. An impending platinum crisis and its implications for the future of the automobile. *Energy Policy.* 37(5):1805-1808. DOI:http://dx.doi.org/10.1016/j.enpol.2009.01.019.

Zhang, Q. & Farrauto, R.J. 2011. A PdZn catalyst supported on stabilized ceria for stoichiometric methanol steam reforming and hydrogen production. *Applied Catalysis A: general.* 395(1–2):64-70. DOI:http://dx.doi.org/10.1016/j.apcata.2011.01.024.

Appendix A Catalyst Preparation and Characterisation

Appendix A.1: ZnO Pore Volume

Pore volume of ZnO support (99.999 wt%, Sigma-Aldrich) was determined by introducing water to the support until the support became saturated (see Table A-1). The ZnO support was subjected under vacuum (~ -90 kPa) so as to force liquid water into the pores of the support. The pore volume was found to be ~ 0.96 ml/g-ZnO.

Table A-1: ZnO support pore volume determination experiments

Category	Experiment #1	Experiment #2	Experiment #3
m_{ZnO}, g	2.0120	2.0095	2.0043
m_{H2O}, g	1.9509	1.9042	1.9216
Pore volume, cm^3/g	0.9696	0.9476	0.9587

Note: density of water = 1 g/cm^3

Appendix A.2: Impregnation Catalyst

Table A-2 provides amounts of materials used in the preparation of impregnation catalyst. The ICP-OES results and BET surface area are also provided.

Table A-2: Impregnation catalyst preparation material and characterisation results

Category	Preparation material, g			ICP-OES		BET
	ZnO	Pd salt	Water	Pd, wt%	Zn, wt%	m^2/g
IMP_1	28.0300	1.8660	26.6000	2.8	78.9	3.3
IMP_2	19.0011	1.2842	18.0100	2.7	77.3	3.2
ZnO	-	-	-	-	-	2.8

Note: Pd salt has 42 wt% Pd according the TGA

Pd salt is 37.0 – 42.0 wt% Pd according to the supplier specifications

Appendix A.3: Co-precipitation Catalyst

Amounts of materials used for the preparation of co-precipitation catalyst, and ICP-OES results and BET surface area of the catalyst are provided in Table A-3.

Table A-3: Co-precipitation catalyst preparation material and characterisation results

Amount, g			Vol, ml	ICP-OES		BET
Pd salt	Zn salt	Water	5M NH_4OH	Pd, wt%	Zn, wt%	m^2/g
1.0000	49.3939	30.00	70.19	1.1	79.9	5.3

The amount of aqueous NH_4OH (i.e. 70.19 ml, 5M) used for precipitating Pd and Zn was 3 mol% more than the stoichiometric amount (refer to the precipitation reaction equations, i.e. Eqn 4.2 and Eqn 4.3.

Appendix B : Summary of the Catalyst Performance Tests

Table B-1 is the summary of the performance tests conducted in this work. Refer to chapter 4.1.3 for test Nomenclature.

Table B-1: Summary of the catalyst performance tests

Test Nomenclature	ToS (h)	GHSV (h^{-1})	X_{MeOH} (%)	SD (-)	RSD (%)
IMP_1-120/180	0-50	1100	16.1	2.9	17.8*
	120-160	1100	11.1	0.1	1.0
IMP_2-120/180	0-35	1060	12.8	1.7	13.0*
	35-121	240	24.7	1.4	5.5
	120-150	1060	12.0	0.5	3.9
IMP_1-200/180	0-50	1100	14.8	2.1	13.8*
IMP_1-450/180	90-150	1100	10.4	0.5	4.8
CP-225/200	0-60	920	36.2	1.6	4.5
	60-121	480	46.5	0.7	1.5
	121-168	760	37.7	0.4	0.9
	168-218	920	29.3	0.8	2.6
CP-450/200	218-295	920	23.8	1.1	4.6
	295-360	410	36.5	0.8	2.3
	360-400	1270	16.4	0.5	2.9
	460-490	920	19.9	1.2	6.2

MeOH conversion: SD = standard deviation, RSD = relative standard deviation, *RSD during catalyst line-in period

Selectivity towards CO_2 was > 99% for all the tests.

Partial Pressure of MeOH in the condenser/catch pot:

Table B-2: Antoine equation parameters (after DDBST GmbH, n.d.)

A	B	C	Tmin (°C)	Tmax (°C)
8.08097	1582.27	239.7	15	100

$$P^0 = 10^{A-\frac{B}{C+T}}, P^0 in\ mmHg\ and\ T\ in\ °C$$

$$P^0_{MeOH@15°C} = 10^{8.08097-\frac{1582.27}{239.7+3}} = 36.4\ mmHg = 0.4732\ kPa$$

$$y_{MeOH@15°C} = \frac{P_{MeOH}}{P_{catchpot}} = \frac{x_{MeOH} * P^0_{MeOH@15°C}}{P_{catpot}} = \frac{0.6 * 0.4734}{200} = 0.14\%$$

It should be noted that the condenser/catch pot was kept at ~ 3°C. However, the partial pressure of CH_3OH is less than 1% at a relatively higher temperature (i.e. 15°C).

Appendix C : Equilibrium Calculations

Equilibrium calculations were calculated using Aspen Plus V8.6 simulation software (supplied by Aspen Technology Inc.). A Non-Random Two-Liquid (NTRL) model and a rigorous equilibrium reactor (Requil) based on the stoichiometric approach was used. Aspen Plus simulations were conducted such that the catalyst testing conditions (i.e. S/C = 1.1, T_{rxn} = 180 - 200°C, P = 1 barg, Ar_{feed} = 5 - 15 mol%) were covered.

Chemical reactions i.e. steam reforming of methanol (SRM) (Eqn 2.18), methanol decomposition (MD) (Eqn 2.19) and water-gas shift (WGS) (Eqn 2.20) were taken into consideration. Figure C-1 is Aspen simulation process flow diagram. Under the investigated conditions the 'LIQUID' stream flowrate was zero.

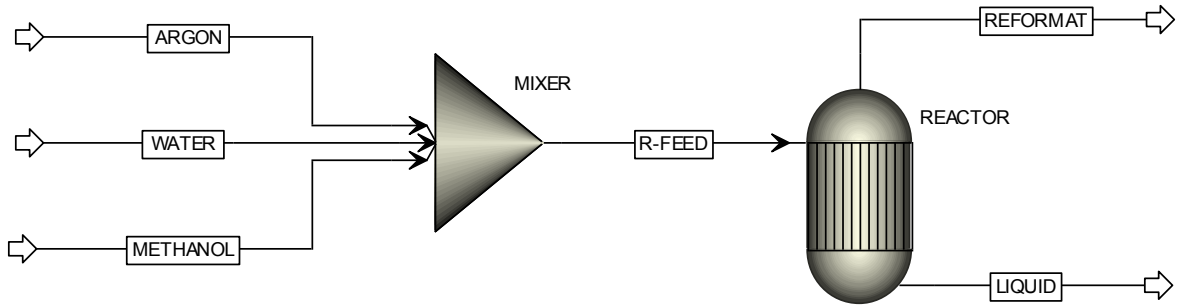

Figure C-1: Flowsheet of the methanol steam reforming simulation

Table C-1 shows specifications as incorporated in the Aspen simulation flowsheet shown in Figure C-1.

Table C-1: Simulation specifications for methanol steam reforming equilibrium calculations

Stream/Block	Specification/Condition
R-FEED	S/C = 1.1, A r= 5 - 15 mol%, T = 30°C, P = 1 barg
REACTOR	$T_{REACTOR}$ = 180 or 200°C, P = 1 barg Equilibrium reactions: SRM, MD and WGS

The results of the simulation (see chapter 5.3.1) show that CH_3OH equilibrium conversion is > 98%. The equilibrium selectivity towards CO_2 (> 99%) is based on the equilibrium conversion (>98%). Since CH_3OH conversion was less than 50% for all the catalyst performance tests in this work, the CO_2 equilibrium selectivity obtained from the simulation does not represent equilibrium selectivity towards CO_2 at lower conversions (< 50%). Hence a WGS equilibrium was simulated at lower conversions (< 50%). For this simulation, it was assumed that CH_3OH is first converted to CO via MD reaction (Eqn 2.19). Hypothetical feed compositions of the WGS equilibrium reactor corresponding to CH_3OH conversion (via MD) were therefore calculated (see Table C-2).

Table C-2: WGS equilibrium reactor feed composition corresponding to CH_3OH conversion

$X_{MeOH, MD}$ (%)	WGS Equilibrium Reactor Feed (mol%)				
	H_2O	Ar	CH_3OH	CO	H_2
5	47.6	4.8	41.1	2.2	4.3
10	45.6	4.6	37.3	4.1	8.3
15	43.8	4.4	33.9	6.0	12.0
20	42.1	4.2	30.7	7.7	15.3
25	40.6	4.1	27.7	9.2	18.5
30	39.1	3.9	24.9	10.7	21.4
40	36.5	3.7	19.9	13.3	26.6
50	34.3	3.4	15.6	15.6	31.2
80	28.9	2.9	5.2	21.0	42.0

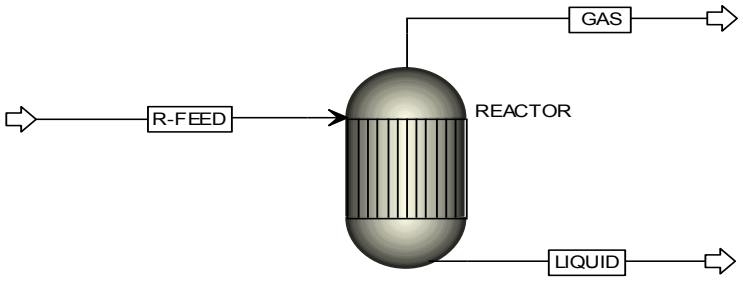

Figure C-2: WGS equilibrium reactor flowsheet

Appendix D : Off-line GC-FID Calibration

Appendix D.1: Off-line GC-FID Calibration Factor

To determine methanol conversion, methanol (MeOH) concentration of the liquid samples was determined using off-line GC-FID system (details on chapter 4.5.2). Ethanol (EtOH), supplied by Kimix, 99.9% purity, was used as an external standard. Acetone, also supplied by Kimix, 99.9% purity, was used to dilute both MeOH in the reactor liquid samples and EtOH used as an external standard (refer to Appendix D.2). The dilution ensured that the GC column was not overloaded with either MeOH or EtOH and that both EtOH and MeOH

exhibited a linear GC response. Figure D-1 shows the concentration range where both EtOH and MeOH give a linear response. It was in this concentration range that a calibration was conducted.

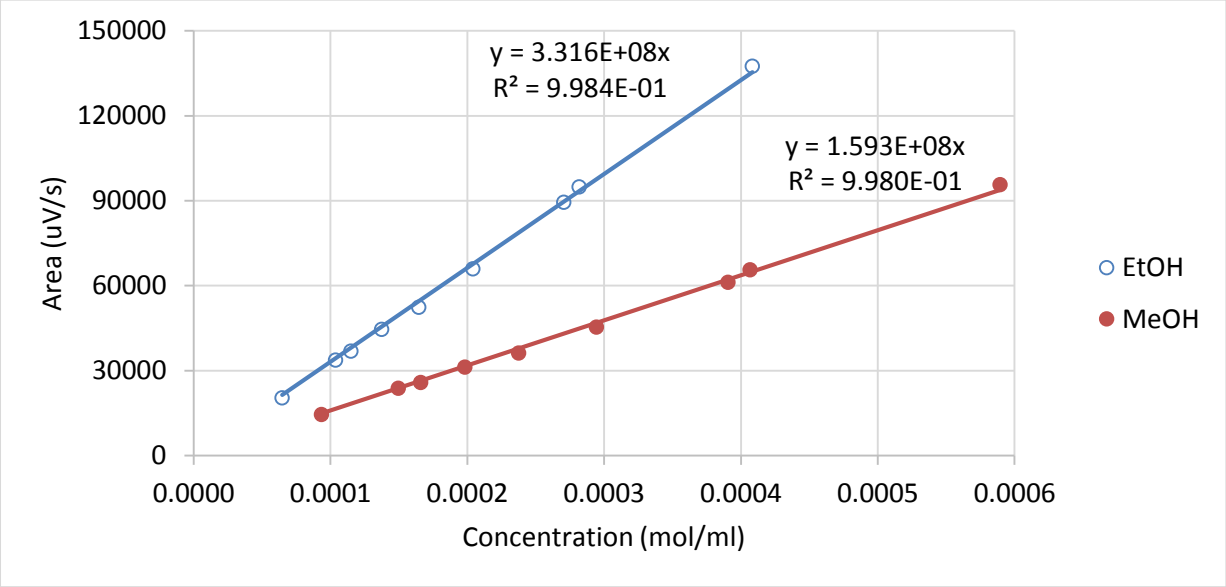

Figure D-1 Concentration range where ethanol and methanol exhibit a linear response

Figure D-2 is the calibration curve of the GC system.

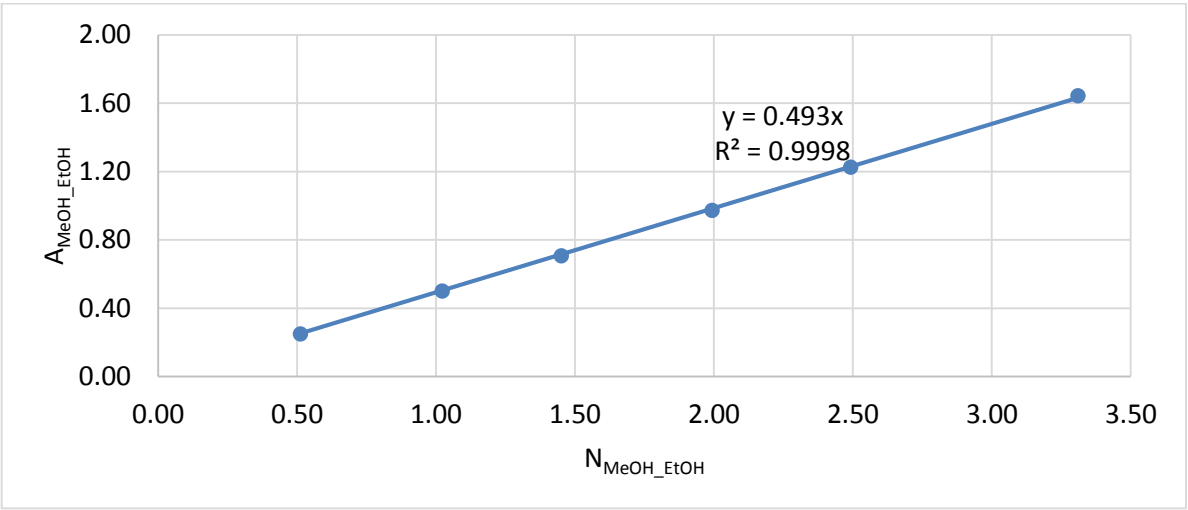

Figure D-2: Off-line GC-FID system calibration curve

Note that in Figure D-2, $A_{MeOH\_EtOH} = A_{MeOH} / A_{EtOH}$ and $nm_{eOH\_EtOH} = nm_{eOH} / N_{EtOH}$, where A_i is an area of a peak of component-i (in a chromatogram), and N_i is a number of moles of component-i. The response factor, $R_{f,MeOH\_EtOH} = A_{MeOH\_EtOH} / nm_{eOH\_EtOH} =$ slope = 0.493.

Appendix D.2: GC Sample Preparation

The samples prepared for GC analysis were such that concentrations of EtOH and MeOH were within the calibration range. The feed molar S/C ratio for catalyst performance test was approximately 1.1 (~ 60 wt% MeOH). Thus the expected maximum MeOH concentration of liquid reactor samples was ~ 60 wt%, and this would happen if there was no MeOH conversion in the reactor. Another extreme case would be when MeOH conversion approached 100 %, then liquid reactor sample concentration would approach 0 wt% MeOH. To accommodate both extremes and also to be within the calibration range, the GC sample was prepared by mixing the liquid amounts indicated in Figure D-1.

Table D-1: Liquid mass used to prepare the sample for GC analysis

Liquid	Reactor sample	Ethanol	Acetone
Amount, g	~ 0.17	~ 0.05	~ 10

Appendix D.3: CH_3OH Conversion Calculation Procedure

MeOH conversion was calculated as follows;

$$R_{f_{MeOH-EtOH}} = \frac{{}^{A_{MeOH}}/_{A_{EtOH}}}{{}^{\Delta N_{MeOH}}/_{N_{EtOH}}} \qquad \text{Eqn I.}$$

$R_{f_{MeOH-EtOH}}$ is equal to the slope of the plot in Figure D-2, and A_i is an area of a peak of component-i in a GC chromatogram.

$$N_{EtOH} = \frac{m_{EtOH}}{M_{R,EtOH}} \qquad \text{Eqn II.}$$

Since the mass of EtOH (m_{EtOH}) added to a sample was known, the number of moles of EtOH (N_{EtOH}) were calculated as per Eqn II.

Subsequently, the number of moles of MeOH (ΔN_{MeOH}) that exit the reactor after a period of time, Δt, was obtained since ΔN_{MeOH} was now the only unknown in Eqn I

$$\Delta N_{MeOH,in} = \frac{wt.\%_{MeOH,feed}}{100} * \frac{\Delta Total\ Mass_{in}}{M_{R,MeOH}} \qquad \text{Eqn III.}$$

$\Delta N_{MeOH,in}$ is the number of moles of MeOH that entered the reactor during the time, Δt

$$X_{MeOH} = \frac{\Delta N_{MeOH,in} - \Delta N_{MeOH}}{\Delta N_{MeOH,in}} \quad \text{Eqn IV.}$$

Note, $\Delta K_i = \Delta t * \dot{K}$, where ΔK_i is K (e.g. moles) of component-i that entered the reactor at a rate $\dot{K}$ within the period of time, Δt. Therefore X_{MeOH} in Eqn IV is the average MeOH conversion over the period of time, Δt

Appendix E : Online GC-TCD Calibration

Appendix E.1: Online GC-TCD Calibration Factors

In order to determine selectivity towards CO_2 the online GC-TCD system (described in 4.5.3) was calibrated. Figure E-1 and Figure E-2 are the calibrations of gas mixtures, i.e. CO in Ar and CO_2 in Ar, respectively.

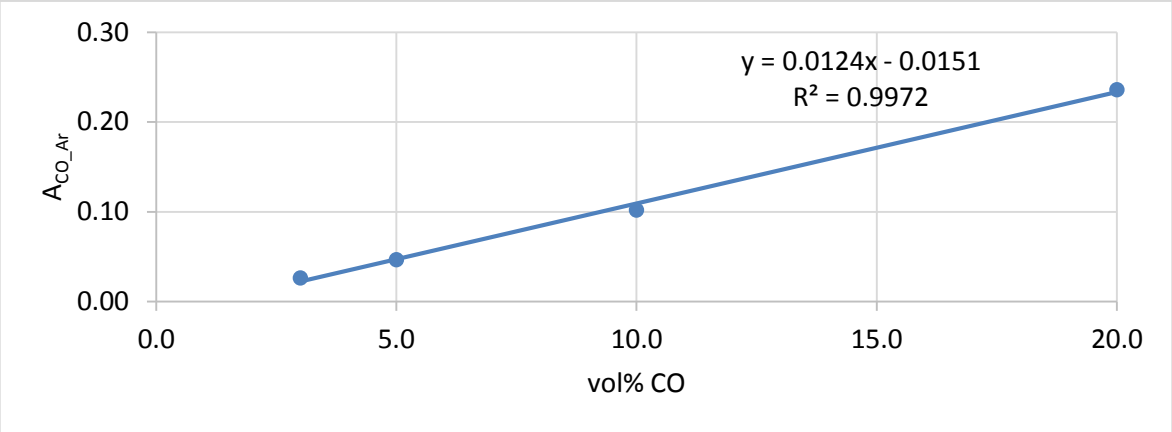

Figure E-1: GC response factor of CO in Ar

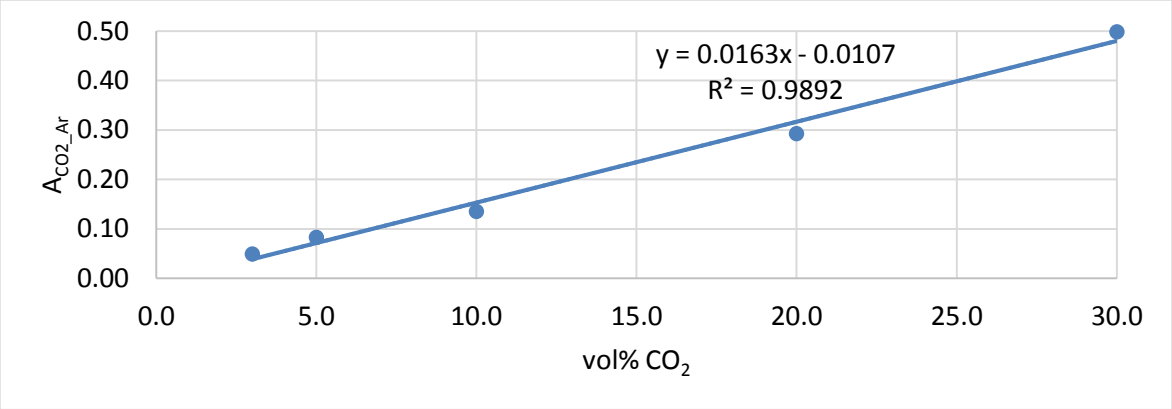

Figure E-2: GC response factor of CO_2 in Ar

Appendix E.2 : CO_2 Selectivity Calculation Procedure

In the following calculation A_i is the area of component-i and is obtained from the GC chromatogram and N_i is the number of moles of component-i. CO_2 selectivity was calculated as follows;

$$R_{f_{CO-Ar}} = \frac{{}^{A_{CO}}/_{A_{Ar}}}{{}^{N_{CO}}/_{N_{Ar}}} \qquad \text{Eqn V.}$$

$R_{f_{CO-Ar}}$ is the slope of the curve in Figure E-1

$$R_{f_{CO_2-Ar}} = \frac{{}^{A_{CO_2}}/_{A_{Ar}}}{{}^{N_{CO_2}}/_{N_{Ar}}} \quad \text{Eqn VI.}$$

$R_{f_{CO_2-Ar}}$ is the slope of the curve in Figure E-2

$$\frac{R_{f_{CO-Ar}}}{R_{f_{CO_2-Ar}}} = \frac{{}^{A_{CO}}/_{A_{CO_2}}}{{}^{N_{CO}}/_{N_{CO_2}}} \quad \text{Eqn VII.}$$

Eqn VII is obtained by combining Eqn V and Eqn VI

$$\frac{N_{CO}}{N_{CO_2}} = \frac{R_{f_{CO-Ar}}}{R_{f_{CO_2-Ar}}} * \frac{A_{CO}}{A_{CO_2}} \quad \text{Eqn VIII.}$$

Eqn VIII is obtained by re-arranging Eqn VII

$$S_{CO_2} = \frac{N_{CO_2}}{N_{CO_2} + N_{CO}} \quad \text{Eqn IX.}$$

Eqn IX is the definition of CO_2 selectivity

$$S_{CO_2} = \frac{1}{1 + {}^{N_{CO}}/_{N_{CO_2}}} \quad \text{Eqn X.}$$

Eqn X is obtained by re-arranging Eqn IX

$$S_{CO_2} = \frac{1}{1 + {}^{R_{f_{CO-Ar}}}/_{R_{f_{CO_2-Ar}}} * {}^{A_{CO}}/_{A_{CO_2}}} \quad \text{Eqn XI.}$$

Eqn XI is a result of substituting Eqn VIII in Eqn X

Appendix F : Sample Calculations

Sample 3 of IMP_1/120/180 performance test is used as an example to demonstrate how CH_3OH conversion (X_{MeOH}) and selectivity towards CO_2 (S_{CO_2}) were calculated.

Appendix F.1: Offline GC-FID Data and CH3OH Conversion Calculation

Liquid flows:

$$m_{in} = 45.00\ g$$

m_{in} is the mass of liquid pumped into the reactor during sample 3 period i.e. 7.8 hours. This mass was obtained from the balance.

$$m_{out} = 40.81\ g$$

m_{out} is the mass of liquid collected from the catch pot after the sample 3 period i.e. 7.8 hours.

Off-line GC Sample Preparation:

$$m_{sample} = 0.1981\ g$$

m_{sample} is the mass of liquid sample used for GC analysis. Otherwise stated, m_{sample} is a portion of m_{out}.

$$m_{EtOH} = 0.0579\ g$$

m_{EtOH} is the mass of EtOH added to m_{sample}. Note, EtOH was used as an external standard.

$$n_{EtOH} = \frac{m_{EtOH}}{M_{R,EtOH}} = \frac{0.0579}{46.07} = 1.2568 * 10^{-3} mols$$

n_{EtOH} is the number of moles of EtOH added to the sample.

MeOH and EtOH in the sample were diluted in acetone before GC analysis.

GC Analysis Results:

Table F-1: Off-line GC-FID Analysis Results

Category	A_i (a.u.)	
	Injection 1	Injection 2
MeOH	53190.1	54243.1
EtOH	37868.7	38753.2
MeOH/EtOH	1.405	1.400

CH_3OH Conversion Calculation:

$$\frac{A_{MeOH}}{A_{EtOH}} = 1.4025$$

This is the ratio of the chromatogram areas (MeOH to EtOH). Refer to Table F-1.

$$N_{MeOH} = \frac{{}^{A_{MeOH}}/_{A_{EtOH}}}{R_{f_{MeOH-EtOH}}} * N_{EtOH} = \frac{1.4025}{0.493} * 1.2568 * 10^{-3} = 3.5818 * 10^{-3}\ mol$$

N_{MeOH} is the number of moles of MeOH in m_{sample} (i.e. 0.1981 g-sample). Note $R_{f\ MeOH\_EtOH}$ is the slope of the plot in Figure D-2.

$$\Delta N_{MeOH,out} = \frac{N_{MeOH}}{m_{sample}} * m_{out} = \frac{3.5818*10^{-3}}{0.1981} * 40.81 = 0.7247\ mol$$

$\Delta N_{MeOH,out}$ is the number of moles of MeOH the exit the reactor during sample 3 period i.e. 7.8 hours.

$$\Delta N_{MeOH,in} = \frac{wt.\%_{MeOH,feed}}{100} * \frac{\Delta Total\ Mass_{in}}{M_{R,MeOH}} = \frac{61.3}{100} * \frac{45.00}{32} = 0.8620\ mol$$

$\Delta N_{MeOH,in}$ is the number of moles that entered the reactor during sample 3 period i.e. 7.8 hours.

$$X_{MeOH,1} = \frac{\Delta N_{MeOH,in} - \Delta N_{MeOH}}{\Delta N_{MeOH,in}} * 100\% = \frac{0.8620 - 0.7247}{0.8620} * 100\% = 15.9\%$$

Likewise, another sample from m_{out} was analysed and $X_{MeOH,2}$ was 13.1%. Thus the average X_{MeOH} = 14.5% (see the third sample or data point of IMP_1/120/180 in Figure 5-14). Note, X_{MeOH} is the average MeOH conversion during sample 3 period.

Appendix F.2: Online GC-TCD Data and CO_2 selectivity Calculation

The data in Table F-2 corresponds to the offline GC-FID data in Table F-1.

Table F-2: Online GC data corresponding to the Offline GC data

			A_i (a.u.)				
	ToS,hr	**Run ID**	**H_2**	**CO**	**Ar**	**CO_2**	**CO/CO_2**
Sample 3	17.61	IMP_1_103	-	-	-	-	-
	18.61	IMP_1_108	-	-	-	-	-
	19.61	IMP_1_113	-	-	-	-	-
	20.61	IMP_1_118	-	-	-	-	-
	21.61	IMP_1_123	2258709	486.0	101378.8	71178.3	0.00479
	22.61	IMP_1_128	2253928	485.6	101051.7	71373.4	0.00481
	23.61	IMP_1_133	2270072	482.7	99688.4	71831.9	0.00484
	24.61	IMP_1_138	2250630	479.5	101530.6	70937.1	0.00472
	25.41	IMP_1_142	2265478	492.8	100674.2	71550.2	0.00489
	Average	-	-	-	-	-	**0.00481**

$$\frac{A_{CO}}{A_{CO_2}} = 0.00481$$

A_{co}/A_{co_2} is the average ratio of chromatogram areas (CO to CO_2) over 7.8 hours, the period over which sample 3 was taken. Only the last five data points (i.e. steady state period) were used for calculations. Refer to Table F-2.

$$\frac{R_{f_{CO-Ar}}}{R_{f_{CO_2-Ar}}} = \frac{0.0124}{0.0163} = 0.7607$$

R_{fCO_Ar} and R_{fCO2_Ar} are the slopes of the plots in respectively.

$$S_{CO_2} = \frac{1}{1 + {R_{f_{CO-Ar}}}/{R_{f_{CO_2-Ar}}} * {A_{CO}}/{A_{CO_2}}} = \frac{1}{1 + 0.7607 * 0.00481} = 99.6\%$$

In summary, X_{MeOH} = 15.9% and S_{CO_2} = 99.6% for sample 3 of IMP_1/120/180. (see the third data point of IMP_1/120/180 in Figure 5-14).